

Republic of Iraq
Ministry of Higher Education and
Scientific Research
University of Kerbala
College of Engineering



**Condition Monitoring of Gas Turbine Shaft in AL-
Hilla Power Station/2 Using Vibration
Measurements in Different Environments.**

A Thesis
Submitted to the Council of the College of
Engineering,
University of Kerbala, in Partial Fulfillment of the
Requirements for the Degree of Master of science in
Mechanical Engineering

By
Hussein Ibrahim Al-Lobawi
BSc. Mechanical Engineering / University of Babylon
2007

Supervised by

Assist Prof.
Dr. Mohsin A. Alshammari

Assist Prof.
Dr. Amjad Al-Hamood

2019 A.D

1440 A.H

بِسْمِ اللَّهِ الرَّحْمَنِ الرَّحِيمِ
بِسْمِ اللَّهِ الرَّحْمَنِ الرَّحِيمِ

وَأَنْتَ يَا مُحَمَّدُ
أَنْتَ يَا مُحَمَّدُ
أَنْتَ يَا مُحَمَّدُ
أَنْتَ يَا مُحَمَّدُ
أَنْتَ يَا مُحَمَّدُ
أَنْتَ يَا مُحَمَّدُ
أَنْتَ يَا مُحَمَّدُ
أَنْتَ يَا مُحَمَّدُ
أَنْتَ يَا مُحَمَّدُ
أَنْتَ يَا مُحَمَّدُ

وَأَنْتَ يَا مُحَمَّدُ
أَنْتَ يَا مُحَمَّدُ
أَنْتَ يَا مُحَمَّدُ
أَنْتَ يَا مُحَمَّدُ
أَنْتَ يَا مُحَمَّدُ
أَنْتَ يَا مُحَمَّدُ
أَنْتَ يَا مُحَمَّدُ
أَنْتَ يَا مُحَمَّدُ
أَنْتَ يَا مُحَمَّدُ
أَنْتَ يَا مُحَمَّدُ

بِسْمِ اللَّهِ الرَّحْمَنِ الرَّحِيمِ
بِسْمِ اللَّهِ الرَّحْمَنِ الرَّحِيمِ

بِسْمِ اللَّهِ الرَّحْمَنِ الرَّحِيمِ
بِسْمِ اللَّهِ الرَّحْمَنِ الرَّحِيمِ (85)

Supervisors Certification

We certify that this dissertation entitled “**Condition Monitoring of Gas Turbine Shaft in AL- Hilla Power Station/2 Using Vibration Measurements in Different Environments**” was prepared by (**Hussein Ibrahim Mansoor**) and had been carried out completely under my supervision at the University of Kerbala, Mechanical Engineering Department in partial fulfillment of the requirement for the degree of Master Science in Mechanical Engineering.

Signature

Assist. Prof. Dr. Mohsin A. Alshammari

Mechanical Engineering Department

University of Kerbala

Data: //2019

Signature

Assist. Prof. Dr. Amjad Al-Hamood

Mechanical Engineering Department

University of Baghdad

Data: //2019

Dedication

To

The big heart " my father" May God have mercy on him and to the great lady "my mother " who always encourage me to reach to the beach of success.

My supporter "My Wife" for his tolerance and assistance to bring my work into completion.

To the flowers who make my life valuable my sons: Muntazir, Adam, and Ibrahim.

My sister for her true feelings and to all friends.

I dedicate this work.

Hussein2019

Acknowledgments

I would like to express my thanks to “**Allah**” the Most Gracious and Most Merciful, and to His prophet “**Mohammad**” for enabling me to complete this study.

I introduce my thanks to my supervisors **Dr. Mohsin A. Alshammari** and **Dr. Amjad Al-Hamood** for their valuable guidance, assistance, cooperation and motivation throughout the course of preparing my thesis.

I would like to thank Assistant Prof. **Dr. Basim K. Nile** the Dean of the College of Engineering–Karbala University.

I would like to thank the Head of Department of Mechanical Engineering **Dr. Hazem Omran Al Jamali** for his help; also, I would like to thank the teaching staff in the Department of Mechanical Engineering for their help and support through my year of study.

I extend my thanks to staff of Mechanical Engineering laboratory in Mechanical Engineering in University of Kufa and anyone who helped me in this work.

Hussein 2019

ABSTRACT

The gas turbine rotors are subjected to different types and directions of loading like axial, bending, shear and thermal loading. This loading is changed periodically during the operation operation which can lead to crack initiation in the rotor shaft. When these cracks propagate to the extreme limit, it will lead to sudden failure of the shaft rotor.

Crack existence can be detected by observing the vibration parameters of the rotor, the vibration parameters is changed when the shaft is cracked. The most observable change in these parameters is the natural frequency and the response of vibration.

In this study, the vibration of Alhilla gas turbine rotor is studied with the existence of cracks and without them. The rotor was modelled analytically, numerically and experimentally. The numerical study was carried out using ANSYS software. For the experimental study, a test rig was built to model the real rotor. During the experiments, the rotor speed range was varied from zero to 10000 rpm. Experimentally two crack depths of 0.2 and 0.4 of the shaft radius was modeled in addition to the uncracked shaft.

The rotor was manufactured with high accuracy and was then balanced to rotate at a higher speed. The vibration of the rotor was measured using an accelerometer connected to a digital oscilloscope. The critical speed was detected when the accelerometer reading reaches to its highest value.

In the analytical study a single and a double crack was modelled having different depths and directions. While in the numerical analysis, the shaft was modeled to have a single crack at different depths.

The results that was obtained from this study show good agreement between analytical, numerical and the experimental modelling. In the case of the proper shaft, the critical velocity was found, and the error ratio between experimental analysis and numerical analysis is (3.07%), and between analytical analysis and experimental analysis is (2.78%). It was conducted from rotor modelling that when the depth of the crack was increased, the critical speed was decreased whereas the response and the orbit size of the shaft was increased.

Contents

NO.	Subject	Page
CHAPTER ONE		
INTRODUCTION		
1.1.	Introduction	1
1.2.	The historical events of the turbine failure due to the crack	4
1.3.	Propagation of Crack	5
1.4.	The Work objectives	6
1.5.	Thesis layout	7
CHAPTER TWO		
LITERATURE Survey		
2.1.	Preview	9
2.2.	History of industrial machines and cracking incidents	10
2.3.	Crack Effect on the Dynamics of rotor	11
2.4.	Concluding Remarks	18
CHAPTER THREE		
THEORETICAL ANALYSIS		
3.1.	Introduction	20
3.2.	The Gas TURBINE ROTOR	21
3.3.	Assumptions for dynamic system	24
3.4.	The system coordinates and the type of support	25
3.5.	The natural frequency for uncrack rotor	26
3.6.	Equation of the motion of a cracked shaft	29
3.6.1.	Crack modelling	31
3.6.2.	Calculation of Direct Compliance	33
3.6.3.	The Response of shaft through Two of Journal Bearings	34
3.7.	The Flexibility for rotor have slant crack	38
3.8.	Analytical study of the rotor has two crack	40
3.9.	The Elliptical orbit path for rotor dynamic system	49
3.10.	Numerical Analysis	50
3.10.1.	The Procedure of Numerical Analysis for Rotor Dynamic System	51
3.10.2.	The flowchart of the constructed ANSYS code	54

CHAPTER FOUR EXPERIMENTAL WORK

4.1.	Introduction	57
4.2.	Test Rig Layout	57
4.3.	Rotor manufacturing	59
4.4.	Rotor Balancing	62
4.5.	Test rig power train	65
4.6.	The lubrication system	67
4.7.	Journal bearings	69
4.8.	Measuring devices	70
4.9.	Experiments procedure	73
4.10.	Cracks Creation	74

CHAPTER FIVE RESULTS AND DISCUSSION

5.1.	INTRODACION	75
5.2.	Analytic Result of single cracked shaft	76
5.2.1.	The dynamic parameters of the rotor at journal bearings	76
5.2.2.	the dimensionless compliance for a single crack in shaft	81
5.2.3.	Detecting of a crack by the shape of Orbit	82
5.2.4.	The response for cracked and uncracked shaft	84
5.3	The Results of numerical results of rotor have single crack	85
5.3.1.	The natural frequency of rotor	85
5.3.2.	The response for uncracked and cracked shaft	87
5.4.	The Experimental Results of rotor have single crack	91
5.4.1.	Free vibration test of uncracked rotor	91
5.4.2.	The response for uncracked and cracked shaft	93
5.5.	The results from analytic analysis for model have Two crack in shaft	101

CHAPTER SIX CONCLUSION AND RECOMMENDATION

6.1.	Conclusions	110
6.2.	The Recommendations	111
	References	113

LIST OF SYMBOLS

Symbols	Description	Units
[A]	Transformation matrix	---
A_1	Cross section area for crack No.1	mm^2
A_2	Cross section area for crack No.2	mm^2
a	Crack depth	mm
b	Crack base length	mm
C_l	Radial clearance	mm
c_{xx}	Horizontal damping coefficient of oil bearing	Ns/m
c_{yy}	Vertical damping coefficient of oil bearing	Ns/m
c_{xy}, c_{yx}	Cross damping coefficient of oil bearing	Ns/m
C_{44}	Compliance of cracked shaft in horizontal direction	m/N
\bar{C}_{44}	Dimensionless Compliance of cracked shaft in horizontal direction	---
C_{55}	Compliance of cracked shaft in vertical direction	m/N
\bar{C}_{55}	Dimensionless Compliance of cracked shaft in vertical direction	---
D	Rotor shaft diameter	mm
E	Modulus of elasticity	$\frac{N}{m^2}$
e	Radial difference between shaft outside diameter and disk inside diameter .	mm
F_t	Tangential force in bearing	N
F_r	Radial force in bearing	N
F_o	Resultant force in bearing	N
$f(t)$	Steering function	---
G_o	Flexibility of uncracked shaft	---
g	Gravity acceleration	$\frac{m}{s^2}$
G	Modulus of rigidity	$\frac{N}{m^2}$
g_ζ	Flexibility of two cracked rotor in perpendicular on crack base line direction	m/N
g_η	Flexibility of two cracked rotor in parallel to crack base line direction	m/N
$g_{\zeta\eta}, g_{\eta\zeta}$	Cross flexibility directions of two cracked rotor	m/N
I	Second moment of area of uncracked shaft	mm^4
I_{cent}	Second moment of area of cracked section about new centroid axis.	mm^4
K	Stiffness of uncracked shaft of rotor	N/m
Kl	Equivalent for overall Stiffness in horizontal direction depend on bearing stiffness.	N/m

$K2$	Equivalent for overall Stiffness in vertical direction depend on bearing stiffness.	N/m
$K12$	Equivalent for overall Stiffness in cross coupling direction depend on bearing stiffness.	N/m
$K21$	Equivalent for overall Stiffness in cross coupling direction depend on bearing stiffness.	N/m
k_{xx}	Horizontal stiffness of oil film bearing	N/m
k_{yy}	Vertical stiffness of oil film bearing	N/m
k_{xy}, k_{yx}	Cross stiffness of oil film bearing	N/m
KI	Stress intensity factor for first mode of crack	$\frac{N}{m^2}$
$KIII$	Stress intensity factor for third mode of crack	$\frac{N}{m^2}$
$K1^{(I)}$	Stress intensity factor of first crack for first mode	$\frac{N}{m^2}$
$K2^{(I)}$	Stress intensity factor of second crack for first mode	$\frac{N}{m^2}$
K_c	Stiffness lost because of crack	N/m
K_{cr}	Stiffness of cracked area of shaft	N/m
K_ζ	Stiffness of two cracked rotor in ζ direction	N/m
K_η	Stiffness of two cracked rotor in η direction	N/m
$K_{\zeta\eta}, K_{\eta\zeta}$	Stiffness of two cracked rotor in cross directions	N/m
L	Length of rotor	mm
L_1	Distance from disk to bearing No.1	mm
L_2	Distance from disk to left bearing No.2	mm
L_b	Length of journal bearing	mm
M	Mass of rotor	Kg
m	Mass of unbalance	Kg
m_{sh}	Mass of shaft of rotor	Kg
M_d	Mass of disk of rotor	Kg
m_u	Unbalance mass residual in disk of rotor	gm
r_f^*	Forward whirl response displacement	mm
r_b^*	backward whirl response displacement	mm
S	Sommerfeld Number	---
S_s	Modified Sommerfeld Number	---
$u_{\zeta 1}$	Displacement of crack No.1 in ζ direction	mm
$u_{\eta 1}$	Displacement of crack No.1 in η direction	mm
$u_{\zeta 2}$	Displacement of crack No.2 in ζ direction	mm
$u_{\eta 2}$	Displacement of crack No.2 in η direction	mm
ζ, η	Rotating coordinate with crack	---
θ_1	Slant angle of crack No.1	degree
θ_2	Slant angle of crack No.2	degree
μ	Lubricant oil absolute viscosity	Ns/m ²

ABBREVIATIONS LIST

Abbrev.	Description
FW	Forward Whirl
BW	Backward Whirl
NF	Natural Frequency
CCL	Crack Closer Line
FEM	Finite Element Method

CHAPTER ONE

Introduction

1.1. Introduction

Stations commonly used in the Arabian Gulf countries are gas stations because of their ease of installation and availability of fuel oil. The generation capacity of gas stations ranges from (100) megawatts to (5000) megawatts, where there are many manufacturing companies and many types of plants and the multiplicity depends on the need of the consumer.

After the year (2003) A.D. most of the stations in Iraq installed were manufactured by GE Energy. the types are Gas Turbine Power Plant - Frame (9) has a generating capacity of (125) MW, and Frame (5) has a generating capacity of (35) MW.

Modern mechanical machines have high speed and large sizes, and the rotor is the important part of rotary machinery, due to its widespread use in several fields such as power plants. This study was about the rotor of a gas turbine in AL_HILLA /2 power plant of the type (GT 9001E).

The rotor of turbine has two shafts; two turbine spacers; and the first, second, and third-stage wheels. The wheels are joined together by bolts to form one mass of high weight. The front wheel shaft is connected to the first stage of the turbine from the front, and the flange of the compressor. The second wheel shaft is connected to the third stage of the turbines and with load coupling from its end. The spacers are placed between the first and second stages, and between the second and third stages of the turbine.

Figure (1.1) shows the rotor parts of the gas turbine. It shows the points of the wheels' connection with each other, as well as their connection with the front and back shafts. This Figure is taken from document of the company.

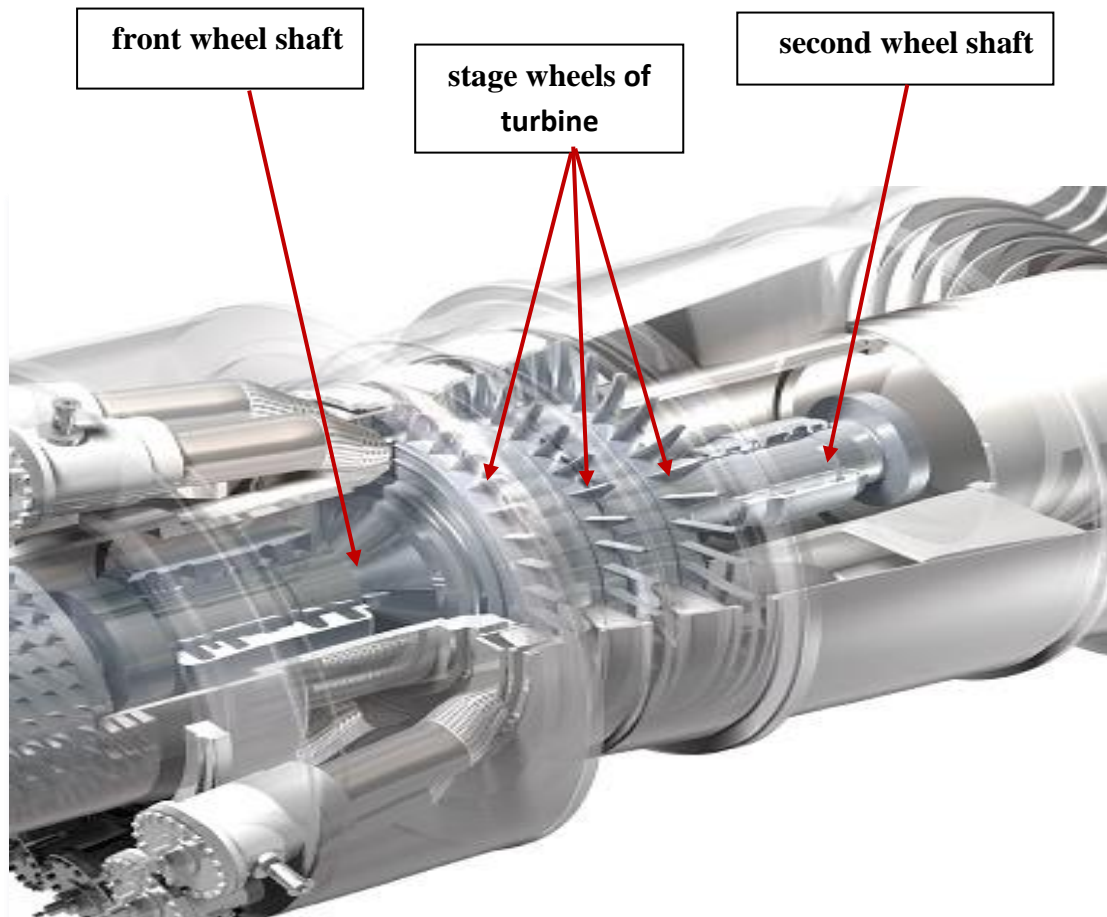


Figure (1.1) The rotor of gas turbine in HILLA power station.

Condition monitoring assesses the operational health of gas-turbine engines which helps in providing early warning of potential failure such that preventative maintenance action may be taken.

One of the most serious problems that occur to the rotor are the cracks because stresses which occurs on it. These stresses include: thermal stresses, bending stress and others. In most cases, these stresses are changing with the rotation.

Since it is the highest stress occurring at the surface, cracks often occur on the surface and begin to grow inside. At first the dimensions of the crack are small and do not affect the work of the rotor, but with time it grows and may reach on dangerous depths, the sudden failure may occur with it and the occurrence of serious damage.

Cracks is expected at the connection section between the shaft and stages wheels' block, because the greatest bending moment will happen in this connection.

It is very difficult to monitor the growth of the crack during rotor work, so researchers have found methods to reveal the relation of vibration to crack growth. Vibration parameters such as displacement and critical velocity were monitoring with a change in the dimensions of the crack. It was reached that once the crack grew, the vibration parameters would change. So it will be very easy to known the growth of the crack by known the rate of change of vibration parameters with work of rotor.

It is necessary to stop the machine when the depth of the crack reaches more than the radius of the rotor so as to expect the sudden failure to occur at any time, and this threaten the safety of workers and equipment.

After detecting the existence of crack by the operating engineer, it is very necessary to inform the maintenance department engineers to make the necessary repairs or replace the rotor in the extreme case.

1.2. The historical events of the turbine failure due to cracks:

The failure of the gas turbine is catastrophic due to equipment and personnel losses. At the Tanners Creek power station in the United States, a failure occurred in part of the Turbine steam turbine, and failure occurred as a result of a crack in the rotary shaft, this was in 1953[2].

In the station Pittsburg USA, at the speed test, there was damage in the Turbine rotor because it exceeded the speed limit, which was 3,920 round per minute, and that was in 1954.

in the Arizona station in the United States, there was damage in the rotor, its speed 3600 revolution per minute, in the workshop During the balancing operations, and this happened in 1954[3].

In the UK and specifically in Downingtown Castle. A shaft was detected and a crack was observed in it, where the remaining area is 25% of the total area of the cross-section.

In Nagasaki, Japan, during the low-pressure Turbine test, a failure occurred in Shaft and more than 50 people have died. Where there was a crack in the shaft before catastrophic failure [4].

A. Muszynska verified in (28) failure Shafts. It was found that (50%) of the shafts had a transverse crack [5]. Many researchers have discovered the cracks in many power plants in United States America and in Germany.

1.3. Propagation of Crack: -

The crack passes through three consecutive stages the first being the initiation of the crack, the crack consists either because of the metal arrangement or the defect in the manufacture or because of the knock or because of thermal stresses and there are many reasons.

The second stage is the crack growth stage where the crack grows with time due to variable loads applied to it. The crack grows until reaches to a critical state of a certain depth, this depth is (80%) from the radius of the shaft then move to third stage, [36].

The third stage is sudden fracture, and it is very dangerous and may lead to damage or disadvantage to the safety of workers and equipment.

So the equipment should be stopped immediately when the depth of the crack is (80%) of the radius of the shaft.

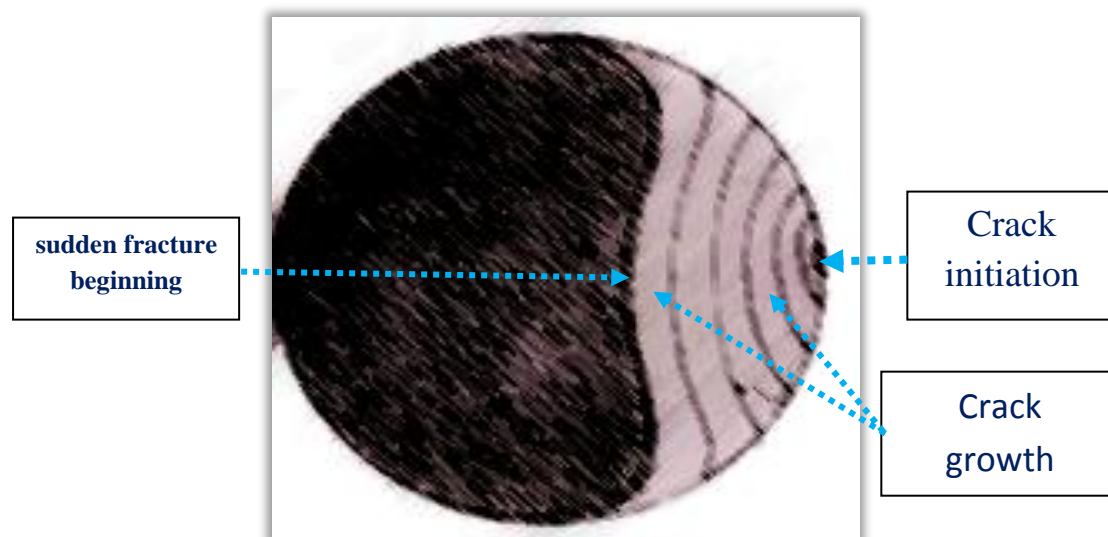


Figure (1.5) The Stages of crack development into failure stage.

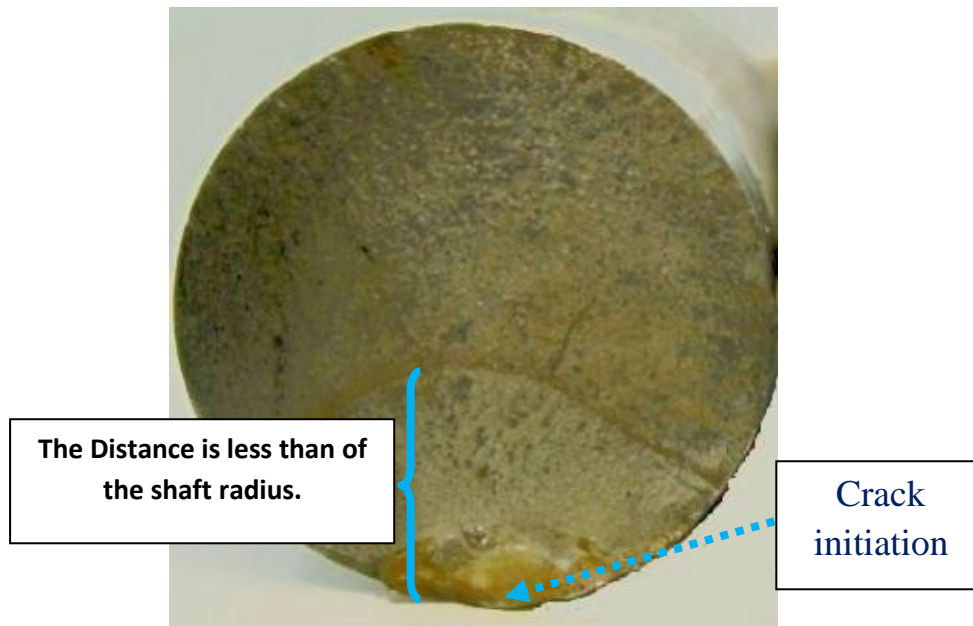


Figure (1.6) Shaft reached to the stage of sudden failure.

1.4. The Work objectives: -

- 1- study rotor containing the shaft and disc, and the disc is at an unequal distance from the bearings, with importance given for the damping and stiffness parameters of the lubrication film in the bearings by its calculation for all directions, horizontal and vertical and cross coupling, after that the amplitude response and critical velocity are calculated also.
- 2- Detecting the presence of the crack during the work of the rotor to avoid the Sudden frailer.
- 3- Studying of the behavior of vibration parameters with changing the dimensions of the crack during the work of the rotor.
- 4- Calculate vibration capacity in Experimental work at each velocity, and through the greatest response determines the critical velocity and in both cases (cracking and non-cracking shaft). so we can get the natural

frequencies of the two states, as well as knowing the depth of the crack by the orbital shapes.

5- Comparing the vibration parameters of an uncrack shaft with a cracked shaft to determine the crack Specifications.

6- Studying of the behavior of the vibration parameters by the presence of more than one of crack, and the investigate of the effect of the crack angle on the vibration parameters also.

7- Studying the effect of the crack on the path of the Orbit at several depths.

8. Investigation on the data in the future by the condition monitoring system equipped to the gas turbine plant in Al- Hilla Power Station /2, To ensure the integrity of the shaft.

1.5. Thesis layout: -

The thesis consists of six chapters which are as following: -

Chapter One: the first chapter contains a definition of gas turbine and the problems which can occur in the rotor, then the stages of the crack growth during the work of the rotor.

Chapter Two: this chapter consists of the introduction about rotor types which were previously designed, and It was mentioned the problems and historical events which occurred in the past, also taken conclusions of the research's which deals the problem of crack in the rotor and its effect on the dynamic system.

Chapter Three: This chapter consists of modeling the real rotor of the turbine to be easy to manufacture or test in other analyses. As well as finding analytical calculations of the vibration parameters when cases are a single and double crack.

Chapter Four: This chapter consists of the introduction the definitions of the components of the test rig, as well as include the operations of the balancing. This chapter also includes the method of measuring vibration parameters by the Oscilloscope.

Chapter Five: In this chapter the results are presented as values in curves or tables, and discuss the behavior of these results which obtained from the analytical, numerical and experimental studies. As well as comparing results with previous research.

Chapter Six: In this chapter several conclusions were reached, which include the effect of the crack on the rotor system, as well as the effect of the crack at different depths and at different angles on the size of the orbit, and its effect on the vibration parameters.

CHAPTER TWO

Literature Survey

2.1. Preview: -

The analysis of cracked rotors is very important for the safety of the rotary shaft. The design of the rotor was simple by the design of H.H. Jeffcott in 1919. It was consisting of a massless shaft and a disc in the middle, and on both sides, there are the hard bearings, [30].

Jeffcott rotor shows the conditions at critical velocity, where the vibration amplitude becomes high, but it cannot explain the rotational effects. This design can include rigid rotor or rotor with uniform parameters and on both sides. In this type the equivalent mass is equal to the mass of part from the shaft and mass of the rotor. The equivalent stiffness of the rotor is equal to the stiffness of the bearings and the stiffness of bending of the shaft [1].

since 1954, research and papers submitted by many researchers with regard to the cracks in shafts are abundant. There are few experimental results for cracked shafts, and few of these results pertain to real rotors, and this gives great importance to any model for the real cracked shafts.

There are many of papers looking at topics related to the presence of a crack in the shafts, such as parameters of the cracked shaft or change the stiffness for material because of fracture mechanics.

2.2. History of industrial machines and cracking incidents: -

The rotary shafts work in continuously with high weights and periodic stresses for long periods, so the crack will have generated as a result of fatigue. In order to avoid sudden accidents in the rotors, it is necessary to develop diagnostic systems for the operational machines, so it is useful to have monitoring system of the equipment, and this will reveal cracks in the early stages of growth. Vibration is an important part to know the cracks in the shafts. The deflection in the cracking shaft generates a breathing crack, which is in the case of closing and opening constantly.

The beginning of the knowledge of the accidents caused by the failure of the rotor of Turbine due to crack in 1950, these incidents were studied numerically and analytically in 1970.

In 1990, the crack was detected at a nuclear power plant in Darlington, and the crack area was more than 25% of the total cross-sectional area. [6] R.A. Gasch, [7] B.E. Oka-Ave, proved that the breathing cracks caused the nonlinear system, and It was solved the equation of the motion, in which the effect of the crack, by the analog computer.

2.3. Crack Effect on the Dynamics of rotor: -

Many of the research deals the physical condition of the crack and its effects on the system. Some of the researchers used Finite Element Approach, and others used analytic solution of the system, and some of them built a test rig to the simulation of the real system for easy data acquisition in the presence of crack and without it.

H.D. Nelson and I.M. Mcvaugh [9], deals the dynamic rotor system, and It was used the Finite Elements Method. It was studied gyroscopic moments, rotary inertia and axial load.

It has been provided an equation of motion in the rotational state and static state. In the Dynamic rotor system, the Finite Elements Method was used to create a thoroughness for the mode. It was providing that the Finite Elements Method can easily be used for several situations in the rotor dynamic system, where It was found the critical velocities of the rotor model, as well as, it was found the response to both stability and unbalance force. It was concluded that the rotor element could generally represent the effect of axial momentum, shear deformation for several states in the shaft. It was provided a numerical solution to the rotor bearing system by Finite Elements Method.

Stefanos A. Paipetis, Thomas G. Chondros [10], introduced a general stiffness matrix for cracked structural members to model the respective dynamic system. It was mentioned, the defects in a shaft may cause also changes in mass distribution and damping properties. It was have reached that change of damping of a shaft in case of crack initiation and growth is important for the estimation of resonance.

E.T. John Penny and I. Michael Friswell [11], studied a cracking shaft to model a rotary shaft. It was mentioned in their research that the close and open cracks produced by the weight of the shaft itself, and this generates excitation during circulation. It was searched and documented the appropriate ways through which the crack was detected, and its location in its initial stages. It was concluded that adding any force would increase the speed of crack growth.

M.A. Mohiuddin and Y.A. Khulief [12], developed a numerical, analytical model and computational scheme, which deals with the analysis of responsiveness to a rotary system, it was used the Finite Element Formulation. It was received the response results when applied the direct load and torsion load. It was reached a dynamic arithmetic scheme for the respond at the presence of a crack in shaft.

A.K. Darpe, K. Gupta, A. Chawla [13], studied two cracks in shaft, and was analyzed the nonlinear behavior of the stiffness. The model was a Jeffcott type with one depth of the crack. It was found that the least value of the stiffness when the angle of rotation is (180) degree, this is because the crack is fully open.

It was divided the line that represents the base of the crack to fifty points, the line is called the Crack Closure Line (CCL), it was Document location of (CCL) of two modes (closing and opening modes) and found the stress intensity factor. The asymmetrical rotor produces a higher harmonic than the symmetrical rotor.

Marc et.al. [14], searching for the effect of the crack (open type) on the rotary shaft. It was studied the effect of rotational speed, crack depth and crack position on the natural frequency. It was used The harmonic balance method.

It was deduced the great effecting to the depth of crack on the natural frequency, and it is larger when the rotation speed (80-120) % of the critical velocity.

J. Darryl Chauvin [15], produced an experimental study on the non-stability of the rotor, the study included the effect of lubrication on the bearings (journal type), its Mission carries the rotor.

The equation of the motion was solved, it is including the parameters of stiffness and dampness in the horizontal and vertical and cross coupling directions, knowing that the type of rotor is a Jeffcott. It was found that the response for both bearings are equally and in all directions due to symmetry.

the natural frequency was found of the system, as well as line instability threshold. If the speed is less than the speed of the threshold, it enters the stability zone. If the speed is higher than the threshold speed, it enters the instability zone.

It was produced the equation of motion, which includes the presence of a crack in the rotor shaft and derived the equation of the 6th order, and from which we find Eigenvalues for critical speed. The Rig is made to get the response by monitoring the system, and to get the largest data, and then analyzes the waves to see the effect of the crack on the resulting wave.

J.J. Sinou [16], studied the parameters of crack (depth and location), and its effects on the rotor at a speed of different. Where it was concluded that the stability decreases significantly with increasing crack depth. The uncertainty was increases with increasing crack depth, and the location of the disc and the value of the stiffness of the bearings effect on the vibration parameters.

P. TODORVIČ et al [18], studied the effect of cracks on the stability of the mechanical system. It was discussed the response of the cracked shafts at the run-up stage, as well as studied the reason for the decrease in natural frequency with the existence of the crack.

It was found that increasing the depth of the crack reduces the critical speed during rotation, i.e., the resonance frequency decreases during rotation with increased crack depth. There is an explanation for a very important point, namely, that resonance frequency is not always equal to critical speed.

The change of stiffness was studied with the change of rotation of the shaft. A rig was constructed from a rotor and a disc, where it was monitored to determine critical velocity and vibration parameters.

José M. Machorro-López, et al [19], studied the effect of the crack on the shaft at an electric power plant. It was shown that the crack represents only 2% of the causes of the vibration of the rotor shaft compared with misalignment and mass imbalance. It was used the finite element method in the numerical study. It was revealed that the change in natural frequency was not enough to detect the crack in the mid-span rotor, Experimental analyzes and Numerical analyzes should be used.

J.J. Sinou [20], investigated the transient response to a rotary shaft containing the open crack, in order to determine the expected response when the crack exists. Where it was studied the vibration parameters of the shaft with and without crack. the vibration parameters were found in One-third of the critical speed and it is one of the important indicators for an open crack.

A.AL Shudeifat and A. Butcher [8], found a new equation for crack type breathing transverse, Harmonic analysis was for critical velocity and

subcritical velocity. The study was divided into two branches: the first is experimental and the second is theoretical.

It was produced a good model that simulated breathing crack and concluded that variable time with inertia torque is a factor its follow the stiffness matrix. It was used the finite element method and solved it by the harmonic equilibrium method. the matrix of stiffness was found with the change of time. The results compared the critical and sub-critical velocities with reliable results.

Z.K. Peng et al [21], have investigated a dynamic rotary system that includes a cracked rotor. It was used the finite element method and the harmonic equilibrium method. The method of harmonic equilibrium is a method of calculating the response in a stable state of nonlinear derivation equations. It was explained The variance between the transmission matrix of the super harmonic components was illustrated with the transponder of the first-mode components, the results were compared with numerical methods and the results were very close.

The results gave a clear vision for crack detection by critical speed data and displacement.

C.D. Untaroiu et.al [23], investigated a system consisting of a disk and shaft, and It was made two types of crack (each type in a separate experiment), the first is an open crack and the second is a breathing crack. It was concluded that the instability increases with existing crack, whether it is the open or breathing type. It is possible to reduce the instability by adding an external dampener.

B.S.N. Murthy et al [24], studied a rotary system of Jeffcott type containing crack from breathing type. It was investigated the effect of the crack on the rotor response, and at the end of the experiment, It was caused damage to the shaft. It was studied the effect of crack depth, eccentricity mass and damping forces on shaft response. It was solved the equation of a fractional order derivative of damping by Runge-Kutta method. The damping parameters were found by using the rotor orbit, the phase diagram, and frequency spectrum. It was explained that the nonlinear vibration of the shaft is affected by fractional order damping.

R. Ramezani et al [25], investigated a dynamic rotor system of the Jeffcott type, one of the rotor components was cracked shaft, and the crack is the slanted type, and at an angle with the vertical. It was studied vibration due to the effect of the oblique crack using the mechanics of fracture theory. the relationship between crack angle with longitudinal displacement, crack angle with the angle of torsional displacement, crack angle with transverse displacement was studied. It was investigated the effect of the crack angle on the flexibility matrix. It was proved that the crack transverse parameters were less than the fully open crack parameters.

M. Serier et al [26], have investigated a dynamic rotary system, it has a breathing crack. A test rig was built for vibration analysis, and during the experiment shows the adoption of the crack on rotor parameters. It was also showed that the length of the crack, the speed of rotation and the diameter of the shafts directly effect on the growth of crack. It was concluded that the finite element method can be used in the regression analysis

M.J. Patil and Ali Vaziri [27], studied the cracking rotor to analyze the resulting vibration. It was built a rig for monitoring to the vibration

parameters. It was concluded that the crack affected on the flexibility, the flexibility is increased with an increase in the depth of the crack.

N. Tenali and S. Kadivendi [28], studied the vibration analysis on a rotary shaft in a steam turbine using finite element method in numerical analytical. the Steam turbines are complex systems and contain a number of discs. It was searched orthogonal vibration on the bearing and calculated the transient response to the bearing. It was confirmed the results by the ANSYS program and the TMS-050 program.

R. Peretz¹, L. Rogel², J. Bortman³, and R. Klein⁴[29], studied stress due to the crack in high-speed equipment. It was found that the continuous monitoring of vibration and the orbital paths was used to detect the crack. Two types of flaws were tested: a straight slot, and a fatigue crack. It was observed during the acceleration and deceleration of the rotor shaft, where the crack open, the Vibration amplitude will decrease in critical speed.

J.F. Al Draji [30], studied experimentally, numerically and analytically the rotary shaft with cracks and without cracks. An asymmetric rotor will use, which includes a disc between unequal two distances. Analytical and numerical techniques have been done to drive an equation for finding the stiffness of two cracked shaft in vertical, horizontal and cross directions with making mathematical model representation for the rotor and compared the results of analytical and numerical, it found in good agreement. The response displacement increases and the critical speed decreases with increasing the crack depths.

Nizar Ferjaoui, Sami Naimi, Mnaour Chouchane [31], investigated the effect of the transverse crack of a rotary shaft carried by hydrodynamic journal bearings. It was used the vibration monitoring method and the orbits of the

turbine to detect the presence of crack. It was assumed short bearing for model analysis and found that the crack depth will be an influence on the movement of Centre Journal and decreases stability limit.

Deepak P Hujare¹, Nitesh R Girase, and Madhuri G Karnik[32], studied the relationship between the natural frequencies and crack parameters such as the depth, Width, and location. The analysis was done for the Single Crack and is evaluated, and found The crack will reduce the natural frequencies and stiffness.

2.4. Concluding Remarks: -

In the previous research, the focus was observed on vibration parameters as an indicator of the presence of cracks in the rotor. The cracks were studied in symmetric and unsymmetrical models. Numerical, experimental and analytical analyses of rotor have been performed, and the focus was on the response of the rotor as a displacement to find the critical speed.

There is a research study of rotor has more than one of crack, and investigated on the vibration parameters with change of crack depths.

Many research has studying the effect of fatigue with time on the cracks of the rotor, and the extent of change the vibration parameters. As the rotor is exposed to many loads that affect it because of continuous rotating which generates periodic stresses.

In this study, the effect of cracks on the rotor of a gas turbine of the type (GT 9001E) was studied by designing and manufacturing model. The model was analyzed analytically, numerically and experimentally. The experimental

study of the effect of the crack on vibration was based on the response. The response was form of acceleration to determine the critical velocity.

CHAPTER THREE

Theoretical Analysis

3. Theoretical Analysis

3.1 Introduction: -

Analytical study of real turbine is complicated, because of the complex geometric shape and its large size. So it was designed a system simulates the real turbine (the shaft and disk system), through which it was predicted the real behavior of the machine [33].

In this work, the study of changing in stiffness, critical speed and response will be addressed with and without the crack. Critical speed is very important, where it is found in two ways, first by solving the equation of motion of the system, and the second by solving the equation obtained from [34]. The study will address the relationship between stiffness and damping with the speed of rotation.

At first, it was calculated the response and the critical speed of shaft have a single transverse crack. Then it was calculated the response and the critical speed of the two cracks, the first transverse crack and the second slant crack, where the inclination in varied angle. It was focus on two important cases; the detection of the crack will be through the form of the wave represented by the response and the critical speed, and the knowledge of the depth of the crack will be by responding to the crack zone.

3.2 The Gas Turbine Rotor: -

The rotor of the turbine consists of two turbine spacers; two wheel shafts; the first, second, and third-stage turbine wheels with buckets. The forward wheel shaft contacting with the first-stage turbine wheel and connected with the compressor flange from the other side. The backward wheel shaft connecting with the third-stage turbine wheel and connected with the load coupling from the other side. The journal for the n° 1 bearing is a part of the wheel shaft. The rotor is unsymmetrical as shown from dimensions in **Figure (3.1)**, and this figure from documents of Manufactured company.

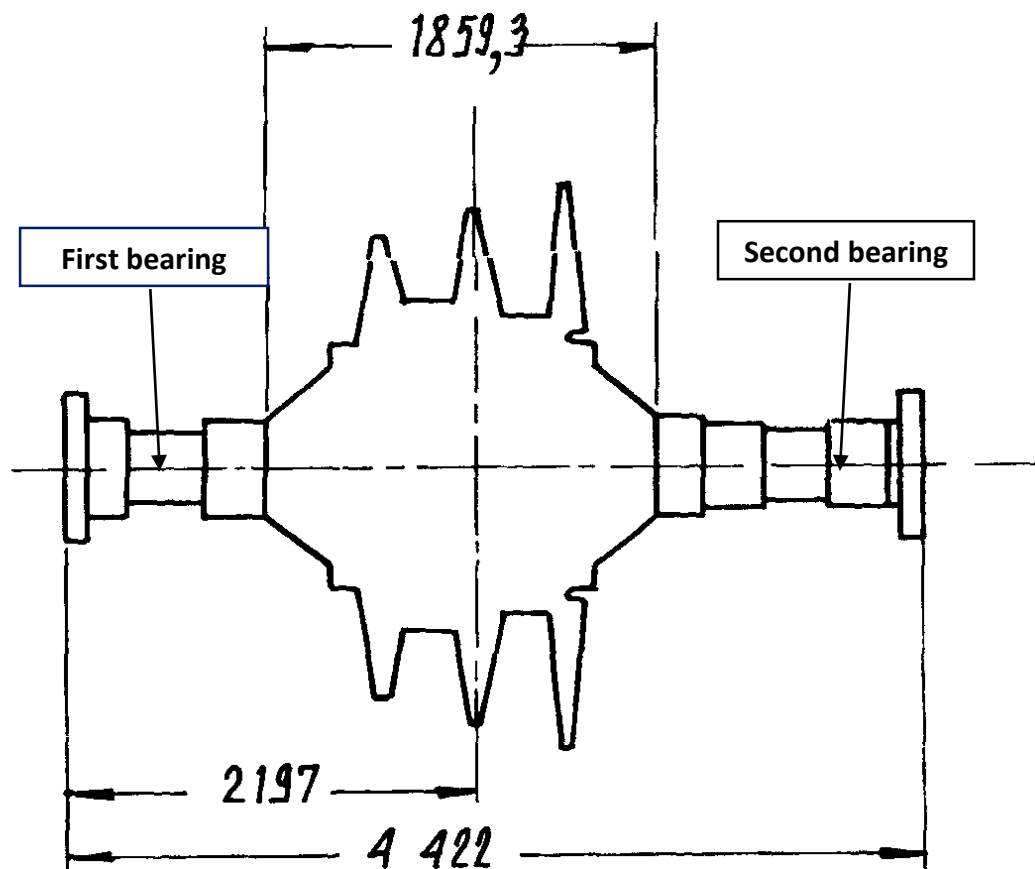


Figure (3.1) the dimensions for the Turbine Rotor by millimeters.

The total mass of the turbine is (**21455 Kg**), and its dimensions are shown in **Figure (3.1)** in millimeter. The simulation will be for the part between the first bearing and the second bearing, this weight will be simulated by shaft and disc (rotor–bearing system) as described in the research references. The representation for the system of the shaft and the disk depends on the **equation (3.1)** and taken from [33].

$$m = \frac{17}{35} \times m_s + m_d \quad 3.1$$

When

m = total mass of turbine.

m_s = mass of shaft.

m_d = mass of disk.

After using simple calculations, it was produced the dimensions and weight of the shaft.

m_s = 3009.3 kg.

d_s = 380 mm.

l_s = 3342.3 mm.

It will be used the values of total mass for turbine and mass of the shaft on **equation (3.1)** to find the disk mass. After finding the disk mass, it was found its dimensions after equalizing the length of the disk to the original length of the turbine, in order to preserve the

location of the possible crack of the turbine (the location of the crack is very close to the turbine rotor flange).

$$m_d = 19993.3 \text{ kg.}$$

$$d_d = 1374.23 \text{ mm.}$$

$$l_d = 1859.3 \text{ mm.}$$

The Large dimensions are one of the obstacles to the experimental, numerical and analytical comparison, so it will be reduced the dimensions to (1/10) from the real dimension, and the Shaft Modelling are shown in **Figure (3.2)**.

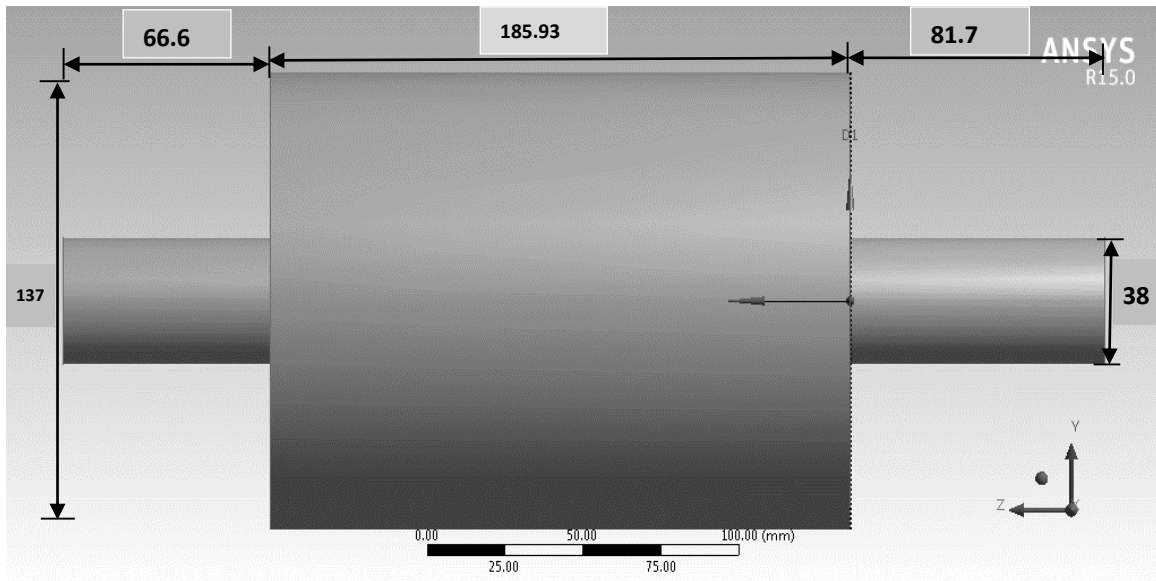


Figure (3.2) the drawing of the rotor Modelling.

3.3. Assumptions for dynamic system: -

The following hypotheses will show the analytical method in a simplified manner and it can be treated with parameters in easily, [33], [1].

- 1 - Suppose that the conveyor is of the short type i.e. ($\frac{L_b}{D} < 1$) where (L_b) is the bearing length and (D) is the diameter of bearing.
- 2 - Reynold equation was applied after it was assumed that the flow was temporary.
- 3 - The Lubricating oil pressure at both edges of the bearing is zero.
- 4 - The Operating conditions are steady state.

From Reynold 's equation, it found that the angle (θ) and the pressure (p) depend on h , r , Ω , and μ , as shown in **equation (3.2)**.

Where (r) is the radius between the center of the shaft and any point for oil film, is (h) is the film thickness, (Ω) is shaft speed, (μ) is the viscosity of the oil, [33].

$$\frac{1}{r^2} * \frac{\partial}{\partial \theta} \left[h^3 * \frac{\partial p}{\partial \theta} \right] + h^3 * \frac{\partial^2 p}{\partial x^2} = 6\mu\Omega \frac{\partial h}{\partial \theta} + 12\mu \frac{\partial h}{\partial t} \quad 3.2$$

Where (h) changes by the change of (θ) as in **equation (3.3)**.

$$h = C_l(1 + \epsilon \cos\theta) \text{ , when } \epsilon = \frac{e}{C_l} \quad 3.3$$

Where (C_l) is radial clearance ,and (ϵ)is eccentricity ratio.

3.4. The system coordinates and the type of support: -

The supports of the rotor shaft system will be represented by Spring and damper in each direction, for X-direction, y-direction, and The Direction Which causes the coupling forces, as shown in **Figure (3.3)**. This is a result of lubricating fluid characteristics.

There are two types of coordinates in the system; the first at the sides when the bushes of bearings; and the second at the middle of the disk.

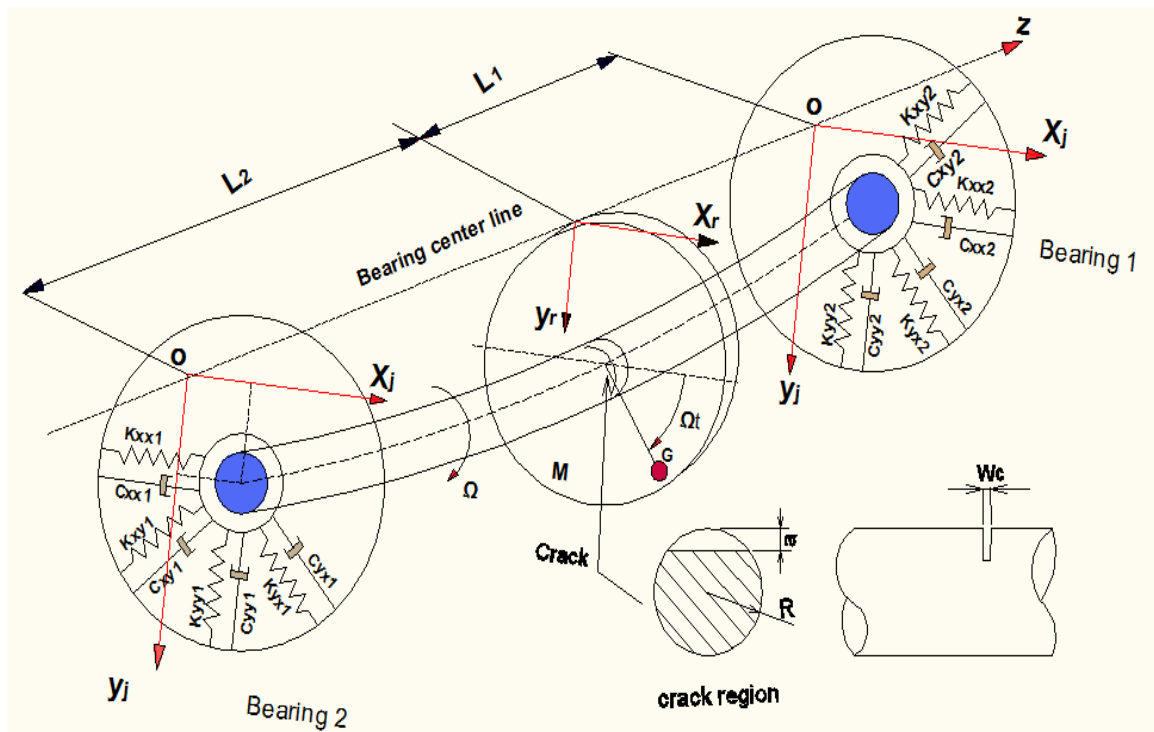


Figure (3.3) the suspension system of the rotor, [30].

3.5. The natural frequency for uncracked rotor: -

Normal frequency is the frequency at which the body oscillates without external force. When the dynamic system approaches from it, the body oscillates at highest response.

Eccentricity is inherent in the journal bearing, so during movement, a dynamic force is generated.

A displacement will be generated towards the (X-axis) and the direction (Y-axis), and this displacement will be relative to the coordinates (X and Y axis) at the bearing holder. The relationship between the load and deformation is nonlinear; and to simplify the dynamic analysis, this relationship can be considered linear if a displacement is too small.

The formed forces are two types, the first is diagonal (F_r), the second is tangential (F_t), They can be found by the following equations, [33].

$$F_r = -\frac{D \Omega \mu L_b^3 \epsilon^2}{2C_l^2 (1 - \epsilon^2)^2} \quad \text{and} \quad F_t = -\frac{\pi D \Omega \mu L_b^3 \epsilon^2}{8C_l^2 (1 - \epsilon^2)^{3/2}} \quad 3.4$$

Then we find the load on the bearing by finding the resultant of the forces.

$$F_o = \sqrt{F_r^2 + F_t^2} = \frac{\pi D \Omega \mu L_b^3 \epsilon}{8C_l^2 (1 - \epsilon^2)^2} \left(\left(\frac{16}{\pi^2} - 1 \right) \epsilon^2 + 1 \right)^{1/2} \quad 3.5$$

After finding the load on the bearing, it is possible to find a value of (Sommerfeld number) by equation (3.6).

$$S_s = \frac{D \Omega \mu L_b^3}{8 F_o C_l^2} \quad 3.6$$

Then it will be used a value of **Sommerfeld number** on the **equation (3.7)** to find *eccentricity ratio*(ϵ),[33].

$$\epsilon^8 - 4\epsilon^6 + \left(6 - S_s^2(16 - \pi^2)\right)\epsilon^4 - (4 + \pi^2 S_s^2)\epsilon^2 + 1 = 0 \quad 3.7$$

Where the value of (ϵ) is found by Newton Raphson Method, using MATLAB program (Appendix-A).

After assess the bearing is short, the damping matrix and the stiffness matrix shall be (2 x 2), provided that the displacement is small, to be the system is linear

$$[k] = \frac{Fo}{C} \begin{bmatrix} a_{xx} & a_{xy} \\ a_{yx} & a_{yy} \end{bmatrix} = \begin{bmatrix} k_{xx} & k_{xy} \\ k_{yx} & k_{yy} \end{bmatrix} \quad 3.8$$

$$[c] = Fo/(C_l \times \Omega) \begin{bmatrix} b_{xx} & b_{xy} \\ b_{yx} & b_{yy} \end{bmatrix} = \begin{bmatrix} c_{xx} & c_{xy} \\ c_{yx} & c_{yy} \end{bmatrix} \quad 3.9$$

Where a_{xx} , b_{xx} , a_{xy} , b_{xy} , a_{yx} , b_{yx} , b_{yy} and a_{yy} values will take from **(Appendix-B)** from **B-1** to **B-8**.

The relationship between eccentricity with stiffness and damping at change in spin speed was represented by the MATLAB program as seen in **(Appendix-A)**.

After that it will be found the parameters of the shaft bearings by the following equations, [35].

$$K = \frac{3EI(L_1^3 + L_2^3)}{L_1^3 \times L_2^3} \quad 3.10$$

$$K1 = \frac{K[(k_{yy1}+k_{yy2})(k_{xx1}+k_{xx2})+K]-((k_{yx1}+k_{yx2})(k_{xy1}+k_{xy2}))]}{((k_{yy1}+k_{yy2})+K)((k_{xx1}+k_{xx2})+K)-((k_{yx1}+k_{yx2})(k_{xy1}+k_{xy2}))} \quad 3.11$$

$$K2 = \frac{K[(k_{xx1}+k_{xx2})(k_{yy1}+k_{yy2})+K]-((k_{yx1}+k_{yx2})(k_{xy1}+k_{xy2}))]}{((k_{yy1}+k_{yy2})+K)((k_{xx1}+k_{xx2})+K)-((k_{yx1}+k_{yx2})(k_{xy1}+k_{xy2}))} \quad 3.12$$

$$K12 = \frac{(k_{yx1} + k_{yx2}) K^2}{((k_{yy1} + k_{yy2}) + K)((k_{xx1} + k_{xx2}) + K) - ((k_{yx1} + k_{yx2})(k_{xy1} + k_{xy2}))} \quad 3.13$$

$$K21 = \frac{(k_{xy1} + k_{xy2}) K^2}{((k_{yy1} + k_{yy2}) + K)((k_{xx1} + k_{xx2}) + K) - ((k_{yx1} + k_{yx2})(k_{xy1} + k_{xy2}))} \quad 3.14$$

Then it is replaced the parameter values in the following equations to find the natural frequency, [36].

$$\Gamma_1^2 = \frac{K1}{M} ; \Gamma_2^2 = \frac{K2}{M} ; \mu_1 = \frac{K12}{K1} ; \mu_2 = \frac{K21}{K2} \quad 3.15$$

$$\omega_n^2 = \frac{1}{2}(\Gamma_1^2 + \Gamma_2^2) \pm \sqrt{(\Gamma_1^2 - \Gamma_2^2)\mu_1\mu_2\Gamma_1^2\Gamma_2^2} \quad 3.16$$

After using the **MATLAB** program, it was found that the fundamental natural frequency is **(8125)** RPM and the response at this frequency is **(0.0295)** mm. When using the **ANSYS** program, it was found that the

fundamental natural frequency is (8150) RPM and the response of (0.0225) mm, and when compared these results, we find it very good.

3.6. Equation of the motion of a cracked shaft: -

The coordinates in the rotor are two, the first is fixed coordinates (X and Y) and the second is the moving coordinates (ζ and η), as shown in **Figure(3.4)**.

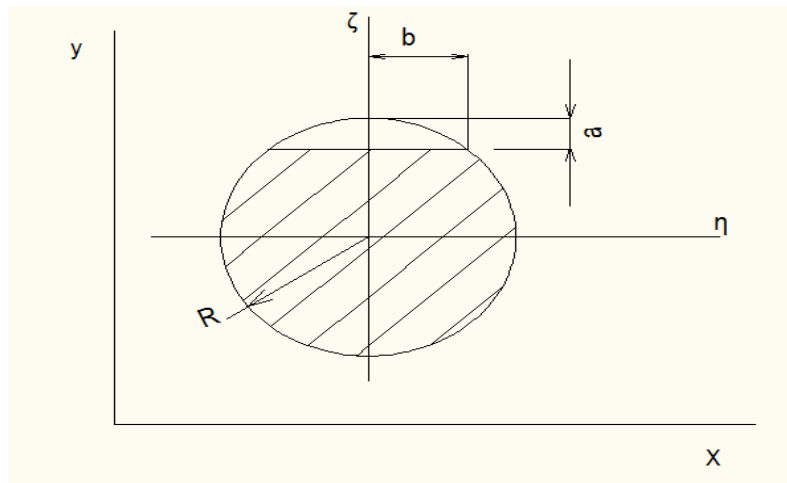


Figure (3.4) fixed and moving coordinates.

So it would be two types of stiffness depending on the coordinates mentioned above. The rigidity in the horizontal direction will be less than the rigidity in the vertical direction, when the crack is in the open state.

After that, the decrease in stiffness will be calculated in both directions (ζ and η), and then transfer the stiffness matrix by the transformation matrix to the fixed coordinates (X and Y), [11].

$$[K_{cr}] = [K] - [K_c(\theta, t)] \quad 3.17$$

Where

$[K]$ is stiffness matrix for uncrack rotor.

$[K_c(\theta, t)]$ is the decrease in stiffness matrix Which happened from the crack effect.

$[K_{cr}]$ is stiffness matrix for crack rotor.

$$[A] = \begin{bmatrix} \cos(\Omega t) & \sin(\Omega t) \\ -\sin(\Omega t) & \cos(\Omega t) \end{bmatrix} \quad 3.18$$

Where $[A]$ is the transformation matrix.

So the stiffness matrix (to crack shaft) will be as follows: -

$$[K_{cr}] = [A]^T [K] [A] - [A]^T [K_c(\theta)] [A] = [K] - [K_c(\theta, t)] \quad 3.19$$

The deformation has two parts, the first is static and the second is dynamic.

$$\mathbf{y} = \mathbf{y}_{st} + \mathbf{y}_{dy} \quad 3.20$$

If (\mathbf{y}_{st}) is a constant part, then $(\dot{\mathbf{y}}_{st})$ equals zero.

$$\dot{\mathbf{y}} = \dot{\mathbf{y}}_{dy} \ \& \ \ddot{\mathbf{y}} = \ddot{\mathbf{y}}_{dy} \quad 3.21$$

$$[M]\{\ddot{\mathbf{y}}_{dy}\} + [[D] + [G]]\{\dot{\mathbf{y}}_{dy}\} + [[K] - [K_{cr}(\theta, t)]]\{\mathbf{y}_{st} + \mathbf{y}_{dy}\} = \mathbf{Q}_u + \mathbf{W} \quad 3.22$$

Where

(W) is rotor weight and (Q_u) is the unbalance force.

If

$$[K]\{y_{st}\} = W \quad 3.23$$

So the equation of the motion will be as follows: -

$$[M]\{\ddot{y}_{dy}\} + [[D] + [G]]\{\dot{y}_{dy}\} + [[K] - [K_c(t)]]\{y_{dy}\} = Qu \quad 3.24$$

3.6.1. Crack modelling: -

The crack in the shaft have many kinds, but the most common is the transverse crack. Multiple vibrations such as (torsional, longitudinal, and transversal) vibrations will be generated, but for ease we will take transversal vibrations.

The theory of beam bending is not active with crack, because the crack is weakening the stiffness of beam (EI), [30].

It is possible to consider the elements of flexibilities in each side are six degrees of freedom, But for ease will ignore all elements except vertical element(\bar{C}_{55}) and the element of cross flexible(\bar{C}_{44}).

If ($a/R < 0.5$) then The effect of (\bar{C}_{44}) is very small, so it will only take (\bar{C}_{55}) into consideration. If ($a/R > 0.5$) then it will take (\bar{C}_{44}) and (\bar{C}_{55}) into consideration.

to find deflection to region near from disk [1]: -

$$\begin{bmatrix} u_\zeta \\ u_\eta \end{bmatrix} = \begin{bmatrix} G_o + \Delta g_\zeta & 0 \\ 0 & G_o + \Delta g_\eta \end{bmatrix} \begin{bmatrix} F_\zeta \\ F_\eta \end{bmatrix} \quad 3.25$$

G_o is the flexibility for uncrack rotor.

Where $(\Delta g_\zeta, \Delta g_\eta)$ is the increase in flexibility due to the existing crack. If the crack is in a closed position, the $(\Delta g_\zeta, \Delta g_\eta)$ is zero.

$$\Delta g_\zeta = \bar{C}_{55} \frac{L^2}{16 * ER^3} \quad 3.26$$

Because of the region of tension and compression in the shaft, we found a steering equation ($f(t)$).

$f(t) = 0$, at compression region.

$f(t) = 1$, at tension region.

So the deflection equation is [1]: -

$$\begin{bmatrix} u_\zeta \\ u_\eta \end{bmatrix} = \left[\begin{bmatrix} G_o & 0 \\ 0 & G_o \end{bmatrix} + f(t) \begin{bmatrix} \Delta g_\zeta & 0 \\ 0 & \Delta g_\eta \end{bmatrix} \right] \begin{bmatrix} F_\zeta \\ F_\eta \end{bmatrix} \quad 3.27$$

$$f(t) = \frac{1}{2} (1 - \cos \Omega t) \quad 3.28$$

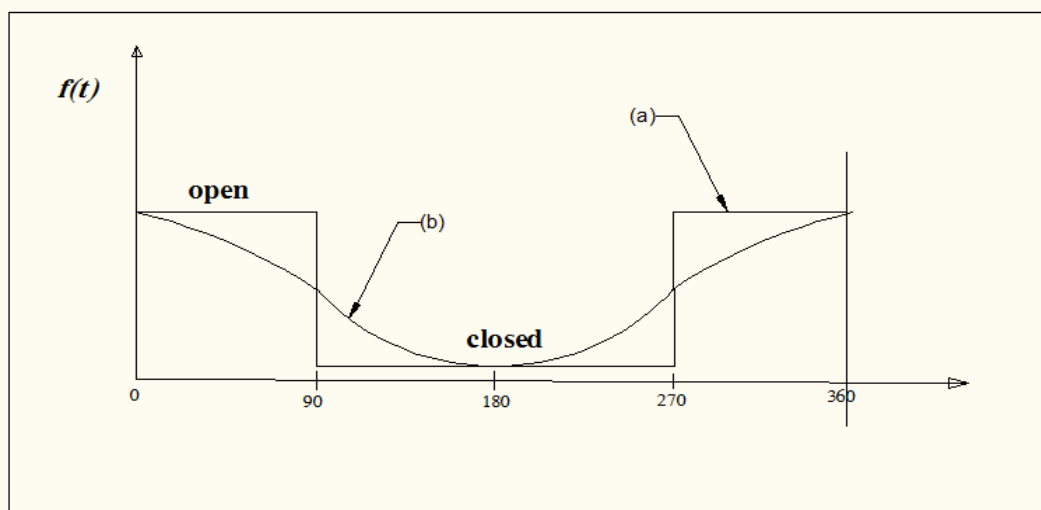


Figure (3.5) The steering function behaves with crack opening [1].

3.6.2. Calculation of Direct Compliance: -

At the vertical plane, an additional cross-sectional shift will occur because of the crack, [1].

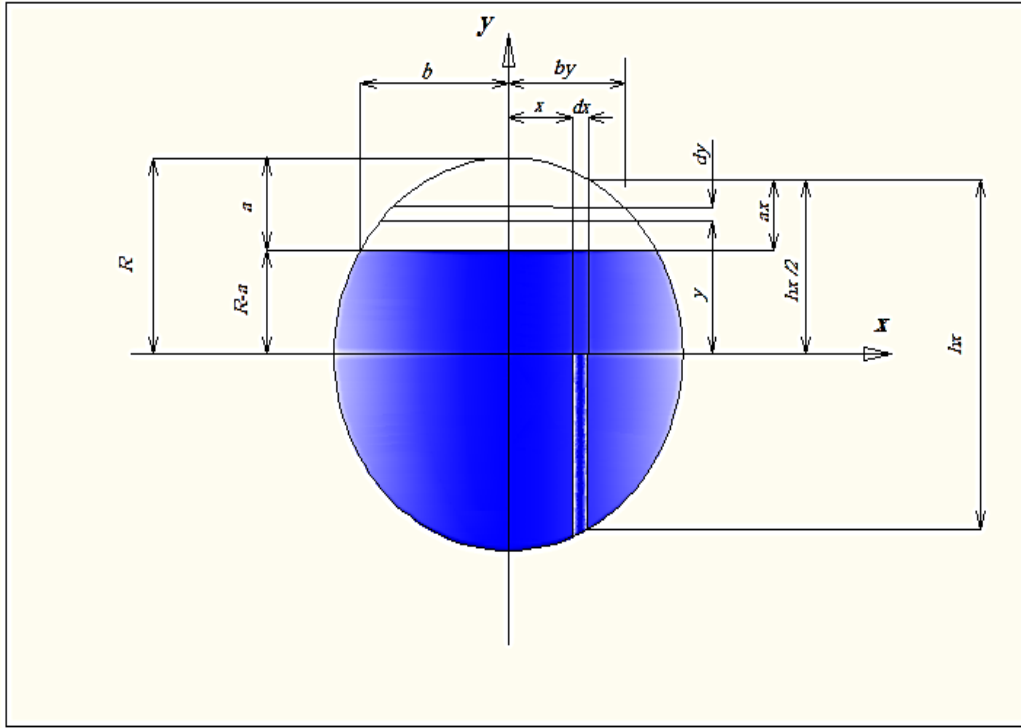


Figure (3.6) transverse crack layout, [30].

$$a_x = \sqrt{1 - \bar{x}^2} - (R - a)$$

$$b = \sqrt{1 - (1 - a)^2} = \sqrt{2a - a^2}$$

$$\bar{h} = \frac{y}{hx} = \frac{y}{R} \times \frac{R}{2\sqrt{R^2 - x^2}} = \frac{\bar{y}}{2\sqrt{1 - \bar{x}^2}}$$

$$\bar{x} = \frac{x}{R}; \quad \bar{y} = \frac{y}{R}; \quad \bar{a} = \frac{a}{R}; \quad \bar{b} = \frac{b}{R}$$

$$\bar{C}_{55} = C_{55} \times \frac{E R^3}{1 - \vartheta^2} = \frac{32}{\pi} \int_{-b}^{\bar{b}} \bar{d}x \int_0^{\bar{ax}} (1 - \bar{x}^2) \bar{y} F2^2 \left(\frac{\bar{y}}{hx} \right) \bar{d}y \quad 3.29$$

$$\bar{C}_{44} = C_{44} \times \frac{E R^3}{1 - \vartheta^2} = \frac{16}{\pi} \int_{-b}^{\bar{b}} \bar{d}x \int_0^{\bar{ax}} \bar{x}^2 \bar{y} F1^2 \left(\frac{\bar{y}}{hx} \right) \bar{d}y \quad 3.30$$

$$C_{55} = \frac{\partial U5}{\partial P5} \quad , \quad C_{44} = \frac{\partial U4}{\partial P4}$$

Where **P4** and **P5** the bending moments for horizontal and vertical plane respectively, [13].

$$C_{55} = \frac{\partial^2}{\partial P5^2} \int_{-b}^b \int_0^{ax} J(y) \cdot dy dx \quad , \quad C_{44} = \frac{\partial^2}{\partial P4^2} \int_{-b}^b \int_0^{ax} J(y) \cdot dy dx \quad 3.31$$

Where $J(y)$ is density of function for strain energy.

$$J(y) = \frac{1}{E'} [(KI5)^2 + (KII5)^2 + M(KIII5)^2] \quad 3.32$$

The parameter of equation (3.32) in Appendix-B , from (B – 9) to (B – 13).

3.6.3. The Response of shaft through Two of Journal Bearings: -

Critical velocity is the speed at which the vibration results from the unbalance and is the response at the greatest value, where mass eccentricity is one of the most important reasons of vibration.

The response will be calculated at the site of the disk because it is at this site has the greatest moment. In our research we cannot consider case is (a rigid bearing rotor) because the stiffness depends on several factors including speed of rotation.

The equation of motion will give us the following [36]: -

$$\begin{aligned} m\ddot{x}_r + K(x_r - x_j) &= m_u e \Omega^2 \cos \Omega t \\ m\ddot{y}_r + K(y_r - y_j) &= m_u e \Omega^2 \sin \Omega t \end{aligned} \quad 3.33$$

Where x_r is the displacement for rotor in X-axis , and x_j is the displacement for journal bearing in X-axis.

$$\begin{bmatrix} K_{xx} & K_{xy} \\ K_{yx} & K_{yy} \end{bmatrix} \begin{Bmatrix} x_j \\ y_j \end{Bmatrix} + \begin{bmatrix} C_{xx} & C_{xy} \\ C_{yx} & C_{yy} \end{bmatrix} \begin{Bmatrix} i\Omega x_j \\ i\Omega y_j \end{Bmatrix} + \begin{bmatrix} K & 0 \\ 0 & K \end{bmatrix} \begin{Bmatrix} x_r \\ y_r \end{Bmatrix} = \begin{bmatrix} K & 0 \\ 0 & K \end{bmatrix} \begin{Bmatrix} x_r \\ y_r \end{Bmatrix} \quad 3.34$$

Where

$$\begin{aligned} x_j &= B e^{i\Omega t} \quad , \quad \dot{x}_j = i\Omega B e^{i\Omega t} = i\Omega x_j \\ y_j &= D e^{i\Omega t} \quad , \quad \dot{y}_j = i\Omega D e^{i\Omega t} = i\Omega y_j \\ K_{xx} &= (K_{xx1} + K_{xx2}), \quad K_{xy} = (K_{xy1} + K_{xy2}) \\ K_{yy} &= (K_{yy1} + K_{yy2}) \quad K_{yx} = (K_{yx1} + K_{yx2}) \\ C_{xx} &= (C_{xx1} + C_{xx2}) \quad C_{xy} = (C_{xy1} + C_{xy2}), \\ C_{yy} &= (C_{yy1} + C_{yy2}) \quad C_{yx} = (C_{yx1} + C_{yx2}) \end{aligned}$$

After simplifying the equation, we will produce the following.

$$\begin{bmatrix} K_{xx} + K + i\Omega C_{xx} & K_{xy} + i\Omega C_{xy} \\ K_{yx} + i\Omega C_{yx} & K_{yy} + K + i\Omega C_{yy} \end{bmatrix} \begin{Bmatrix} x_j \\ y_j \end{Bmatrix} = \begin{bmatrix} K x_r \\ K y_r \end{bmatrix} \quad 3.35$$

Then we solve the equation to produce

$$x_j = \frac{K[(K_{yy} + K + i\Omega C_{yy})x_r - (K_{xy} + i\Omega C_{xy})y_r]}{(K_{xx} + K + i\Omega C_{xx})(K_{yy} + K + i\Omega C_{yy}) - (K_{xy} + i\Omega C_{xy})(K_{yx} + i\Omega C_{yx})} \quad 3.36$$

$$y_j = \frac{K[(K_{xx}+K+i\Omega C_{xx})x_r - (K_{yx}+i\Omega C_{yx})y_r]}{(K_{xx}+K+i\Omega C_{xx})(K_{yy}+K+i\Omega C_{yy}) - (K_{xy}+i\Omega C_{xy})(K_{yx}+i\Omega C_{yx})} \quad 3.37$$

We compensate equation (3.36) and equation (3.37) in equation (3.33) to produce the following.

$$m\ddot{x}_r + K_1 x_r + K_{12} y_r = m_u e \Omega^2 \cos \Omega t \quad 3.38$$

$$m\ddot{y}_r + K_2 y_r + K_{21} x_r = m_u e \Omega^2 \sin \Omega t \quad 3.39$$

Where

$$K_1 = \frac{K[(K_{xx}+i\Omega C_{xx})(K_{yy}+K+i\Omega C_{yy}) - (K_{xy}+i\Omega C_{xy})(K_{yx}+i\Omega C_{yx})]}{(K_{xx}+K+i\Omega C_{xx})(K_{yy}+K+i\Omega C_{yy}) - (K_{xy}+i\Omega C_{xy})(K_{yx}+i\Omega C_{yx})} \quad 3.40$$

$$K_2 = \frac{K[(K_{yy}+i\Omega C_{yy})(K_{xx}+K+i\Omega C_{xx}) - (K_{xy}+i\Omega C_{xy})(K_{yx}+i\Omega C_{yx})]}{(K_{xx}+K+i\Omega C_{xx})(K_{yy}+K+i\Omega C_{yy}) - (K_{xy}+i\Omega C_{xy})(K_{yx}+i\Omega C_{yx})} \quad 3.41$$

$$K_{12} = \frac{K^2(K_{xy}+i\Omega C_{xy})}{(K_{xx}+K+i\Omega C_{xx})(K_{yy}+K+i\Omega C_{yy}) - (K_{xy}+i\Omega C_{xy})(K_{yx}+i\Omega C_{yx})} \quad 3.42$$

$$K_{21} = \frac{K^2(K_{yx}+i\Omega C_{yx})}{(K_{xx}+K+i\Omega C_{xx})(K_{yy}+K+i\Omega C_{yy}) - (K_{xy}+i\Omega C_{xy})(K_{yx}+i\Omega C_{yx})} \quad 3.43$$

It is possible to write solve of equations (3.38) and (3.39) as follows [36].

$$x_r = x_r^+ e^{i\Omega t} + x_r^- e^{-i\Omega t} \quad y_r = y_r^+ e^{i\Omega t} + y_r^- e^{-i\Omega t} \quad 3.44$$

Where x_r^+ and y_r^+ are the radius of whirl for the forward precession, and x_r^- and y_r^- are the radius of whirl for the backward precession.

Then we compensate equation (3.44) in equation (3.33) to produce: -

$$x_r^+ = \frac{(Mu\Omega^2/2)[(K_2 - M\Omega^2) + iK_{12}]}{(K_1 - M\Omega^2)(K_2 - M\Omega^2) - K_{12}K_{21}}, \quad y_r^+ = \frac{(-iMu\Omega^2/2)[(K_1 - M\Omega^2) - iK_{21}]}{(K_1 - M\Omega^2)(K_2 - M\Omega^2) - K_{12}K_{21}} \quad 3.45$$

$$x_r^- = \frac{(Mu\Omega^2/2)[(K_2-M\Omega^2)-iK_{12}]}{(K_1-M\Omega^2)(K_2-M\Omega^2)-K_{12}K_{21}}, y_r^- = \frac{(-iMu\Omega^2/2)[(K_1-M\Omega^2)+iK_{21}]}{(K_1-M\Omega^2)(K_2-M\Omega^2)-K_{12}K_{21}} \quad 3.46$$

then the formula unbalance response will be as follows: -

$$r^* = \frac{x_r + iy_r}{u} \quad 3.47$$

This equation (3.47) can be written as follows [35].

$$r^* = r_f^* e^{i\Omega t} + r_b^* e^{-i\Omega t} \quad 3.48$$

Where

$$r_f^* = \frac{\Omega^2 \{ (\Omega_1^2 + \Omega_2^2 - 2\Omega^2) - i(\mu_2 \Omega_2^2 - \mu_1 \Omega_1^2) \}}{2[(\Omega_1^2 - \Omega^2)(\Omega_2^2 - \Omega^2) - \mu_1 \mu_2 \Omega_1^2 \Omega_2^2]}, r_b^* = \frac{\Omega^2 (\Omega_1^2 - \Omega_2^2) + i(\mu_2 \Omega_2^2 + \mu_1 \Omega_1^2)}{2[(\Omega_1^2 - \Omega^2)(\Omega_2^2 - \Omega^2) - \mu_1 \mu_2 \Omega_1^2 \Omega_2^2]}$$

$$\mu_1 = \frac{K_{12}}{K_1}, \mu_2 = \frac{K_{21}}{K_2}, \Omega_1^2 = \frac{K_1}{M}, \Omega_2^2 = \frac{K_2}{M}$$

Where

(r_f^*) is the component of forward unbalance response,

(r_b^*) is the component of backward unbalance response.

$$|r^*|_{maj} = |r_f^*| + |r_b^*| \quad |r^*|_{min} = |r_f^*| - |r_b^*| \quad 3.49$$

where $|r^*|_{maj}$ is the major radius, and $|r^*|_{min}$ is the minor radius.

Critical velocity occurs when the response is greatest, i.e. when the response is equal to $(|r|_{maj})$.

By using equation (3.49) we can find the critical velocity after knowing the great response.

3.7. The Flexibility for rotor have slant crack: -

In the cracking rotor the amount of elasticity in the slit area will decrease due to a decrease in cross section area. Total energy of strain is two parts, the first is the energy of strain without cracking, and the second part is the energy of strain that comes from crack.

$$E_{total} = U_{uncracked} + W_{cracked} \quad 3.50$$

If we look at the **figure (3.7)** we will notice that there are three forces (F_x, F_y, F_z) and a moment about Z direction, where the energy of a non-cracking shaft is in **equation (3.51)**, [21].

$$U = \frac{F_x^2 L^3}{96EI} + \frac{F_y^2 L^3}{96EI} + \frac{T^2 L}{4GJp} + \frac{T^2 L}{4AE} \quad 3.51$$

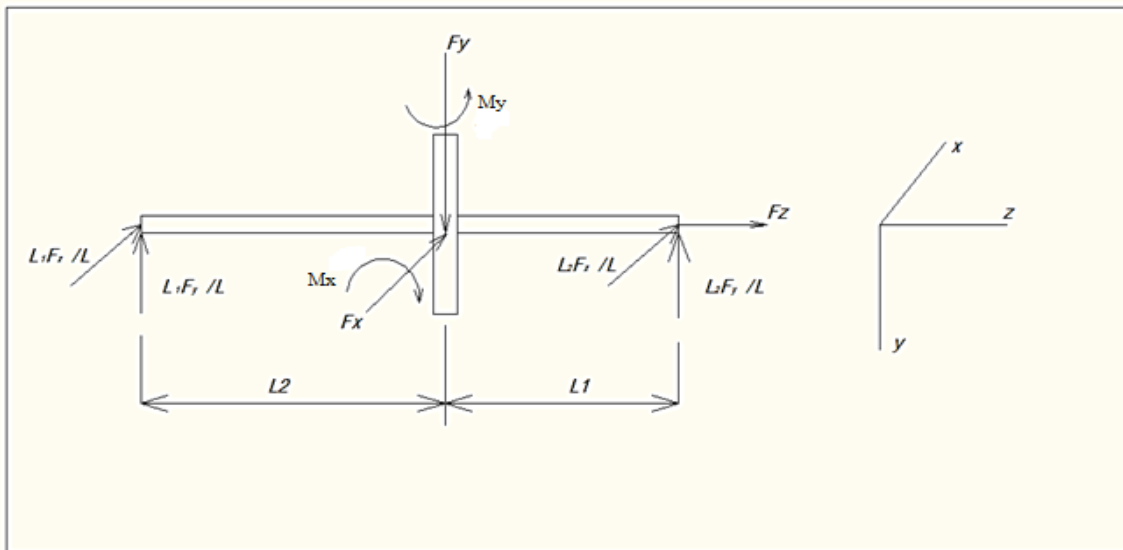


Figure (3.7) The forces and moment affecting on the cracked shaft, [21].

By using Equation (3.50), we conclude that a local flexibility of any point on the rotor is: -

$$\frac{\partial 2E}{\partial F_i \partial F_j} = \frac{\partial 2U}{\partial F_i \partial F_j} + \frac{\partial 2W}{\partial F_i \partial F_j} \quad 3.52$$

And by using the moments (M_x) and (M_y) can be found the relations: -

$$q_4 = \frac{F_y \times L_2 \times L_1}{L} \quad , \quad q_5 = \frac{F_x \times L_2 \times L_1}{L} \quad 3.53$$

By using Chain rule and equation (3.53), we will get, [25]: -

$$[C_o] = \begin{pmatrix} \frac{L_2^2 L_1^2}{L^2} \left(\frac{\partial 2W}{\partial M_y^2} \right) & \frac{L_2^2 L_1^2}{L^2} \left(\frac{\partial 2W}{\partial M_y \partial M_x} \right) & \frac{L_2 L_1}{L} \left(\frac{\partial 2W}{\partial M_y \partial T} \right) & \frac{L_2 L_1}{L} \left(\frac{\partial 2W}{\partial M_y \partial M_z} \right) \\ & \frac{L_2^2 L_1^2}{L^2} \left(\frac{\partial 2W}{\partial M_x^2} \right) & \frac{L_2 L_1}{L} \left(\frac{\partial 2W}{\partial M_x \partial T} \right) & \frac{L_2 L_1}{L} \left(\frac{\partial 2W}{\partial M_x \partial M_z} \right) \\ & & \frac{\partial 2W}{\partial T^2} & \frac{\partial 2W}{\partial M_z \partial T} \\ & \text{Symmetric} & & \frac{\partial 2W}{\partial M_z^2} \end{pmatrix} +$$

$$diag. \left(\frac{L_2^2 L_1^2}{3EI}, \frac{L_2^2 L_1^2}{3EI}, \frac{L}{2GJ_p}, \frac{L}{2AE} \right) \quad 3.54$$

If

$$[K_{cr}] = [C_o]^{-1}$$

So the global matrix is: -

$$[K]_g = [A]^{-1} [K_{cr}] [A] \quad \text{where } [A] = \begin{pmatrix} \cos\theta & \sin\theta & 0 & 0 \\ -\sin\theta & \cos\theta & 0 & 0 \\ 0 & 0 & 1 & 0 \\ 0 & 0 & 0 & 1 \end{pmatrix} \quad 3.55$$

Figure (3.8) shows the dimensions of the slant crack, Where θ is slant angle for crack.

In **Appendix –B**, we finding flexibility of the shaft.

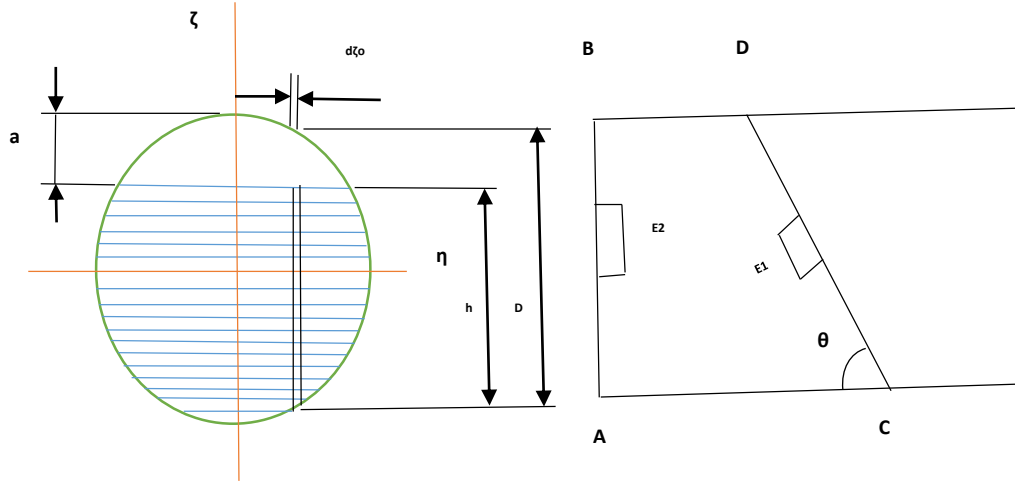


Figure (3.8) a slant crack in the rotating shaft, [30].

3.8. Analytical study of the rotor with two crack (transverse and slant cracks): -

The stresses generated by the crack are the most important causes of failure in the rotor, where these stresses are concentrated on the edge of the crack, so you must enter (stress intensity factor) into the calculations. The (stress intensity factor) will be its symbol (**KI**). The (**KI**) consists of two parts, the first being the direction (ζ) and the second is in the direction (η), [13].

The equation of the first crack: -

$$K1^{(I)} = KQ\zeta1^{(I)} + KQ\eta1^{(I)} \tag{3.55}$$

And the equation of the second crack: -

$$K2^{(I)} = KQ\zeta2^{(I)} + KQ\eta2^{(I)} \tag{3.56}$$

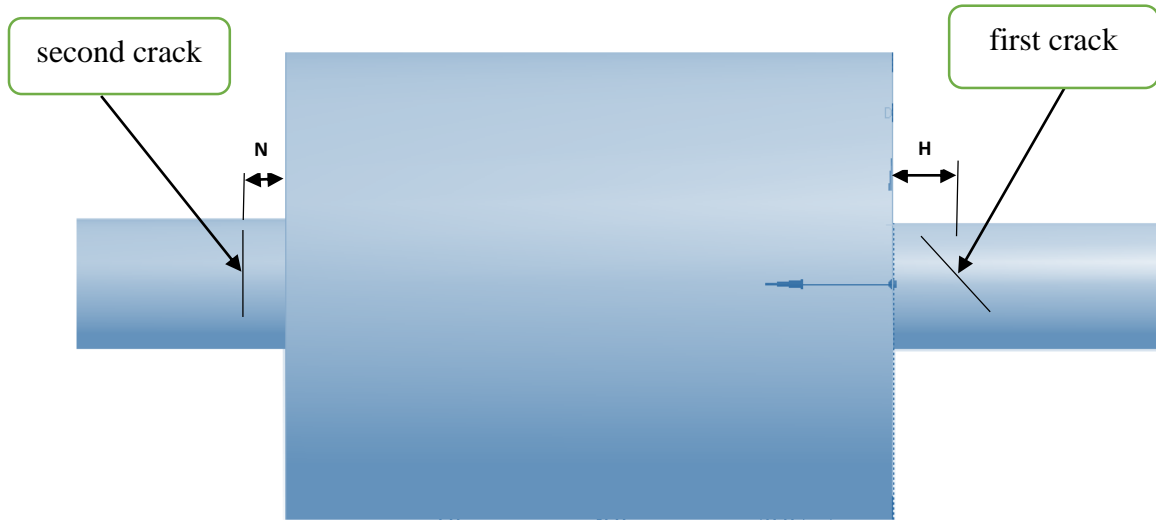


Figure (3.9) Location of the two cracks.

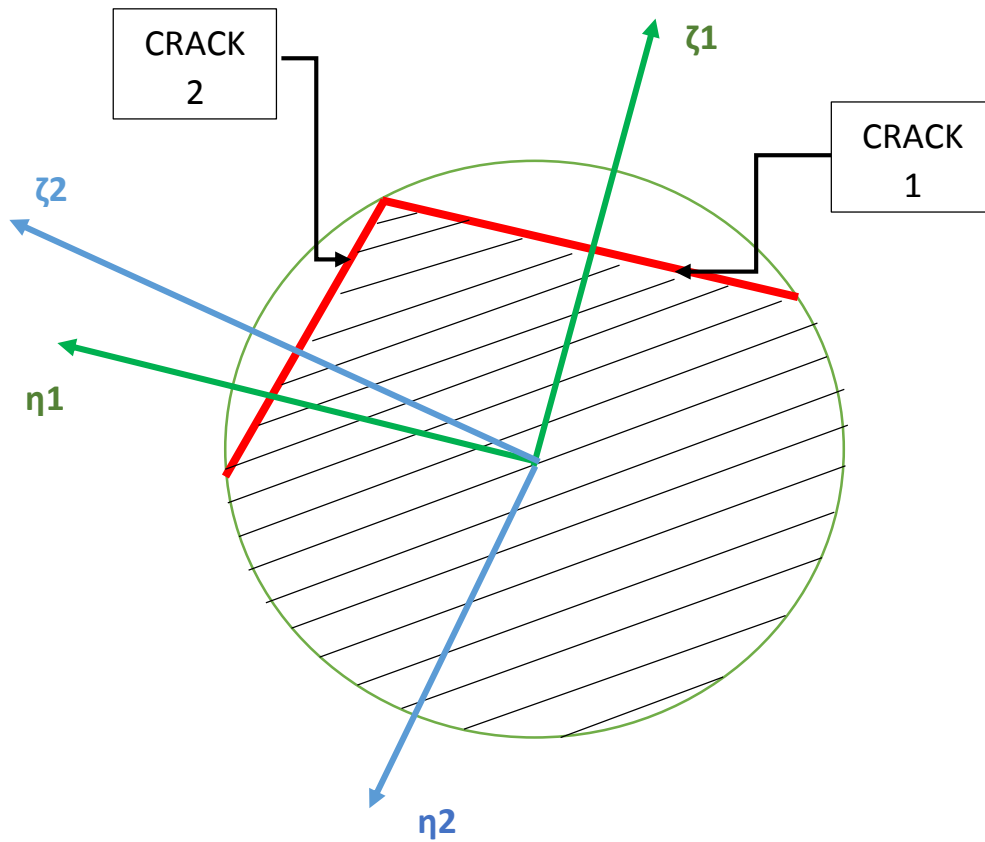


Figure (3.10) coordinates of the first and second cracks.

Now we will take the first crack equations (oblique crack), [13].

$$KQ\zeta_1^{(I)} = \sigma\zeta_1 \sqrt{\pi\alpha} \times F \quad 3.57$$

$$\sigma\zeta_1 = \frac{\left(\frac{Q\zeta_1 \times (L1 - H)}{4}\right) \times \frac{\alpha'}{2}}{I} \quad 3.58$$

Equation (3.58) is compensated in equation (3.57) to produce follows: -

$$KQ\zeta_1 = \frac{Q\zeta_1 \times (L1 - H) \times \alpha'}{8I} \sqrt{\pi\alpha} \times F \quad 3.59$$

Where F is the stress configuration factors in ζ directions.

$$KQ\eta_1^{(I)} = \sigma\eta_1 \sqrt{\pi\alpha} \times \tilde{F} \quad 3.60$$

$$\sigma\eta_1 = \frac{(Q\eta_1 \times (L2 - N)) \times w}{I} \sin \theta \quad 3.61$$

Equation (3.61) is compensated in equation (3.60) to produce follows: -

$$KQ\eta_1 = \frac{Q\eta_1 \times (L2 - N) \times w}{I} \sqrt{\pi\alpha} \times \tilde{F} \sin \theta \quad 3.62$$

Where \tilde{F} is the stress configuration factors in η directions.

The equations of F and \tilde{F} are :-

$$F = \sqrt{\frac{2\tilde{\alpha}}{\pi\alpha} \tan \frac{\pi\alpha}{2\tilde{\alpha}}} \times \frac{0.923 + 0.199[1 - \sin(\frac{\pi\alpha}{2\tilde{\alpha}})]^4}{\cos(\frac{\pi\alpha}{2\tilde{\alpha}})} \quad 3.63$$

$$\tilde{F} = \sqrt{\frac{2\tilde{\alpha}}{\pi\alpha} \tan \frac{\pi\alpha}{2\tilde{\alpha}}} \times \frac{0.752 + 2.02(\frac{\alpha}{\tilde{\alpha}}) + 0.37[1 - \sin(\frac{\pi\alpha}{2\tilde{\alpha}})]^3}{\cos(\frac{\pi\alpha}{2\tilde{\alpha}})} \quad 3.64$$

So the density of strain energy ($J_1(\alpha)$) is

$$J_1(\alpha) = \frac{1}{E} [KQ\zeta_1^{(I)} + KQ\eta_1^{(I)}]^2 \quad 3.63$$

Figure (3.11) and Figure (3.12) shows the mechanism of opening and closing of crack with the coordinates of the first crack.

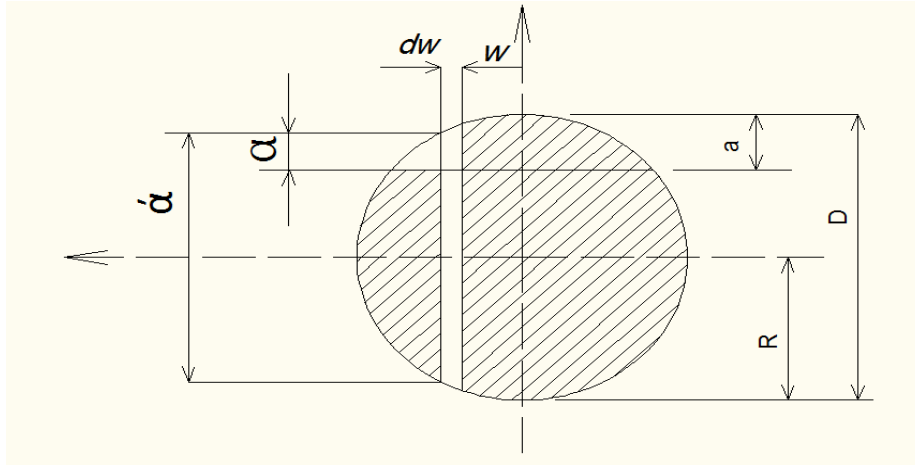


Figure (3.11) area of cross section for crack, [30].

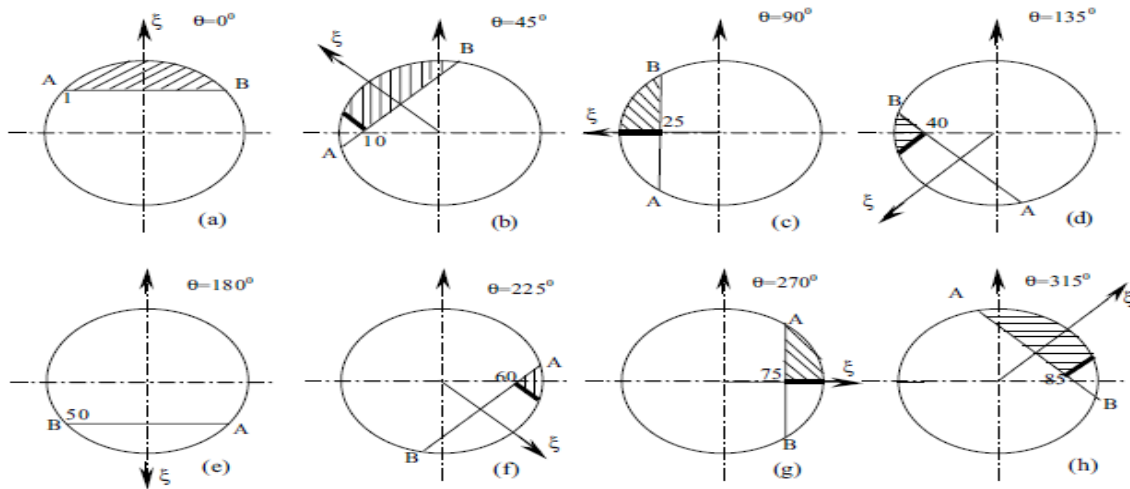


Figure (3.12) the mechanism of opening and closing of crack with rotating angle (θ), [13].

The additional deflection will be calculated through the following equation:

$$u_{i1} = \frac{\partial}{\partial Q_{i1}} \left[\int J_1(\alpha) d\alpha \right] \tag{3.64}$$

Where (i) is (ζ_1) or (η_1).

$$u_{\zeta_1} = \frac{2}{E} \iint_{A_1}^{A_2} \left(\frac{Q_{\zeta_1} \times (L_2 - N) \times \alpha' \times \sqrt{\pi \alpha} \times F}{2I} + \frac{Q_{\eta_1} \times (L_2 - N) \times w \times \sqrt{\pi \alpha} \times \bar{F}}{I} \right) \frac{(L_2 - N) \times \alpha' \times \sqrt{\pi \alpha} \times F}{2I} d\alpha dw \tag{3.65}$$

$$u\eta_1 = \frac{2}{E} \iint_{A_1} \left(\frac{Q\zeta_1 \times (L_2 - N) \times \alpha' \times \sqrt{\pi\alpha} \times F}{2I} + \frac{Q\eta_1 \times (L_2 - N) \times w \times \sqrt{\pi\alpha} \times \tilde{F}}{I} \right) \frac{(L_2 - N) \times w \times \sqrt{\pi\alpha} \times \tilde{F}}{4I} \sin\theta \, d\alpha \, dw \quad 3.66$$

Now it was taken the second crack (transverse crack) using $\zeta_2 - \eta_2$ coordinate: -

$$u\zeta_2 = \frac{2}{E} \iint_{A_2} \left(\frac{Q\zeta_2 \times (L_1 - H) \times \alpha' \times \sqrt{\pi\alpha} \times F}{8I} + \frac{Q\eta_2 \times (L_1 - H) \times w \times \sqrt{\pi\alpha} \times \tilde{F}}{I} \right) \frac{(L_1 - H) \times \alpha' \times \sqrt{\pi\alpha} \times F}{8I} \, d\alpha \, dw \quad 3.67$$

$$u\eta_2 = \frac{2}{E} \iint_{A_2} \left(\frac{Q\zeta_2 \times (L_1 - H) \times \alpha' \times \sqrt{\pi\alpha} \times F}{8I} + \frac{Q\eta_2 \times (L_1 - H) \times w \times \sqrt{\pi\alpha} \times \tilde{F}}{I} \right) \frac{(L_1 - H) \times w \times \sqrt{\pi\alpha} \times \tilde{F}}{4I} \, d\alpha \, dw \quad 3.68$$

If the terms ($\tilde{u}\zeta_1$) and ($\tilde{u}\eta_1$) fellows can be given by the equations: -

$$\tilde{u}\zeta_1 = u\zeta_1 + u\eta_2 \sin\gamma + u\zeta_2 \cos\gamma + u\zeta_1^0 \quad 3.69$$

$$\tilde{u}\eta_1 = u\eta_1 + u\zeta_2 \sin\gamma + u\eta_2 \cos\gamma + u\eta_1^0 \quad 3.70$$

And,

$$\begin{pmatrix} Q\zeta_2 \\ Q\eta_2 \end{pmatrix} = \begin{bmatrix} \cos\gamma & \sin\gamma \\ -\sin\gamma & \cos\gamma \end{bmatrix} \begin{pmatrix} Q\zeta_1 \\ Q\eta_1 \end{pmatrix} \quad 3.71$$

So,

$$\begin{aligned} \tilde{u}\zeta_1 = & \frac{2}{E} \iint_{A_1} \left(\frac{Q\zeta_1 \times (L_2 - N) \times \alpha' \times \sqrt{\pi\alpha} \times F}{4I} \right. \\ & + \left. \frac{Q\eta_1 \times (L_2 - N) \times w \times \sin\theta \sqrt{\pi\alpha} \times \tilde{F}}{2I} \right) \frac{(L_1 - H) \times \alpha' \times \sqrt{\pi\alpha} \times F}{8I} \, d\alpha \, dw \\ & + \frac{2}{E} \iint_{A_2} \left[\left(\frac{(L_1 - H)^2 \alpha'^2 \pi \alpha F^2}{32I^2} \cos\gamma - \frac{(L_1 - H)^2 \alpha' w \pi \alpha F \tilde{F}}{8I^2} \sin\gamma \right) Q\zeta_1 \right. \\ & + \left(\frac{(L_1 - H)^2 \alpha'^2 \pi \alpha F^2}{32I^2} \sin\gamma \right. \\ & + \left. \left. \frac{(L_1 - H)^2 \alpha' w \pi \alpha F \tilde{F}}{8I^2} \cos\gamma \right) Q\eta_1 \sin\theta \right] \cos\gamma \, d\alpha \, dw \\ & - \frac{2}{E} \iint_{A_2} \left[\left(\frac{(L_1 - H)^2 \alpha' w \pi \alpha F \tilde{F}}{16I^2} \cos\gamma - \frac{(L_1 - H)^2 w^2 \pi \alpha \tilde{F}^2}{4I^2} \sin\gamma \right) Q\zeta \right. \\ & + \left(\frac{(L_1 - H)^2 \alpha'^2 w \pi \alpha F \tilde{F}}{16I^2} \sin\gamma \right. \\ & + \left. \left. \frac{(L_1 - H)^2 w^2 \pi \alpha \tilde{F}^2}{4I^2} \cos\gamma \right) Q\eta_1 \sin\theta \right] \sin\gamma \, d\alpha \, dw \\ & + \frac{Q\zeta_1 L_2^2 L_1^2}{3EIL} \end{aligned} \quad 3.72$$

$$\begin{aligned}
& \tilde{u}_{\eta 1} \\
&= \frac{2}{E} \iint_{A_1} \left(\frac{Q\zeta 1 \times (L2 - N) \times \alpha' \times \sqrt{\pi\alpha} \times F}{8I} \right. \\
&+ \left. \frac{Q\eta 1 \times (L2 - N) \times w \times \sin\theta \sqrt{\pi\alpha} \times \tilde{F}}{2I} \right) \frac{(L1 - H) \times w \times \sqrt{\pi\alpha} \times \tilde{F}}{4I} d\alpha dw \\
&+ \frac{2}{E} \iint_{A_2} \left[\left(\frac{(L1 - H)^2 \alpha'^2 \pi \alpha F^2}{32I^2} \cos\gamma - \frac{(L1 - H)^2 \alpha' w \pi \alpha F \tilde{F}}{8I^2} \sin\gamma \right) Q\zeta 1 \right. \\
&+ \left. \left(\frac{(L1 - H)^2 \alpha'^2 \pi \alpha F^2}{32I^2} \sin\gamma + \frac{(L1 - H)^2 \tilde{\alpha} w \pi \alpha F \tilde{F}}{16I^2} \cos\gamma \right) Q\eta 1 \sin\theta \right] \sin\gamma d\alpha dw \\
&+ \frac{2}{E} \iint_{A_2} \left[\left(\frac{(L1 - H)^2 \alpha' w \pi \alpha F \tilde{F}}{16I^2} \cos\gamma - \frac{(\alpha' - H)^2 w^2 \pi \alpha \tilde{F}^2}{4I^2} \sin\gamma \right) Q\zeta 1 \right. \\
&+ \left. \left(\frac{(L1 - H)^2 \alpha' w \alpha F \tilde{F}}{8I^2} \sin\gamma \right. \right. \\
&+ \left. \left. \frac{(L1 - H)^2 w^2 \pi \alpha \tilde{F}^2}{4I^2} \cos\gamma \right) Q\eta 1 \sin\theta \right] \sin\gamma d\alpha dw \\
&+ \frac{Q\eta 1 \sin\theta L2^2 L1^2}{3EIL} \tag{3.73}
\end{aligned}$$

Where

$$u_{\zeta 1}^0 = \frac{Q\zeta 1 L2^2 L1^2}{3EIL} \tag{3.74}$$

$$u_{\eta 1}^0 = \frac{Q\eta 1 L2^2 L1^2}{3EIL} \tag{3.75}$$

And,

$u_{\zeta 1}^0$ is a deflection for un cracked rotor in $\zeta 1$ axis.

$u_{\eta 1}^0$ is a deflection for un cracked rotor in $\eta 1$ axis.

$u_{\zeta 1}$ is a deflection by reason the first crack in ζ direction.

$u_{\zeta 2}$ is a deflection by reason the second crack in ζ direction.

$u_{\eta 1}$ is a deflection by reason the first crack in η direction.

$u_{\eta 2}$ is a deflection by reason the second crack in η direction.

Then it was calculated the flexibilities in any direction ($g\eta, g\zeta, g\eta\zeta, g\zeta\eta$), [30].

$$g\zeta = \frac{\partial \tilde{u}\zeta_1}{\partial Q\zeta_1} \quad 3.76$$

$$\begin{aligned} g\zeta = & \frac{\pi(L2 - N)^2}{16EI^2} \iint_{A1} \alpha'^2 \alpha F^2 d\alpha dw + \frac{\pi(L1 - H)^2 \cos^2 \gamma}{32EI^2} \iint_{A2} \alpha'^2 \alpha F^2 d\alpha dw \\ & - \frac{\pi(L1 - H)^2 \sin \gamma \cos \gamma}{16EI^2} \iint_{A2} \alpha'^2 \alpha w F \tilde{F} d\alpha dw \\ & - \frac{\pi(L1 - H)^2 \sin \gamma \cos \gamma}{16EI^2} \iint_{A2} \alpha' \alpha w F \tilde{F} d\alpha dw \\ & + \frac{\pi(L1 - H)^2 \sin^2 \gamma}{4EI^2} \iint_{A2} w^2 \alpha \tilde{F}^2 d\alpha dw \\ & + \frac{L2^2 L1^2}{3EIL} \end{aligned} \quad 3.77$$

$$g\eta = \frac{\partial \tilde{u}\eta_1}{\partial Q\eta_1} \quad 3.78$$

$$\begin{aligned} g\eta = & \frac{\pi(L2 - N)^2 \sin \theta}{4EI^2} \iint_{A1} w^2 \alpha \tilde{F}^2 d\alpha dw \\ & + \frac{\pi(L1 - H)^2 \sin^2 \gamma \sin \theta}{16EI^2} \iint_{A2} \alpha'^2 \alpha F^2 d\alpha dw \\ & + \frac{\pi(L1 - H)^2 \sin \gamma \cos \gamma \sin \theta}{8EI^2} \iint_{A2} \alpha' \alpha w F \tilde{F} d\alpha dw \\ & + \frac{\pi(L1 - H)^2 \sin \gamma \cos \gamma \sin \theta}{8EI^2} \iint_{A2} \alpha' \alpha w F \tilde{F} d\alpha dw \\ & + \frac{\pi(L1 - H)^2 \cos^2 \gamma \sin \theta}{4EI^2} \iint_{A2} w^2 \alpha \tilde{F}^2 d\alpha dw \\ & + \frac{\sin \theta L2^2 L1^2}{3EIL} \end{aligned} \quad 3.79$$

$$g\zeta\eta = \frac{\partial \tilde{u}\zeta_1}{\partial Q\eta_1} \quad 3.80$$

$$\begin{aligned}
g\zeta\eta = g\eta\zeta = & \frac{\pi(L2-N)^2}{8EI^2} \sin\theta \iint_{A1} \alpha' \alpha w F\tilde{F} d\alpha dw + \\
& \frac{\pi(L1-H)^2 \sin\gamma \cos\gamma \sin\theta}{16EI^2} \iint_{A2} \alpha'^2 \alpha F^2 d\alpha dw + \frac{\pi(L1-H)^2 \cos^2\gamma \sin\theta}{8EI^2} \iint_{A2} \alpha' \alpha w F\tilde{F} d\alpha dw - \\
& \frac{\pi(L1-H)^2 \sin^2\gamma \sin\theta}{8EI^2} \iint_{A2} \alpha' \alpha w F\tilde{F} d\alpha dw - \\
& \frac{\pi(L1-H)^2 \sin\gamma \cos\gamma \sin\theta}{8EI^2} \iint_{A2} w^2 \alpha \tilde{F}^2 d\alpha dw
\end{aligned} \tag{3.81}$$

The equations of flexibility can be written as follows, [13]: -

$$\begin{aligned}
g\zeta = & \frac{\pi(L2-N)^2}{16EI^2} \bar{I}g1 + \frac{\pi(L1-H)^2 \cos^2\gamma}{32EI^2} \bar{I}g1 - \frac{\pi(L1-H)^2 \sin\gamma \cos\gamma}{16EI^2} \bar{I}g2 \\
& + \frac{\pi(L1-H)^2 \sin^2\gamma}{16EI^2} \bar{I}g3 - \frac{L2^2 L1^2}{3EIL}
\end{aligned} \tag{3.82}$$

$$\begin{aligned}
g\eta = & \frac{\pi(L2-N)^2 \sin\theta}{4EI^2} \bar{I}g2 + \frac{\pi(L1-H)^2 \sin^2\gamma \sin\theta}{16EI^2} \bar{I}g1 + \frac{\pi(L1-H)^2 \sin\gamma \cos\gamma \sin\theta}{8EI^2} \bar{I}g2 + \\
& \frac{\pi(L1-H)^2 \cos^2\gamma \sin\theta}{8EI^2} \bar{I}g3 + \frac{L2^2 L1^2}{3EIL}
\end{aligned} \tag{3.83}$$

$$\begin{aligned}
g\zeta\eta = & \frac{\pi(L2-N)^2}{8EI^2} \sin\theta \bar{I}g3 + \frac{\pi(L1-H)^2 \sin\gamma \cos\gamma \sin\theta}{16EI^2} \bar{I}g1 + \\
& \frac{\pi(L1-H)^2 (\cos^2 - \sin^2)\gamma \sin\theta}{8EI^2} \bar{I}g2 - \frac{\pi(L1-H)^2 \sin\gamma \cos\gamma \sin\theta}{8EI^2} \bar{I}g3
\end{aligned} \tag{3.84}$$

Where $\bar{I}g2, \bar{I}g3, \bar{I}g1, \bar{I}g1, \bar{I}g2, \bar{I}g3$, are listed in **Appendix – B**, from equation (B – 25) to equation (B – 30).

After that it was found the stiffness using the flexibilities equations as following.

$$K_\zeta = \frac{g\eta}{g\eta g\zeta - g\zeta\eta^2} ; K_\eta = \frac{g\zeta}{g\eta g\zeta - g\zeta\eta^2} ; K_{\zeta\eta} = \frac{-g\zeta\eta}{g\eta g\zeta - g\zeta\eta^2} \tag{3.85}$$

So the equation of motion for the two directions (ζ) and (η) will be as follows: -

$$M(\ddot{\zeta}1 - 2\Omega \dot{\eta}1 - \Omega^2 \zeta1) + C(\dot{\zeta}1 - \Omega\eta1) + K_{\zeta} \zeta1 + K_{\zeta\eta} \eta1 = m ec \Omega^2 \cos\beta - Mg\cos\theta' \quad 3.86$$

$$M(\ddot{\eta}1 - 2\Omega \dot{\zeta}1 - \Omega^2 \eta1) + C(\dot{\eta}1 - \Omega\zeta1) + K_{\eta} \eta1 + K_{\eta\zeta} \zeta1 = m ec \Omega^2 \sin\beta - Mg\sin\theta' \quad 3.87$$

By equation (3.86) and equation (3.87), it was found the response to the cracked rotor, and then find the forces applicable on the cross section of the crack.

$$\begin{Bmatrix} Q\zeta1 \\ Q\eta1 \end{Bmatrix} = \begin{bmatrix} K_{\zeta} & K_{\zeta\eta} \\ K_{\eta\zeta} & K_{\eta} \end{bmatrix} \begin{Bmatrix} \zeta1 \\ \eta1 \end{Bmatrix} \quad 3.88$$

Equations (3.86) and (3.87) can be written as follows: -

$$\ddot{\zeta} + 2\zeta ro \dot{\zeta} + 2\dot{\eta} + (r\zeta^2 - 1)\bar{\zeta} + (r\zeta\eta^2 - 2\zeta ro)\bar{\eta} = e\cos\beta - ro^2\cos t \quad 3.89$$

$$\ddot{\eta} + 2\zeta ro \dot{\eta} + 2\dot{\zeta} + (r\eta^2 - 1)\bar{\eta} + (r\eta\zeta^2 + 2\zeta ro)\bar{\zeta} = e\sin\beta + ro^2\sin t \quad 3.90$$

Where

$$\omega n = \sqrt{\frac{K}{M}} ; \omega\eta = \sqrt{\frac{K\eta}{M}} ; \omega\zeta = \sqrt{\frac{K_{\zeta}}{M}} ; \omega\zeta\eta = \sqrt{\frac{K_{\zeta\eta}}{M}} ; \varsigma = \frac{c}{2\sqrt{KM}}$$

$$ro = \frac{\omega n}{\Omega} ; r\eta = \frac{\omega\eta}{\Omega} ; r\zeta = \frac{\omega\zeta}{\Omega} ; r\zeta\eta = \frac{\omega\zeta\eta}{\Omega} ; r\eta\zeta = \frac{\omega\eta\zeta}{\Omega}$$

$$\bar{\eta} = \frac{\eta1}{\delta st.} ; \bar{\zeta} = \frac{\zeta1}{\delta st.} ; \tau = \Omega t ; e = \frac{ec}{\delta st.} ; \bar{a1} = \frac{a1}{R} ; \bar{a2} = \frac{a2}{R}$$

It should be noted that the equations (3.89) and (3.90) do not include the effect for bearings.

In Appendix-A, we have MATLAB program to find the critical velocity and response to cracked shaft, taking into consideration the effect of bearings.

3.9. The Elliptical orbit path for rotor dynamic system:

In the dynamic rotor system, have two natural frequencies (ω_{nx} and ω_{ny}), this frequency gives the limits of system stability.

If the velocity is between the two critical speeds, the type of orbit is (backward orbit). and if the velocity is before or after the two velocities, the orbit type (forward orbit), Figure (3.13) shows the direction of the orbit path Compared with the rotation of the shaft, the horizontal axis is the natural frequency, and the vertical axis is the radius of whirl, [35]. The radius of the whirl depends on the value of the eccentricity in the shaft and disk system.

It is important to mention that when a crack occurs, the shape of the orbit path is external.

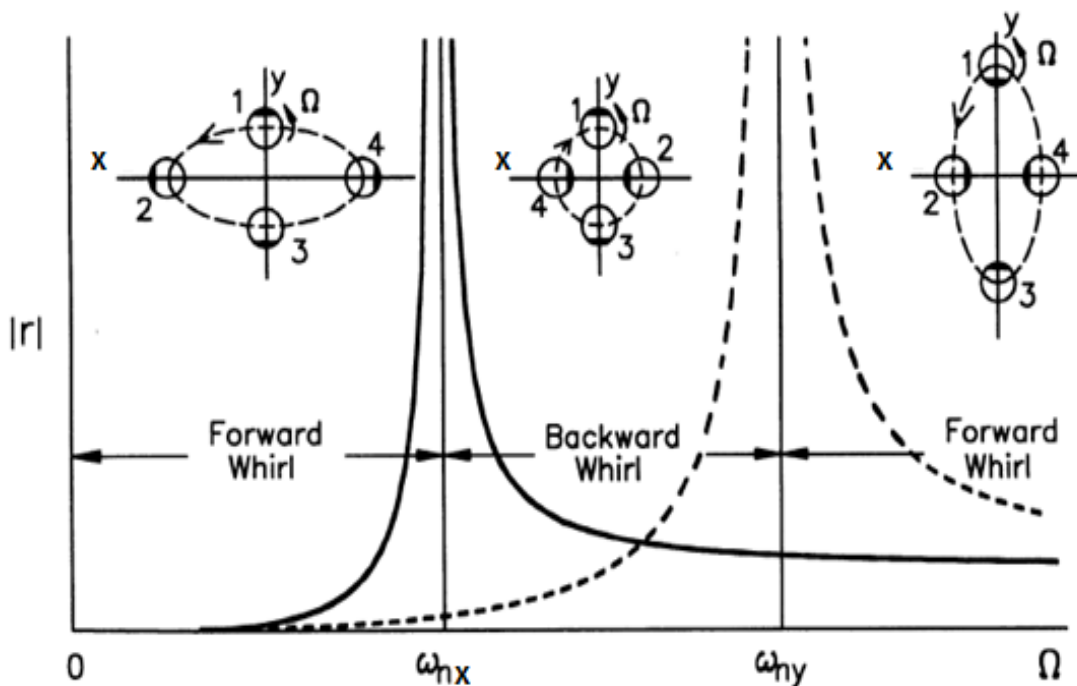


Figure (3.13) Path of the orbit and its relation with the rotation of the shaft, [35].

3.10. Numerical Analysis

Numerical analysis of the rotary shaft system is done to verify vibration behavior during the rotation, and verification of the results obtained from analytical solution in this chapter. In the numerical, the **ANSYS** software will be used.

Elements of the shaft are (17) element of type (**beam188**), where its type is affected by crack. It is necessary to mention is when using an element from type (solid), the response does not sense the existence of a crack, so we used (**beam188**). In Rotor dynamics ANSYS guide, there is a note is that the solid element is not used, because it is not affected by the existence of the crack, [37].

The disc can be used an element from type (**Mass21**), where the effect of the disk as a mass on the shaft with their dimensions, [37].

The bearings can be represented by element (**COMBI 214**), where this element is affected by the oil properties, as stiffness and damping, [37].

The numerical analysis will be for two tests. The first test is to find the critical velocity and response for uncrack shaft, and the second test is to find the critical velocity and response for the cracked shaft and multiple depths (**0.2R, 0.4R, 0.6R, 0.8R**).

After finding the results of the two tests, it was compared with the results obtained from the analytical study. This comparison was in the results and discussion chapter.

3.10.1. The Procedure of Numerical Analysis for Rotor Dynamic System: -

The Steps of numerical analysis for the rotor dynamic system are represented in the following:

- 1. Building model:** - Model construction is carried out on the basis of identifying the parts of the system and the relationship which connect these parts to each other.
- 2. Define Element type:** - the Gyroscopic effect should be among the basic principles for selecting the type of element, the selected elements must support the principle of CORIOLIS, where this principle proves the existence of the gyroscopic effect in the system. The shaft element is (**Beam188**), and the disc element (**MASS21**), and the bearing element (**COMBI214**).
- 3. Define the material:** - The material must be defined to know its properties whether linear or nonlinear, where the material was chosen linearly in our research.
- 4. Define rotation speed:** - The speed is defined either by **OMEGA** or **CMOMEGA**. If there are fixed parts of the rotor, we use **CMOMEGA**. In this search was used **CMOMEGA**.
- 5. Meshing the model:** - In this model, the shaft was divided into (17) elements of type (**Beam188**), and more data was given to the site of the crack in the shaft.

The response will be more accurate whenever we give a more accurate and more detailed data about the location of the crack as the depth and distance from the disk and its width relative to the cross section area.

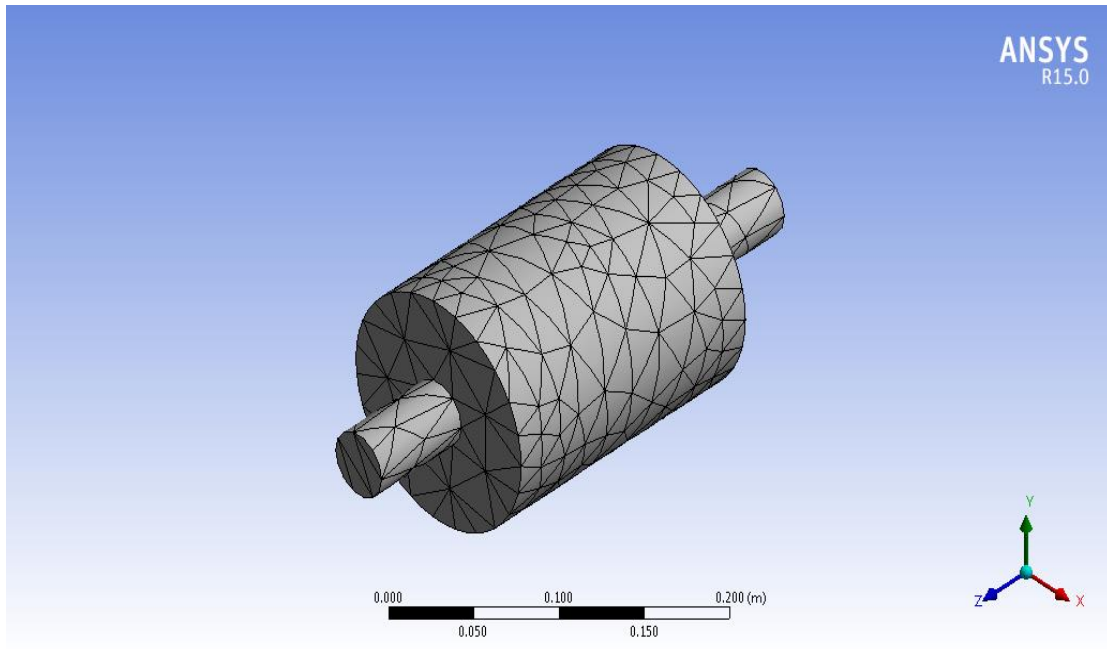


Figure (3.14) The Meshing of dynamic rotor.

6. the boundary conditions: - the type of bearing is determining the boundary conditions of the rotor, the type is the journal bearing, where its boundary condition is on form of damping and stiffness forces in the horizontal and vertical and cross coupling direction.

The values of the matrix of stiffness and damping will take from the products of analytical study at each speed of the rotor from chapter three, [30]. The values of the damping and stiffness matrix changing with the rotating speed alteration because the oil specification changes with it.

Figure (3.15) shows boundary condition of the Journal bearing. Where two axes were defined - the vertical and the horizontal axis. Because of the specific boundary conditions of the journal bearing, the oil layer is represented by spring and damper in each direction.

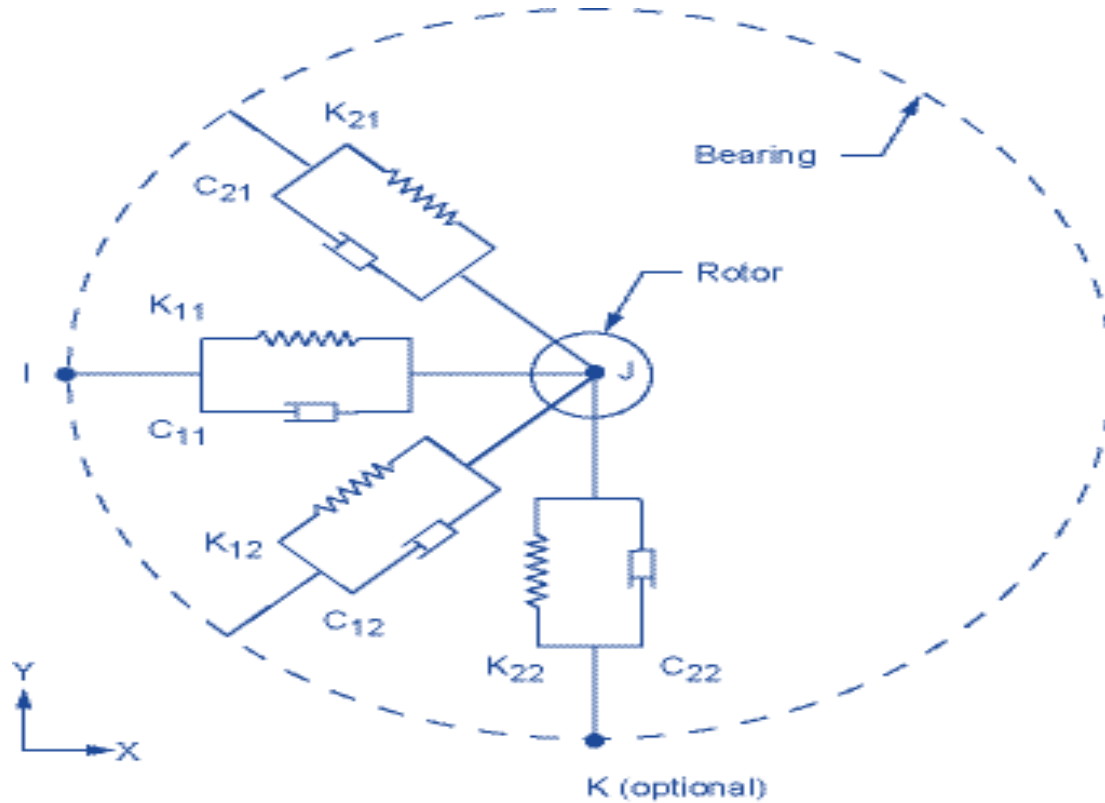


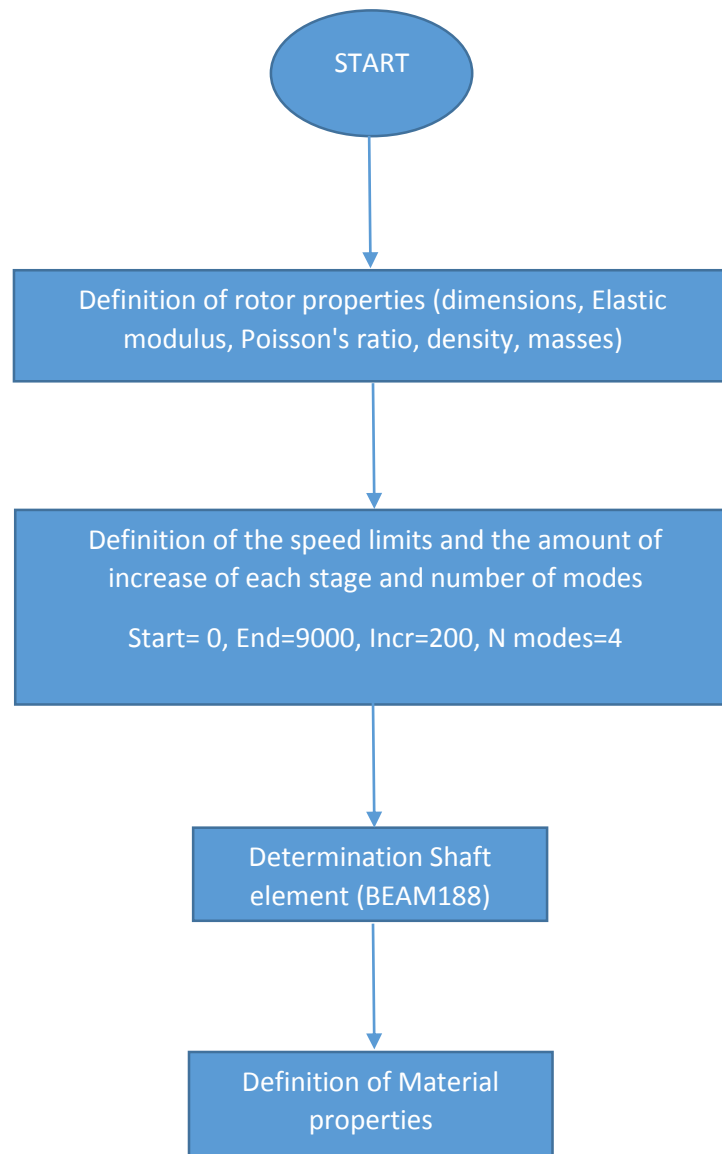
Figure (3.15) The boundary condition of the Journal bearing, [1].

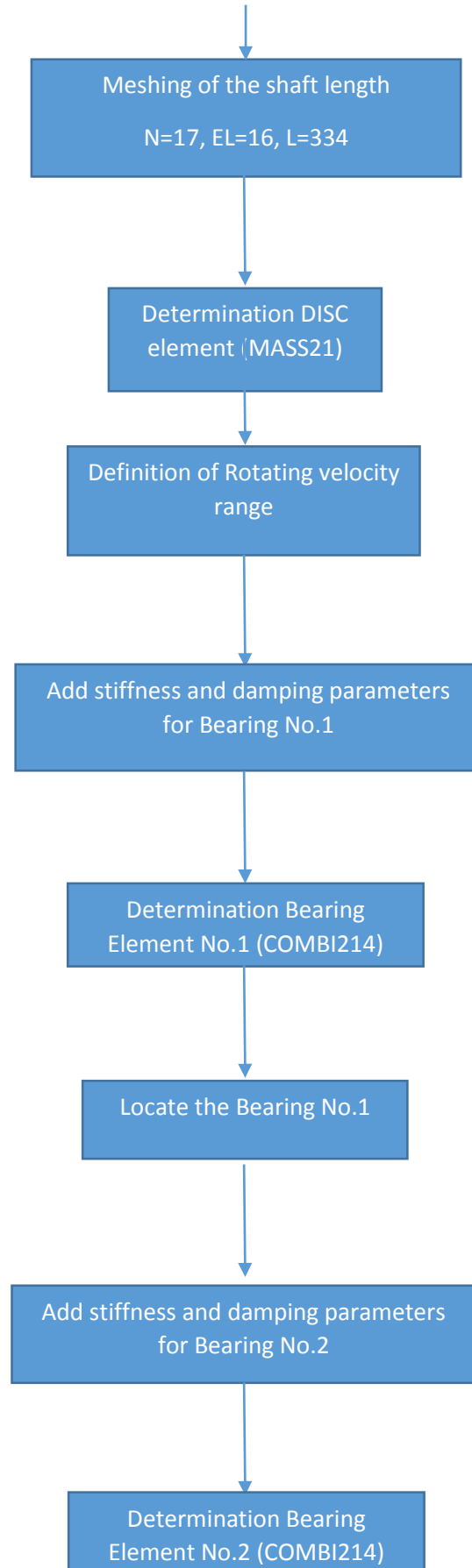
7. Solving the model: - The dynamic rotor model was solved by standard ANSYS Software, and the analysis was performed in two cases, transient and harmonic.

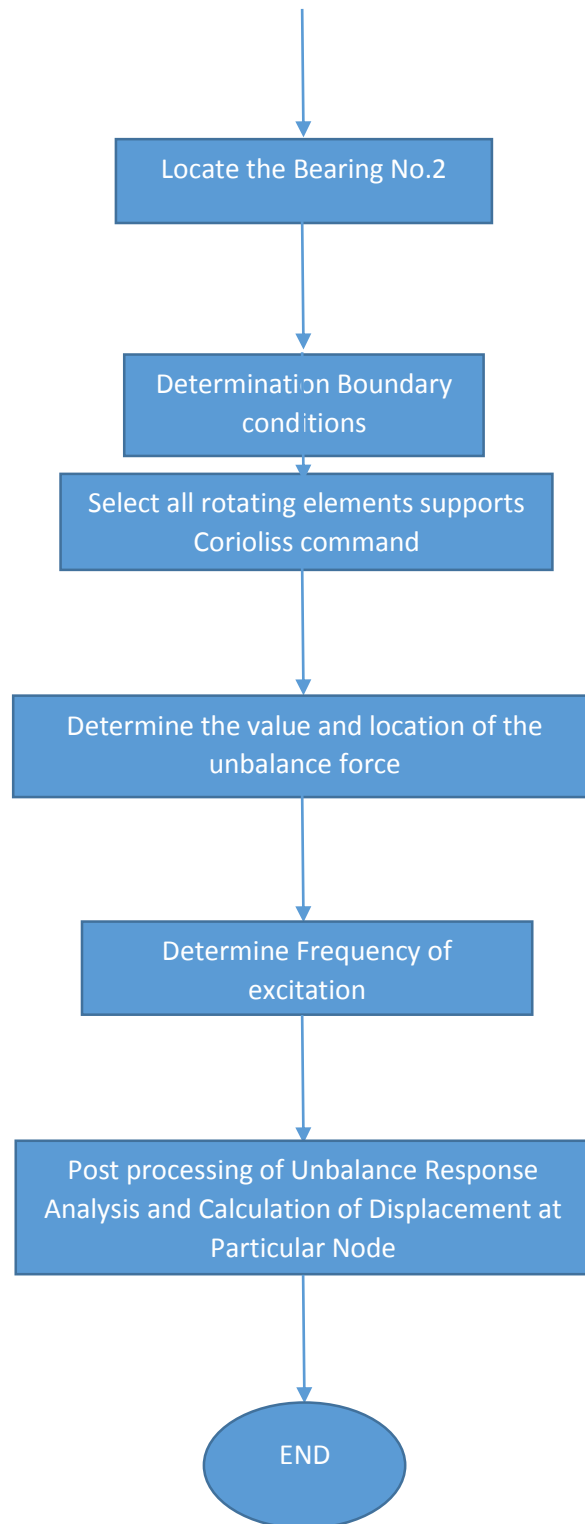
8. Analyses of Results: - To analyze the data from uncrack shaft and crack shaft, the **(POST1)** and **(POST26)** were used. **(POST1)** Is used as a generic processor, and **(POST26)** is used for determination the time history [37].

3.10.2. The flowchart of the constructed ANSYS code: -

An outline of the program construction process was illustrated by flowchart indicating all inputs, outputs and commands.







CHAPTER FOUR

EXPERIMENTAL WORK

4.1. Introduction: -

In this chapter, full description of the design and manufacturing of the test rig is presented. The test rig in this work is aimed to simulate the dynamics and vibration of the gas turbine rotor at Al-Hilla power station. The rig was designed and manufactured in to model similar conditions of that in the real rotor gas power station. Additionally, this rotor will be modeled analytically and numerically for results verifications. The shaft and the disk were designed and configured with a reduction ratio of 1/10 to the original dimensions of the rotor, adjusting none equal length of both ends of the shaft outside the disk i.e. ($L_1 \neq L_2$). The rotor is supported by two journal bearings at both ends. These bearings and the lubrication system are also designed and manufactured to present conditions similar to the real conditions too. There are two measuring devices that are fitted to the test rig; these are an accelerometer and rotational speed reader; this will be described in the next sections in this chapter

It should be mentioned that the manufacture of the device was very accurate by sophisticated equipment to obtain more accurate results.

4.2. Test Rig Layout: -

The tes rig which is designed and manufactured during the current work is shown in figure (4.1). In this rig, a reletively heavey rotor is designed to rotate at high speed about 10000 rpm. So that, the frame of the rig is made of steel memebers with a 4 mm thickness.

Due to the expected vibrations, rubber bases are used to support the whole rig and the sub-base of the rotor as shown in figure (4.1). This will result in absorbing the undesired source of vibrations that might come from the motor itself. Additionally, it can be also seen that the rotor is linked to the motor via a rubber belt where this can reduce transferring vibration from the motor.

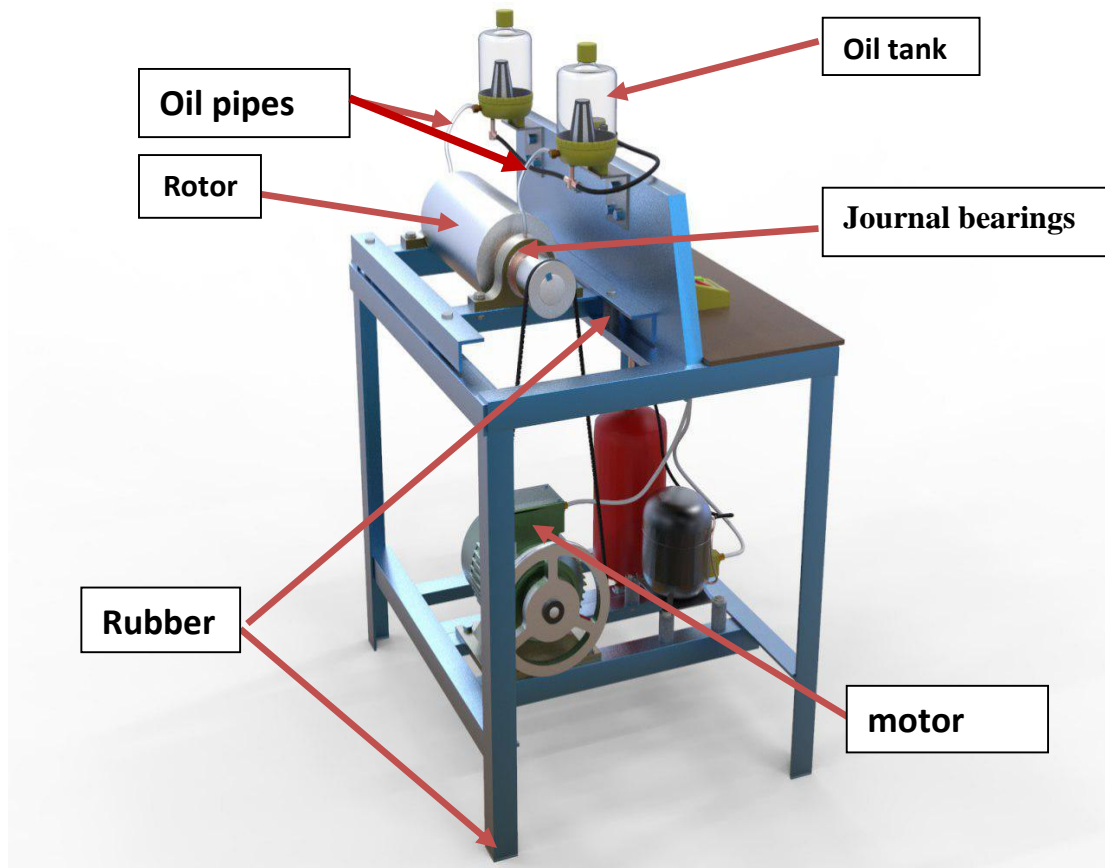


Figure (4.1) layout of the test rig

4.3 Rotor manufacturing: -

The material used to manufacture the rotor shaft is of carbon steel while the disk is made from iron. This is due to the fact that the disk paly as a rigid body where its mass and moment of inertia are the only effective parameters. The shaft material is of chromium- molybdenum alloy steel (AISI 4140), the chemical composition of this alloy is shown in table (4.1)

Table (4.1): The chemical composition of the shaft material.

C%	Si%	Mn%	P%	S%	Cr%	Mo%	Ni%	Al%	Co%	Cu%	V%	Fe%
0.39	0.27	0.80	0.005	0.027	1.14	0.225	0.077	0.02	0.005	0.064	0.004	96.673

The disk was fitted to the shaft via interference fit (I.F). In this type of fit, the shaft size is made slightly larger than the disk hub size with a tapered angle of 10° as shown in figure (4.2). For installation, the shaft is pressed inside the disk during installation giving high binding contact. This will prevent relative slippage between the disk and the shaft.

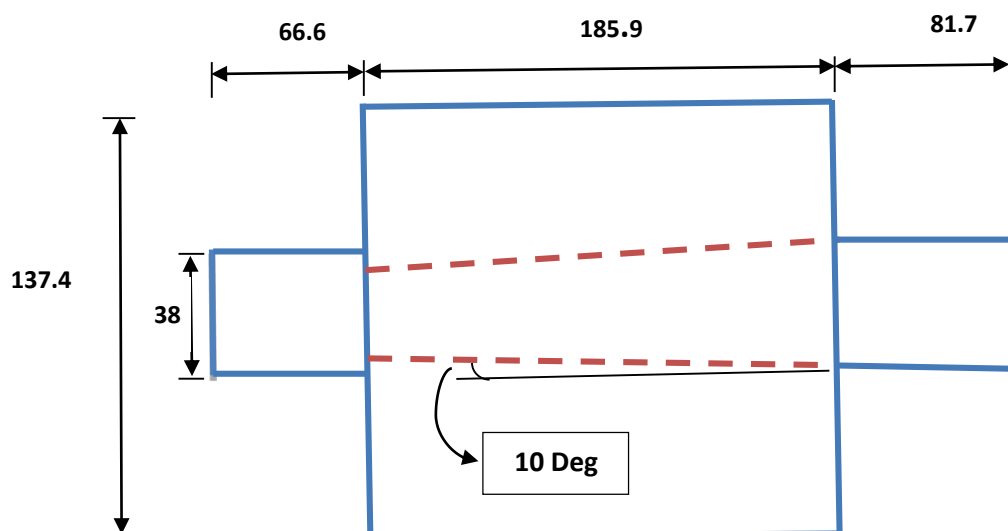


Figure (4.2) The rotor layout showing the interference fit between the shaft and disk and dimensions in millimeter.

For more secure contact, the outside circular edges are welded at both ends, where this also increase the safety during running the rig. The welded area is shown in Figure (4.3).

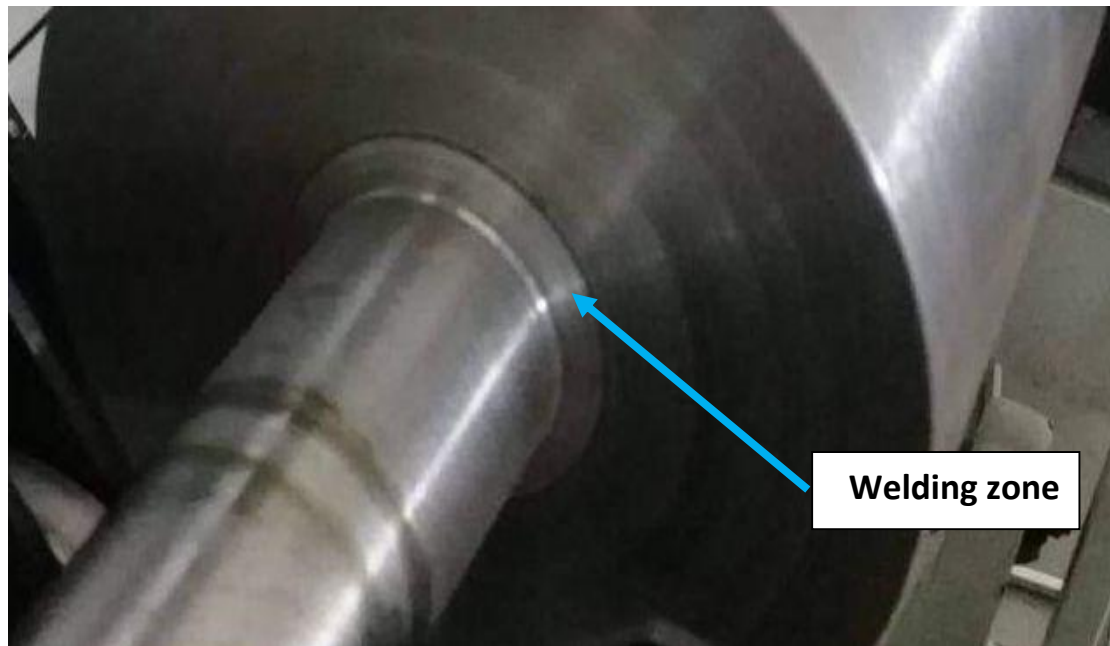


Figure (4.3): The welded edge between the shaft and disk.

The compression and welding processes formed a relatively tortuous surface, so that diameter of the lips 2 mm was increased before the process of contact between the disc and the shaft. After the welding and pressing process, the scrap surface was removed.

In order to achieve accurate diameter of the shaft, a dial gauge was used for this aim, this is shown in Figure (4.4). All dimensions of the shaft and the disk are accurately checked using digital Vernier, this is shown in figures (4.4) and (4.5).

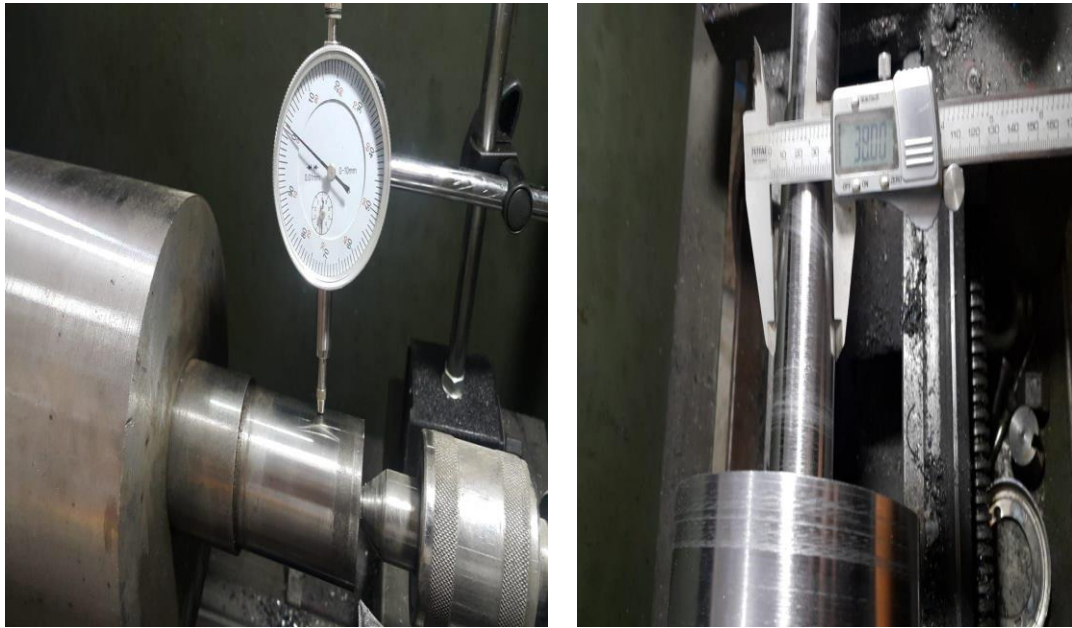


Figure (4.4) Accurate measurements during shaft manufacturing.

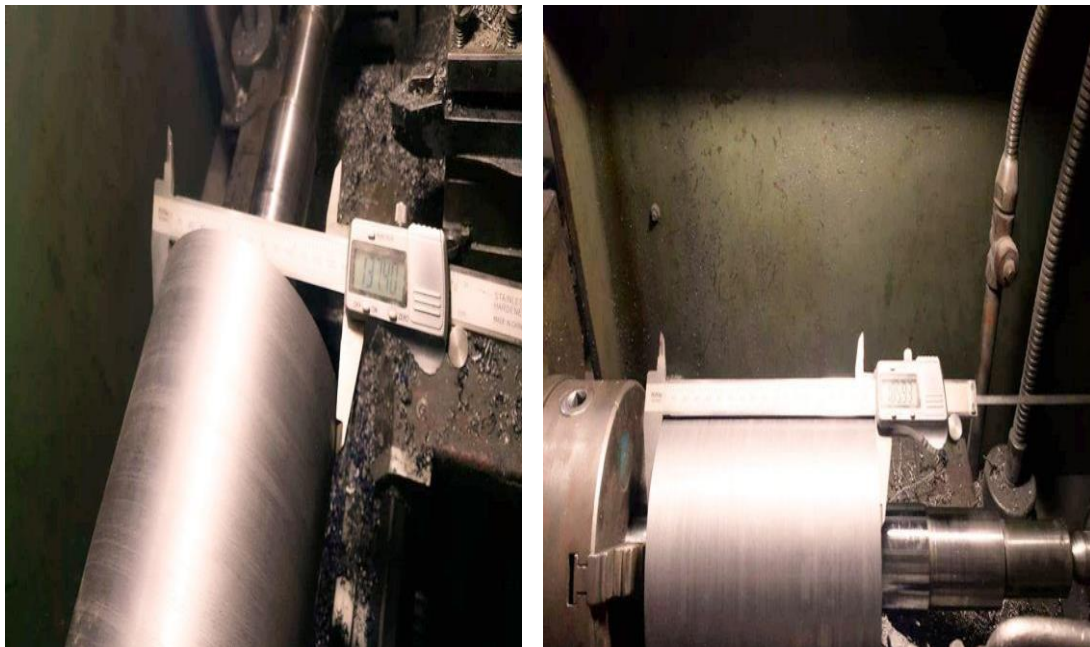


Figure (4.5) Accurate measurements during disk manufacturing.

4.4. Rotor Balancing:

After manufacturing the rotor, it has to be tested to investigate for any unbalanced rotating mass. The balancing process are commonly used for the majority of rotors after manufacturing. The existitnce of unbalanced masses can resulted during manufacturing the disk and shaft followed by the process of fitting them together. Balancing process should first determine the amount and location of the unbalanced masses, secondly balance these masses by removing them or by adding equivalent masses.

The balancing of the rotor manufactured for the current work was balanced using the very specialized balancing equipment at DORA refinery. Figure (4.6) shows the rotor installed on the Schenck balancing machine, where this company belongs to the globally active technology group of DÜRR AG based in Stuttgart.

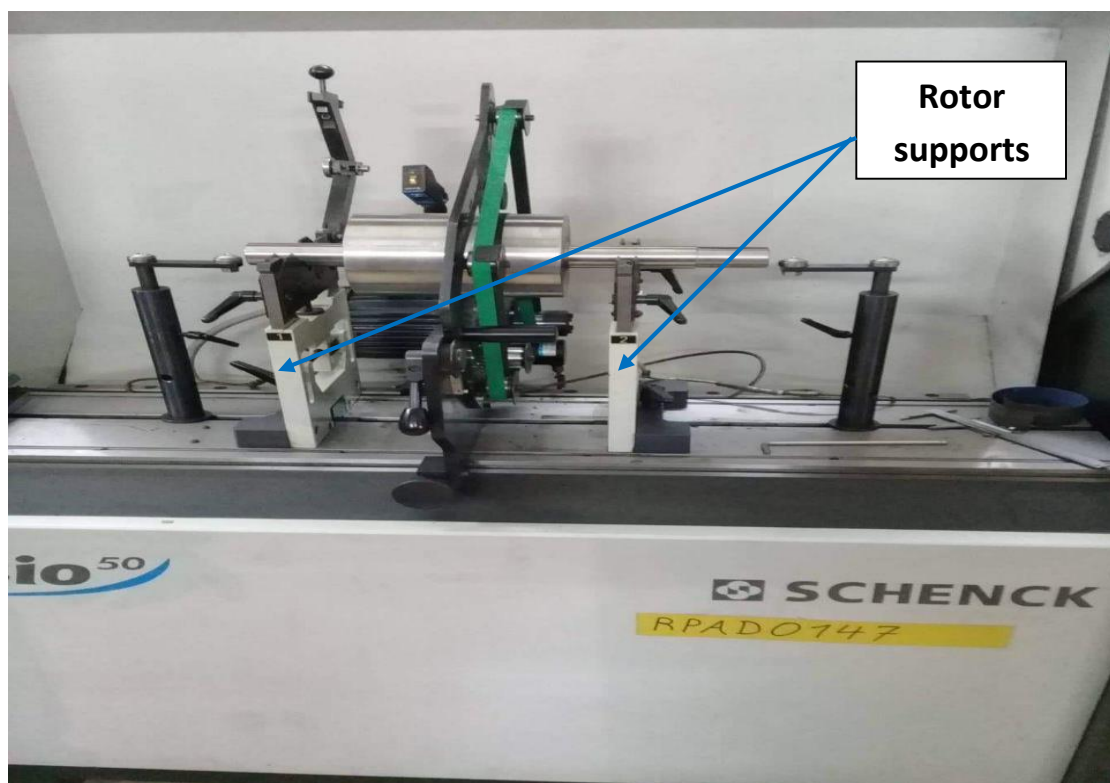


Figure (4.6) The rotor of the current work installed on the Schenck balancing machine.

In the balancing process, the rotor was rotated at a speed (750) rpm. During that, the sensors determine the amount and position of the unbalanced masses, this is shown in Figure (4.7). In this figure, the maximum unbalance mass (M.U.M), for the right and left side are (87.2 g.mm) and (93.3 g.mm) respectively.

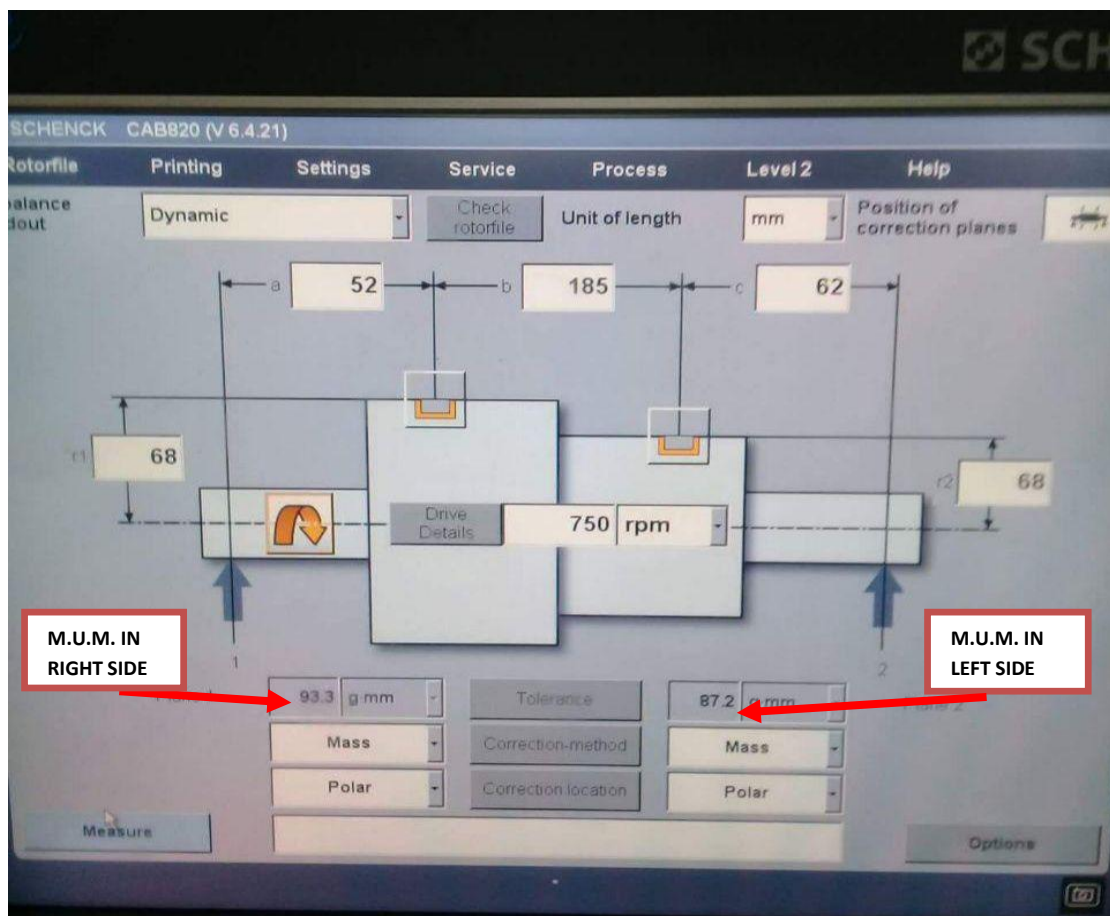


Figure (4.7) The screen of the Schenck device showing the (M.U.M).

Figure (4.8) shows that there are two regions of unbalanced masses, the first is the green circle which represents the permissible limits, and the second is the white region, which represents the **not** allowed limits.

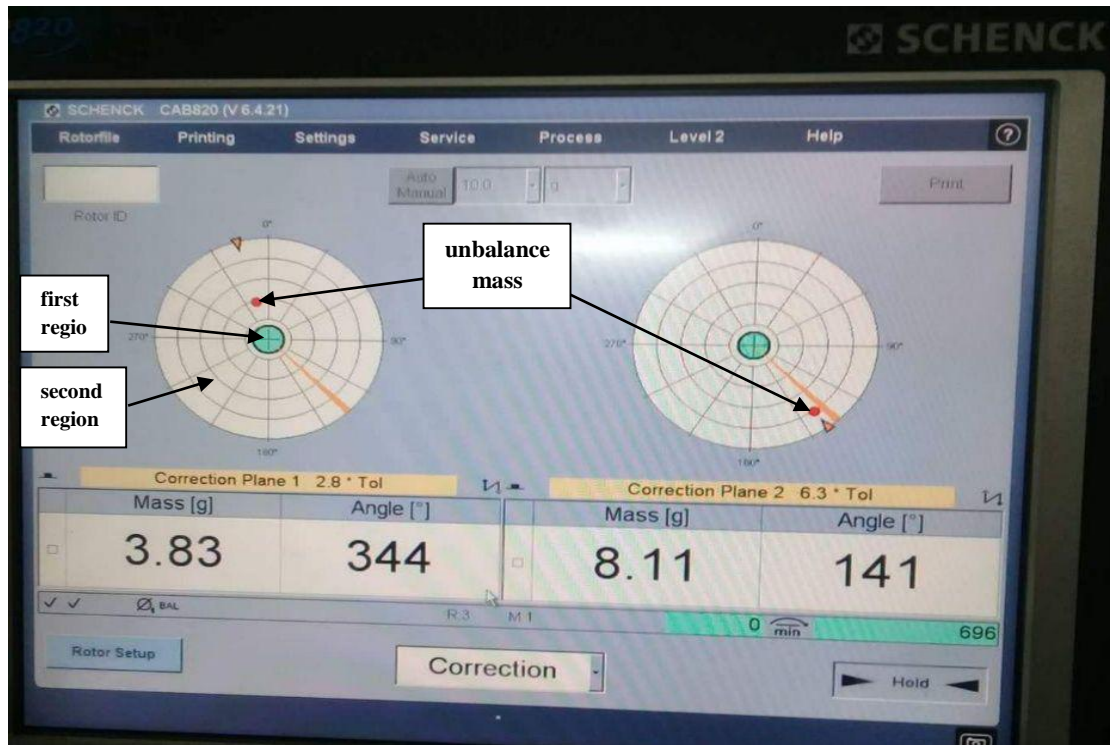


Figure (4.8) the value and location of the unbalance masses.

The balancing approach was carried out by removing masses from the disk in the same direction of the unbalanced masses, this can be seen in figure (4.9)

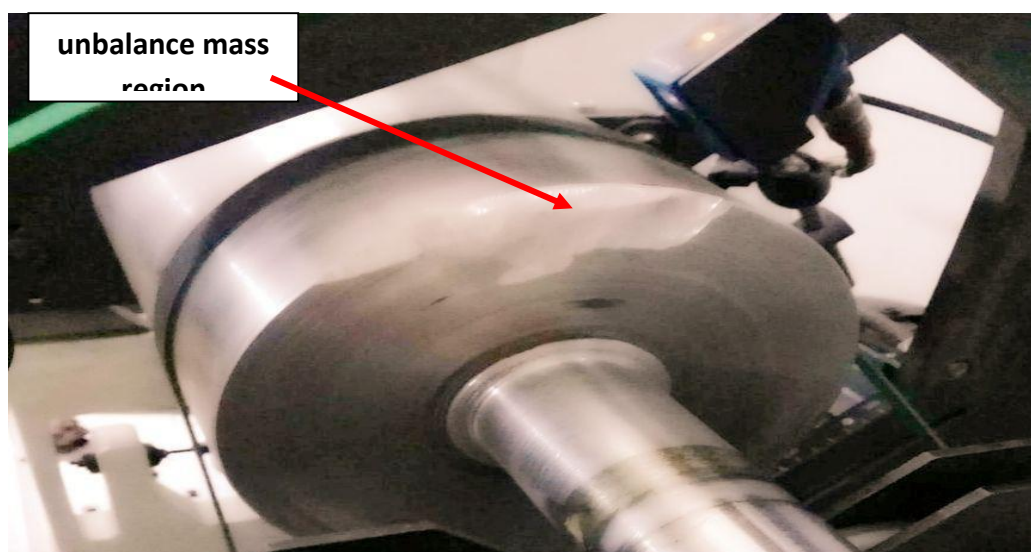


Figure (4.9) Removing of the unbalance mass.

The process of removing masses was repeated 12 times resulted in unbalanced mass of 0.936 g and 0.534 g for the two planes and this can be considered as an acceptable value. This is shown in figure (3.10) where the unbalanced masses are located at the green zone.



Figure (4.10) The final state of rotor balancing.

4.5. Test rig power train:

The rotor is driven by three-phase electric motor via a V-belt and a pair of pulleys with diameter ratio of 3:1 (the driver is of 150 mm diameter and the driven is of 50 mm), this is shown figure (4.11). the reason behind using rubber belt is to reduce the vibration that can transform from the motor and may add measurement noises. The speed of the electric motor is controlled by an inverter. The full specifications of the motor and the inverter can be seen in table (4.2) and (4.3) respectively.

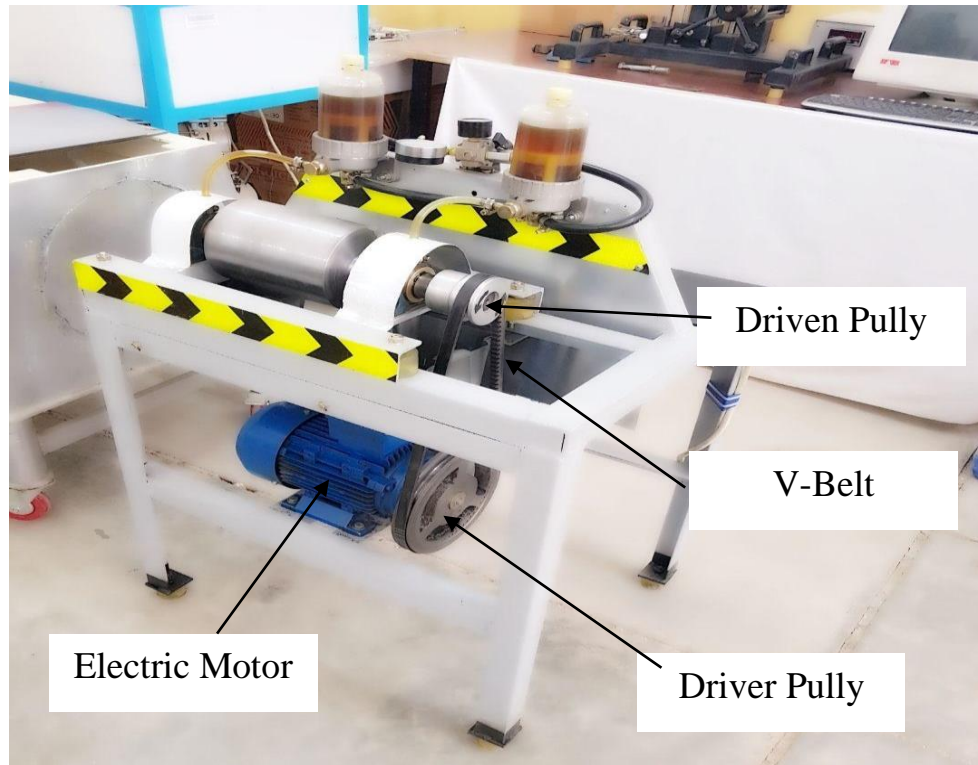


Figure (4.11) The power train of the test rig

Table (4.2) Specification of the electric motor.

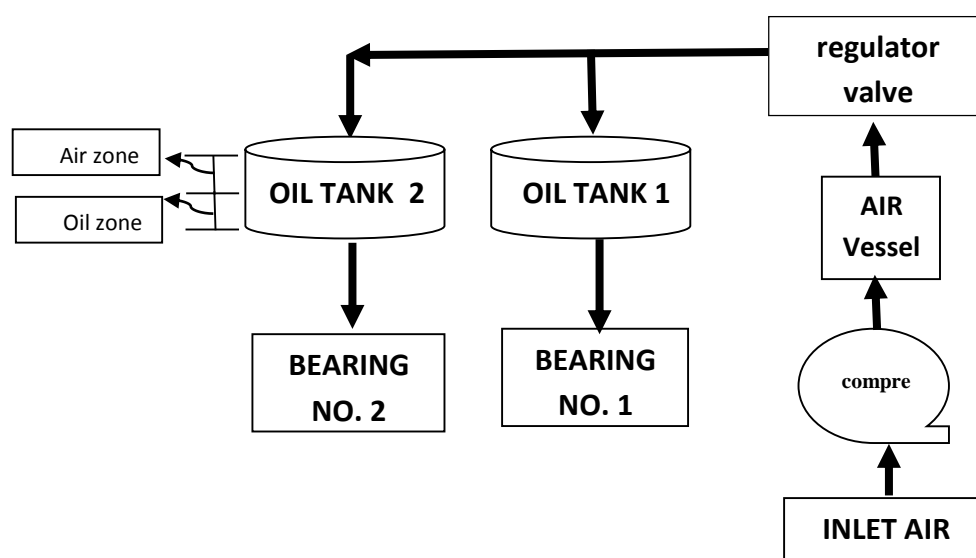
Input voltage	220-230
Frequency	50
HP	3
Input Current	8.4/4.9
RPM	2855-3426

Table (4.3) Specification of the inverter.

Input voltage	3Phase -220-230 V AC
Frequency	50-60 Hz
Output voltage	3Phase - 0 to input V AC
Output current	5 A
Frequency	0.1 - 400 Hz

4.6. The lubrication system: -

As mentioned previously, the rotor is supported by two journal bearings. These bearings should be lubricated continuously during the operation of the test rig. The lubrication system consists of the air compressor which pressurized air to an air vessel, the air pressure is controlled by regulating valve. The constant pressured air is moved via pipes to the closed oil tanks making the bearing deliver the oil at constant pressure. The lubrication system can be seen in figures (4.12), (4.13) and (4.14).

**Figure (4.12) layout of the lubrication system.**

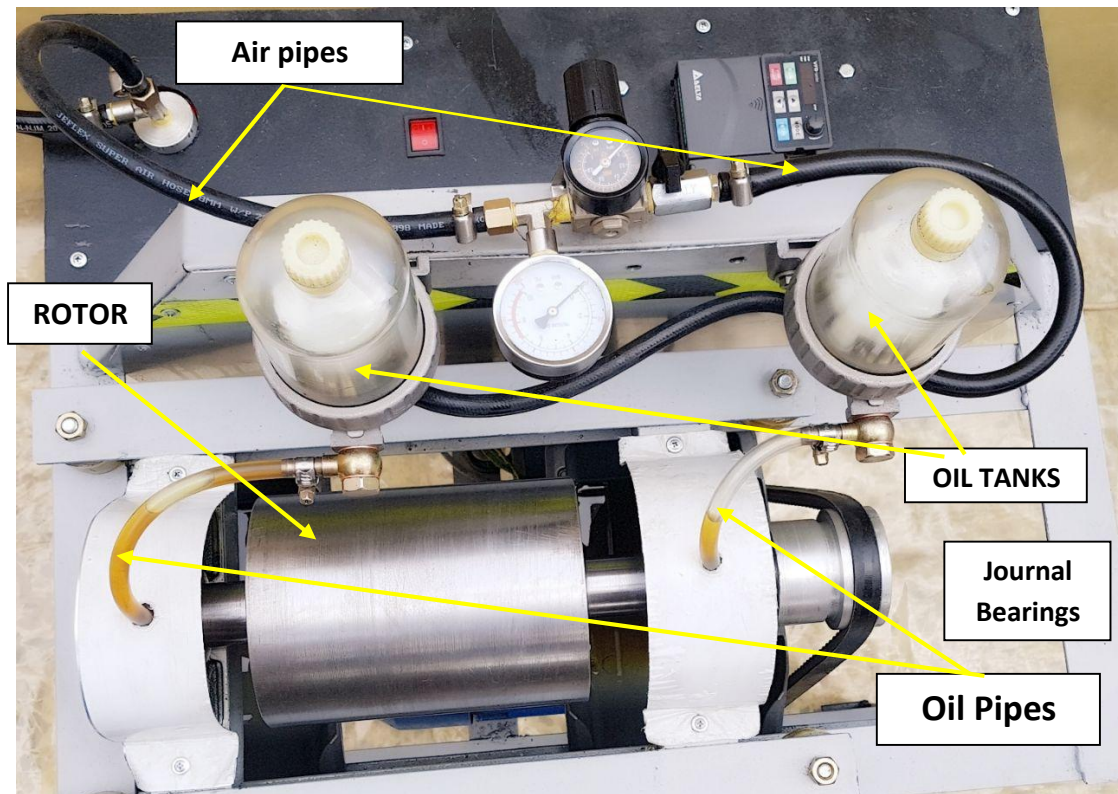


Figure (4.13) A view on the lubrication system of the test rig

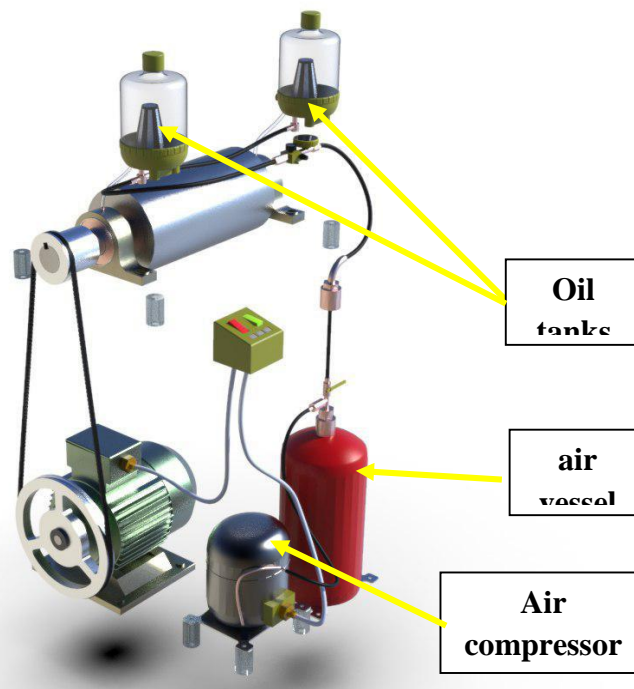


Figure (4.13) A general view on the lubrication system of the test rig

The oil that used for lubrication in the test rig is **SAE 10W** which has the specifications shown in Table (4.4).

Table (4-4): specifications of the oil SAE 10W

The Kinematical viscosity at 40 C° and at 20 C°	28 mm²/s and 104 mm²/s
The Dynamic viscosity at 40 C° and at 20 C°	0.032 Pa.s and 0.12 Pa.s
The density of oil at 40 C°	870 kg/m³

4.7. Journal bearings: -

The two journal bearings are made of brass, they are supported by external bushes to stand for higher loads. The diameter of the shaft is (38) mm, accordingly, the diameter of bushes should be greater than this value, a 0.2 mm clearance is selected for this aim. The length of the bush is 25 mm, with these dimensions, the bearing is considered as a short bearing where this was imposed in the analysis carried out in chapter three.

4.8. Measuring devices

The vibration of the rotor is measured by an accelerometer which is fixed on the housing of one of the journal bearing. The signal of the accelerometer is amplified by a charge amplifier, the signal then displayed and stored in a digital oscilloscope.

The accelerometer is of **352C68** type where its measurement limits are **491 m/s²**. The Figure (4.14) shows the acceleration used in the current work. The accelerometer is mounted rigidly on the bearing housing using glue, this is shown in figure (4.15). Accordingly, when the structure vibrates, the mass inside the accelerometer is vibrated which leads to change the resistance of the sensing element. This resistance change will form a signal which should be amplified and read to give the vibration specifications.

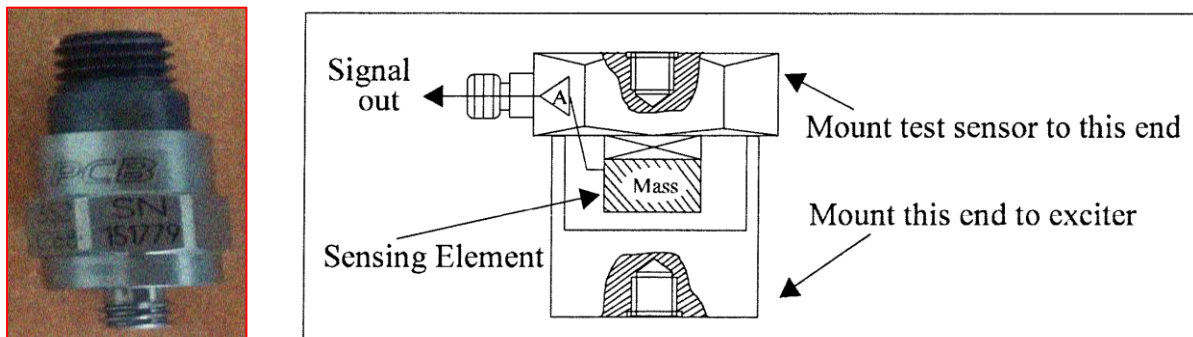


Figure (4.14) the accelerometer, left: outside photo, right: schematic diagram on its configuration

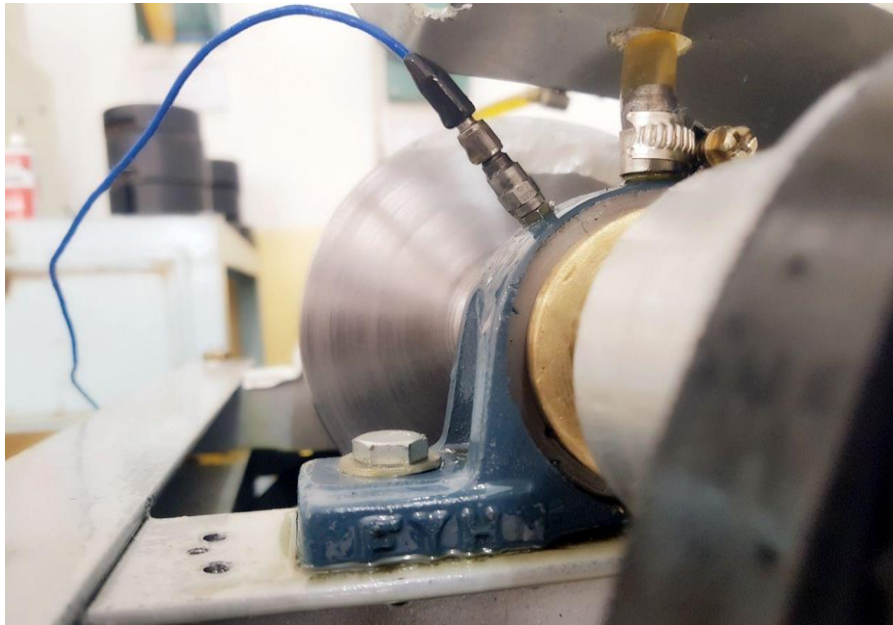


Figure (4.15) Mounting of the accelerometer.

The electric signal of the accelerometer has small amplitude which is amplified using charge amplifier of the model **480E09**. It was choosing. The signal is amplified proportional to the size of the wave. Amplification magnitude is depended on the possibility of displaying the oscilloscope screen, the amplification is often adjusted on the gain value of 10.



Figure (4.16) the Charge Amplifier instrument.

A digital oscilloscope is used in this work to display and store data of vibration wave. The vibration data are stored in spread sheets which can be analyzed and studied or can be stored as screen capture. The greatest sample rate that can be processed by the oscilloscope is **500 MSa/s.** and frequency of **200 MHz.** At any time after the experiments, the data can be exported from this device using USB memory data. Figure (4.17) shows the digital oscilloscope used in the current work.

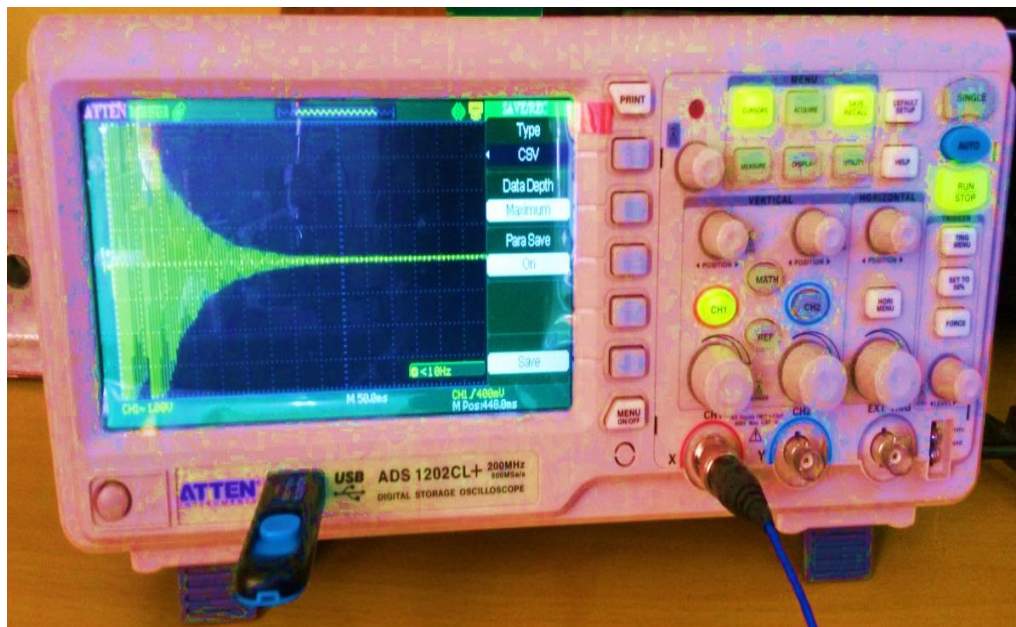


Figure (4.17) the Digital oscilloscope instrument.

4.9. Experiments procedure

In order to carry out a vibration experiment, the oil tanks should be filled with oil keeping a space for the compressed air at each tank. Then the compressor is turned on and the pressure is raised inside the pressure vessel. After that, the main air valve is opened and adjusting the valve regulator to 1.25 bar. When enough amount of oil flows through the journal bearings, the electric motor is turned on and is adjusted to particular speed with 1000 rpm step. After the experiments, the data is exported to the computer and analyzed using the **FFT** function that provided by Sig-View software. Figure (4.18) shows a signal of an experiments after processing using the Sig-View software. it can be seen in this figure the values of the response and the natural frequency is determined using this software.

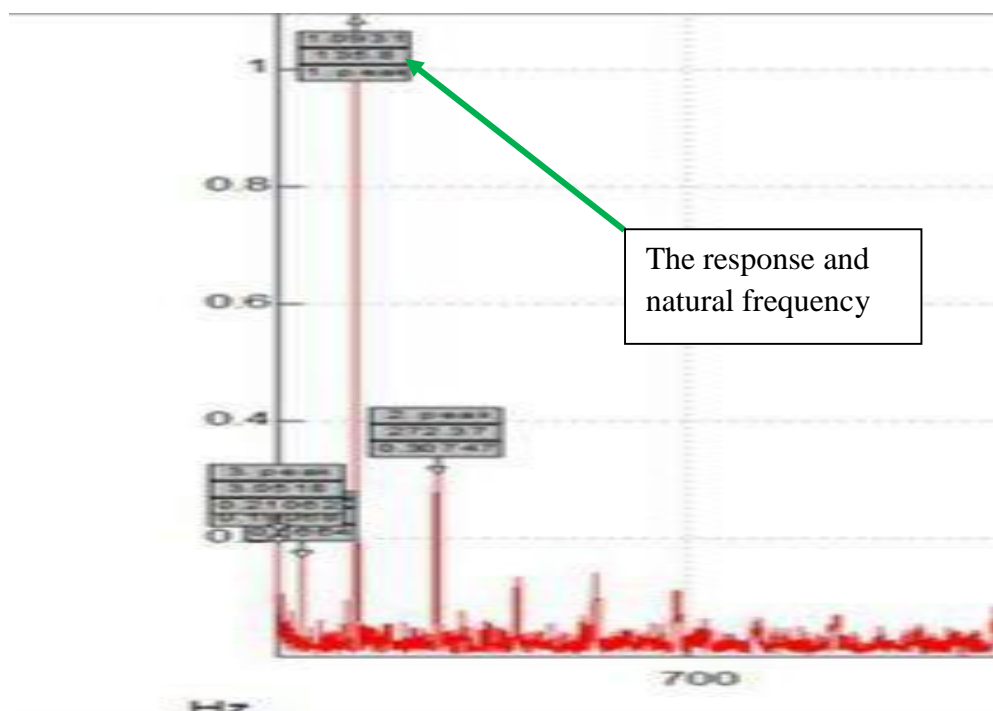


Figure (4.18) the vibration signal after processing using Sig-view software.

4.10. Cracks Creation

An important part in this work is studying the effect of existing cracks on the vibration of the rotors. The cracks are created at the shaft of the rotor using manual saw of 0.47 mm thickness which is shown in figure (4.19). this is approximately similar to that used in [30] where the saw has a thickness of (0.5) mm.



Figure (4.19) the saw used for crack creation.

The location of the cracks where selected at (8) mm apart from the disk, where the greatest stresses are induced at this position and depths of 0.2R and 0.4R were considered. Figure (4.20) shows the location of the 0.2R crack at the shaft of the rotor.

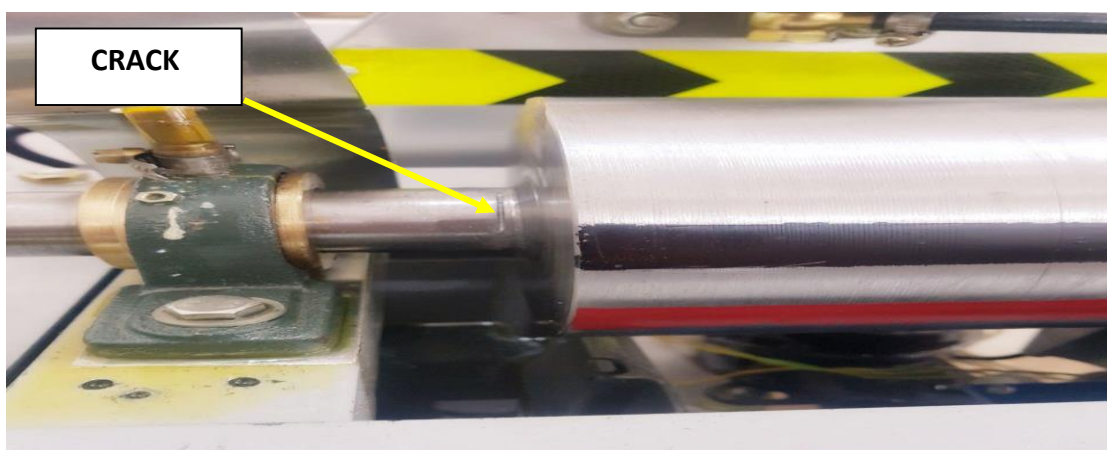


Figure (4.20) the location of the 0.2R crack depth

Chapter Five

Results and Discussion

5.1. Introduction: -

In this chapter, the results obtained from analytical, numerical, and experimental studies are illustrated, discussed, and compared in details.

The basis of the study was to found the effect of crack on vibration parameters, Analytical study was on the presence of a single crack, and the presence of two crack each one on the side from the disc.

The effect of crack on the rotor was studied numerically, experimental, and analytically. Changes in vibration parameters were observed when the depth of the incision was changed.

It is important to mention that the parameters of the journal bearings were estimated at each speed, the step of change of speed was (1000) RPM, because these variables dependent on the velocity of rotation, and as a result, the number of the Sommerfeld would change.

The results were compared, calculated and discussed the error ratio between the analytical and numerical and the experimental studies with regard to the critical speed and response.

5.2. Analytical Result of single cracked shaft:

5.2.1. The dynamic parameters of the rotor at journal bearings: -

The dynamic parameters are varied with the speed of rotation for the shaft due to changes in oil specifications between the shaft and the bush. The Parameters can be represented by stiffness and damping, where it was calculated in the horizontally, vertically, and cross section direction. It is worth mentioning that the dynamic parameters were found by the Matlab program.

The oil viscosity is (0.023 Pa. s), which works on the lubrication of the bearing of short type, the diameter of the bearing (38) mm and thickness (25) mm, and clearance (0.1) mm.

It was observed that there was no significant change in the parameters before reaching to change rate (1000) RPM, So the calculations will be based on a change of speed of (1000) step change.

In table (5.1) and table (5.2) it was displayed the results of the parameters of the stiffness and damping for the first and second bearings receptively, and their change with the speed of rotation. In Figure (5.1) it was explained the change of the parameters for the stiffness with changing the speed of rotation, and compare it with the figures (5.2) and (5.3) in the sources [30] and [39].

In Figure (5.4) it was explained the change of the parameters for the damping with changing the speed of rotation, and compare it with the figures (5.5) and (5.6) in the sources [30] and [39]. The results were realistic, where the curve behavior was very similar when compared.

Table (5.1) Stiffness and damping parameters for first bearing.

RPM	K_{xx1} $\times 10^3$ (N/m)	K_{xy1} $\times 10^3$ (N/m)	K_{yx1} $\times 10^3$ (N/m)	K_{yy1} $\times 10^3$ (N/m)	C_{xx1} $\times 10^3$ (N*S/m)	C_{xy1} $\times 10^3$ (N*S/m)	C_{yx1} $\times 10^3$ (N*S/m)	C_{yy1} $\times 10^3$ (N*S/m)
500	2310.5	-1834.5	-5285.7	6531.9	262.88	-435.98	-435.98	158.16
1000	2468.1	3706.9	-3028.6	4423.1	261.31	40.68	40.68	740.24
1500	2574.8	3446.3	-150.24	3509.2	221.31	-105.2	-105.2	491.96
2000	2653	3192.7	1056.7	2984.6	200.26	-230.31	-230.31	377.54
2500	2712.3	3022.3	1912.7	2644.3	187.41	-325.84	-325.84	313.43
3000	2758.1	3139.2	2302.5	2407.6	178.89	-428.58	-428.58	273.3
3500	2794.1	3248.4	2606.2	2235.6	172.9	-519.61	-519.61	246.32
4000	2822.8	3452.6	2925.4	2106.4	168.53	-611.75	-611.75	227.24
4500	2845.8	3653.5	3169.2	2007.1	165.25	-676.99	-676.99	213.23
5000	2864.5	3852.1	3495.2	1929.2	162.72	-726.34	-726.34	202.64
5500	2879.7	4249.1	3929.2	1867.1	160.73	-750.48	-750.48	194.45
6000	2892.4	4644.8	4292.5	1816.9	159.14	-774.61	-774.61	187.97
6500	2902.9	5039.6	4824.2	1775.7	157.85	-801.69	-801.69	182.78
7000	2911.8	5433.7	5278.6	1741.7	156.79	-810.85	-810.85	178.55
8000	2925.6	6220.4	6158.2	1689.2	155.17	-828.54	-828.54	172.14
9000	2935.8	7005.7	6950.5	1651.2	154.02	-833.62	-833.62	167.61

Table (5.2) Stiffness and damping parameters for second bearing.

RPM	K_{xx1} $\times 10^3$ (N/m)	K_{xy1} $\times 10^3$ (N/m)	K_{yx1} $\times 10^3$ (N/m)	K_{yy1} $\times 10^3$ (N/m)	C_{xx1} $\times 10^3$ (N*S/m)	C_{xy1} $\times 10^3$ (N*S/m)	C_{yx1} $\times 10^3$ (N*S/m)	C_{yy1} $\times 10^3$ (N*S/m)
500	1767.6	-4724.9	-1948.7	8188.7	247.10	-177.39	-177.39	279.46
1000	2299.9	4886.9	-4404.4	3908.9	252.48	-222.40	-222.408	682.03
1500	2399.7	9747.5	-4299.2	3101.9	215.01	-155.13	-155.13	456.49
2000	2471.8	1419.1	-4321.8	2641.7	195.41	-119.45	-119.45	352.81
2500	2525.7	1843.2	-4419.6	2345.7	183.53	-974.05	-974.05	294.91
3000	2566.7	2256.2	-4569.0	2141.3	175.70	-823.44	-823.44	258.81
3500	2598.6	2662.5	-4757.2	1994.0	170.24	-713.59	-713.59	234.64
4000	2623.6	3064.6	-4975.7	1884.3	166.28	-629.73	-629.73	217.61
4500	2643.5	3463.8	-5218.5	1800.6	163.32	-563.53	-563.53	205.16
5000	2659.5	3861.1	-5481.0	1735.3	161.05	-509.91	-509.91	195.79
5500	2672.4	4256.9	-5760.0	1683.6	159.28	-465.56	-465.56	188.55
6000	2683.1	4651.8	-6052.5	1642.0	157.87	-428.28	-428.28	182.86
6500	2691.9	5045.9	-6356.4	1608.0	156.73	-396.49	-396.49	178.30
7000	2699.3	5439.4	-6670.0	1580.1	155.79	-369.06	-369.06	674.60
8000	2710.7	6225.2	-7320.7	1537.2	154.37	-324.15	-324.15	1690.1
9000	2719.1	7009.8	-7995.8	1506.4	153.36	-288.93	-288.93	165.07

From Figure (5.1), it was observed the curves behavior similar to the curves behavior of the Figures (5.2) from [30] and (5.3) from [39]. The continuous increase in the cross coupling components was observed with increasing rotational speed in Figure (5.1), and stability of the (K_{xx}) and (K_{yy}) components values of high velocity. This indicates that the stresses in the cross coupling axes are higher and are prone to failure. The reason for increased stiffness in the cross coupling direction was explained, and it was that the increased oil pressure leads to resulted in an increase in oil density and This results in an increase in hardness. A negative signal is Indicate that the force direction reversed what was imposed.

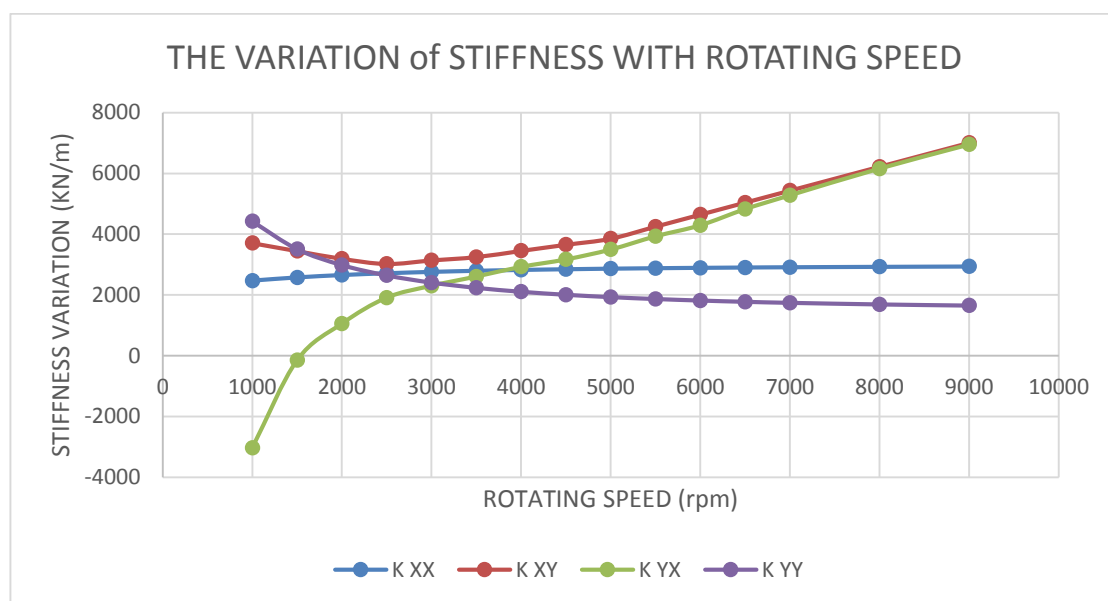


Figure (5.1) The variation of stiffness with rotating speed for the current work.

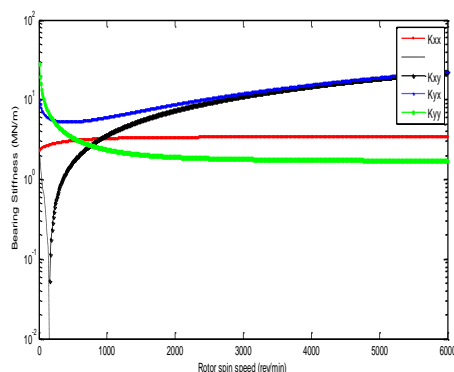


Figure (5.2) The variation of stiffness with rotating speed, [30].

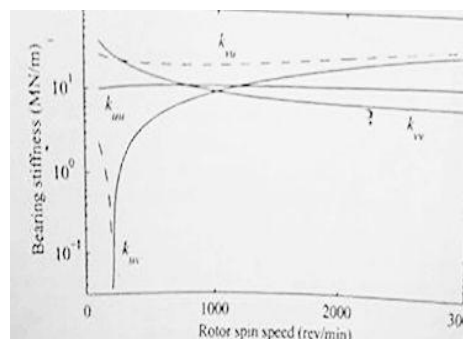


Figure (5.3) The variation of stiffness with rotating speed, [39].

From Figure (5.4), it was observed that the curves behavior similar to the curves behavior of the Figures (5.5) in [30] and (5.6) in [39]. It was observed the stability of all damping compounds after the rotation speed (6000) RPM.

The reason for the negative signal of (C_{xx}) and (C_{yy}) indicates that the speed of the oil is decreasing, where the damping depends on the speed. The reason for the decrease in the speed of oil is to increase the pressure, where the kinetic energy turns to a latent energy, and this justifies the increase of the potential energy Represented by (K_{xx}) and (K_{yy}).

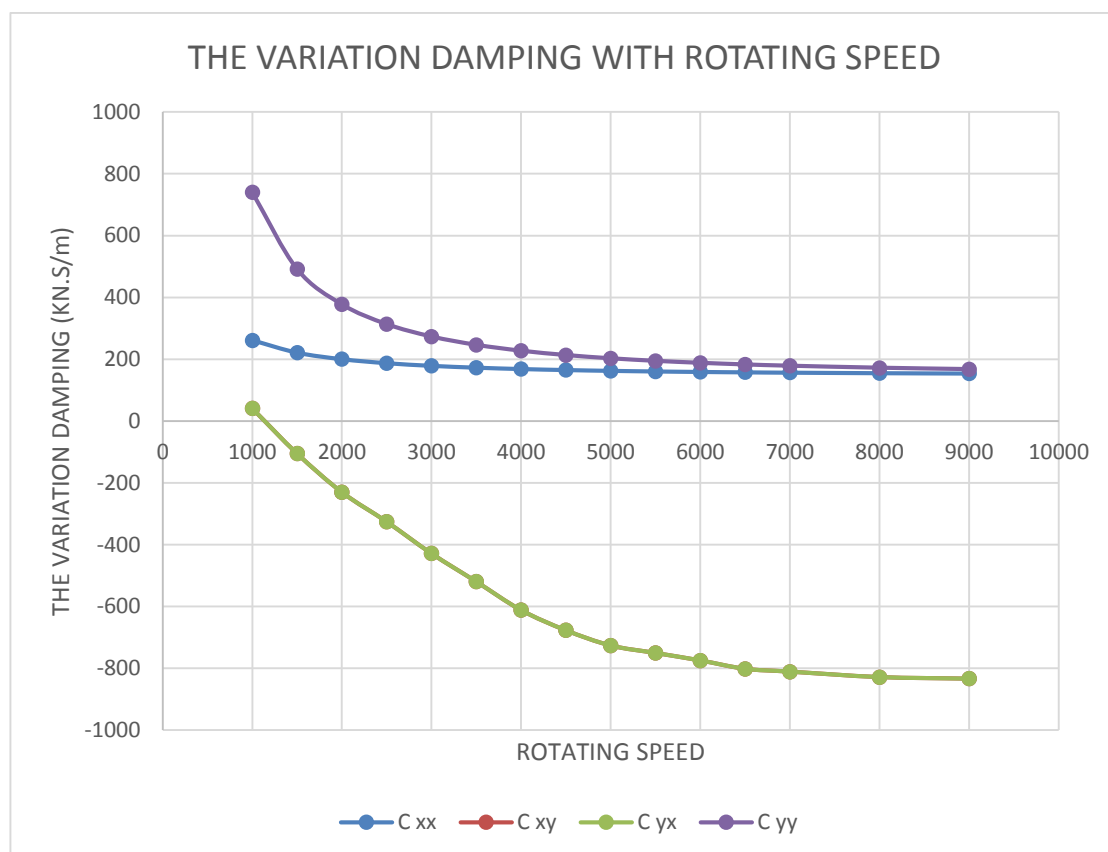


Figure (5.4) The variation of damping with rotating speed.

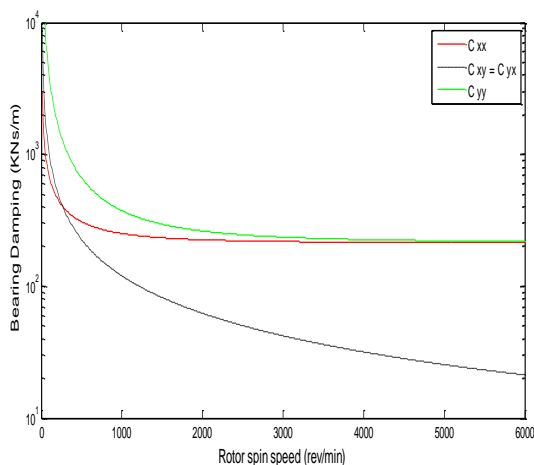


Figure (5.5) The variation of damping with rotating speed, [30].

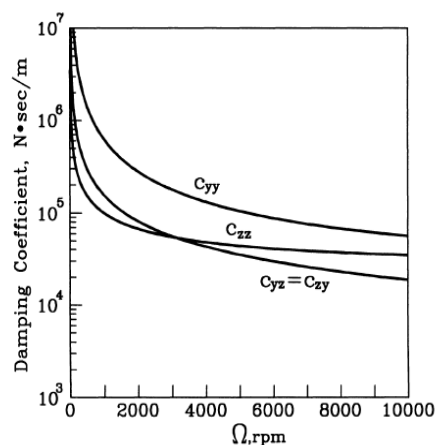


Figure (5.6) The variation of damping with rotating speed, [39].

5.2.2. the dimensionless compliance for a single crack in shaft: -

The value of dimensionless compliance depends on the type of crack, as well as crack site. Bending moment will generate two areas of stresses, tensile stresses and compression stresses, When the crack is lies in the tensile area, the flexibility will increase because the area of the cross section will decrease.

In Ref[1], the dimensionless compliance was calculated in the vertical (\bar{C}_{55}) and cross coupling directions (\bar{C}_{44}), depending on the ratio ($\mathbf{a/R}$), Where the ratio of ($\mathbf{a/R}$) is less than ($\mathbf{0.5}$) then the value of (\bar{C}_{44}) is neglected because it is few compared to (\bar{C}_{55}). **Figure (5.7)** shows the behavior of the dimensionless compliance with ($\mathbf{a/R}$).

The values of the dimensionless compliance in vertical and cross coupling directions in Appendix C.

It was observed from Figure (5.7) that when the ratio of (a / R) is less than (0.5), the (C_{44}) is very small so it will be neglected.

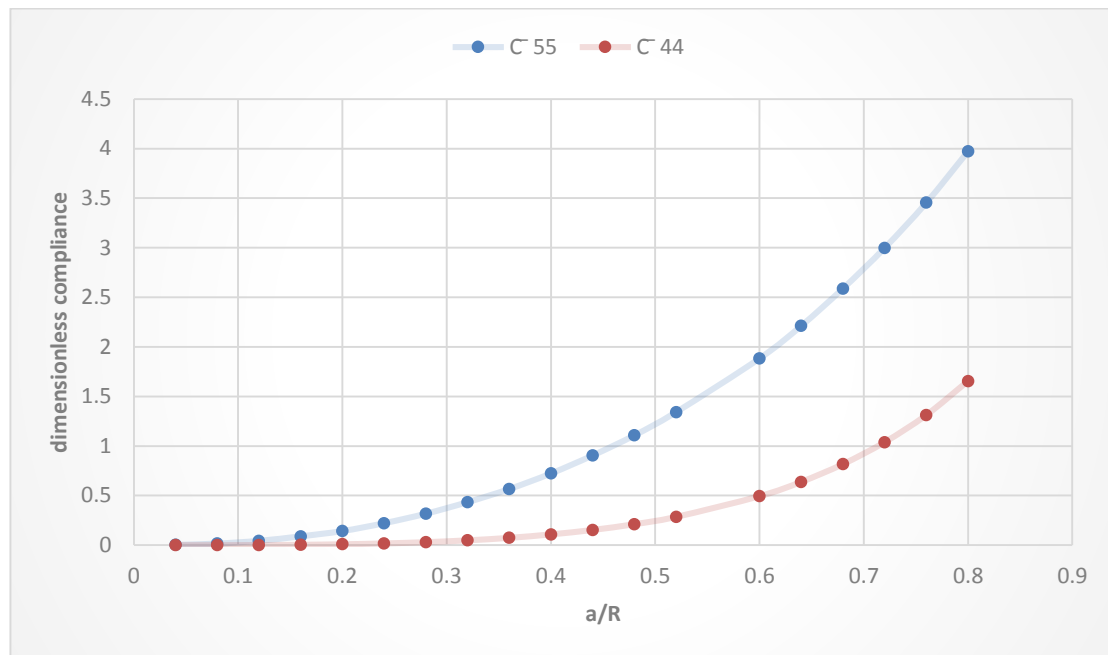


Figure (5.7) The dimensionless compliance with ratio of crack depth.

5.2.3. Detecting of a crack by the shape of Orbit: -

The orbit is a pathway formed by two compounds of response, in horizontal and vertical direction, for point on the shaft. The reason for the formation of orbit is due to the presence of unbalance in the elements of the distributed mass in rotor. The unbalanced forces depend on the speed of rotation of the shaft, the unbalance mass, and the position of the unbalance mass about the center of shaft. Many factors affect the response of the shaft which determine the shape of the orbit, these factors include the speed of rotation, the stiffness, the damping, the depth of the crack, the number of crack, the weight of the shaft and its dimensions.

The Matlab program was used to find the shape of the orbit and in different depths (UNCRACK,0.2R,0.4R,0.6R,0.8R). from the orbit

pathways in **Figure (5.8)**, it is clear that when the depth of the crack increases, the volume of the orbit increases also, and this is a good indication of the presence of the crack in the rotor.

When the depth of the crack is increased, the rotor hardness in the crack zone will decrease, it is giving more area for movement about axis of the shaft, this leads to an increased size of orbit path

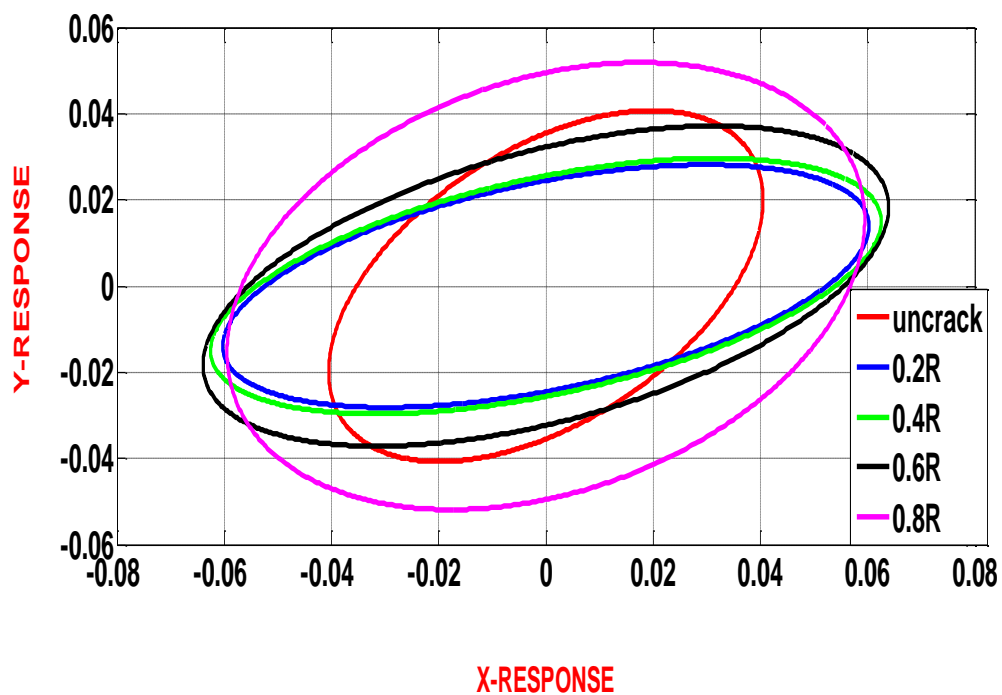


Figure (5.8) The Orbit path for different depths.

5.2.4. The response for cracked and uncracked shaft

The most important vibration components that give a good indicator of the existence of crack are the response and critical speed, So the focus will be on the response and critical speed in analytical analysis as well as in numerical analysis and experimental analysis.

In analytical study it was found that when the depth of the crack increased, the shaft stiffness will decrease, leading to a decrease in critical speed because it depends on the stiffness and mass. the response would increase with a decrease in critical speed, and this is shown in **Figure (5.9)**. It was noted that the percentage of variation between **uncrack** test and **(0.8R)** crack test is about **(15.69%)** for critical speed and **(39.79%)** for response.

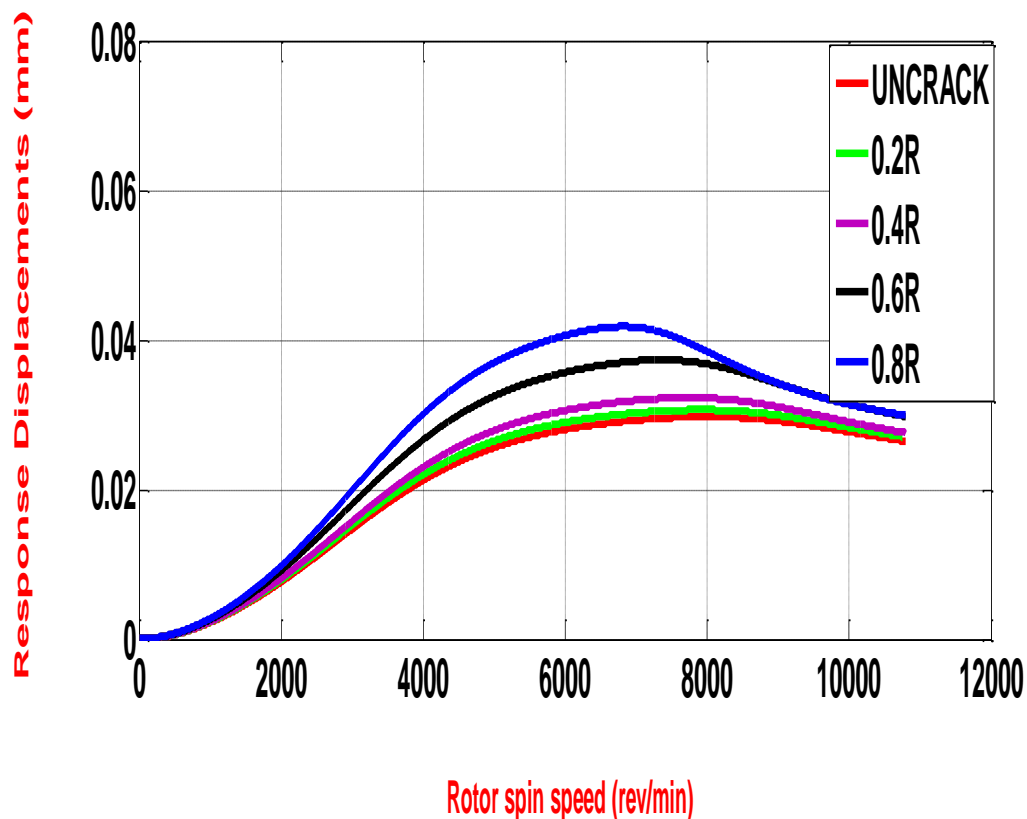


Figure (5.9) The Response rotor with multiple depths for crack.

Table (5.3) The values of response and critical speed with different crack depths.

CRACK DEPTH RATIO	CRITICAL SPEED (RPM)	RESPONSE (mm)
UNCRACK	8125	0.029507
0.2R	7925	0.03069
0.4R	7750	0.03231
0.6R	7370	0.03732
0.8R	6850	0.04125

5.3. The Results of numerical analysis of rotor have single crack: -

5.3.1. The natural frequency of rotor: -

The natural frequencies of the rotor for the first six modes were determined. The ANSYS software was used, the six values shown at the bottom of **Figure (5.10)** are natural frequencies. There are two benefits to finding natural frequencies, the first is to ensure from the results of the first models of the rotor by comparison the experimental with numerical, and these results are proving that the model will give correct results to another cases. The second benefit is to ensure that natural frequencies close to the critical speed, where the greatest response to the rotor is occurs.

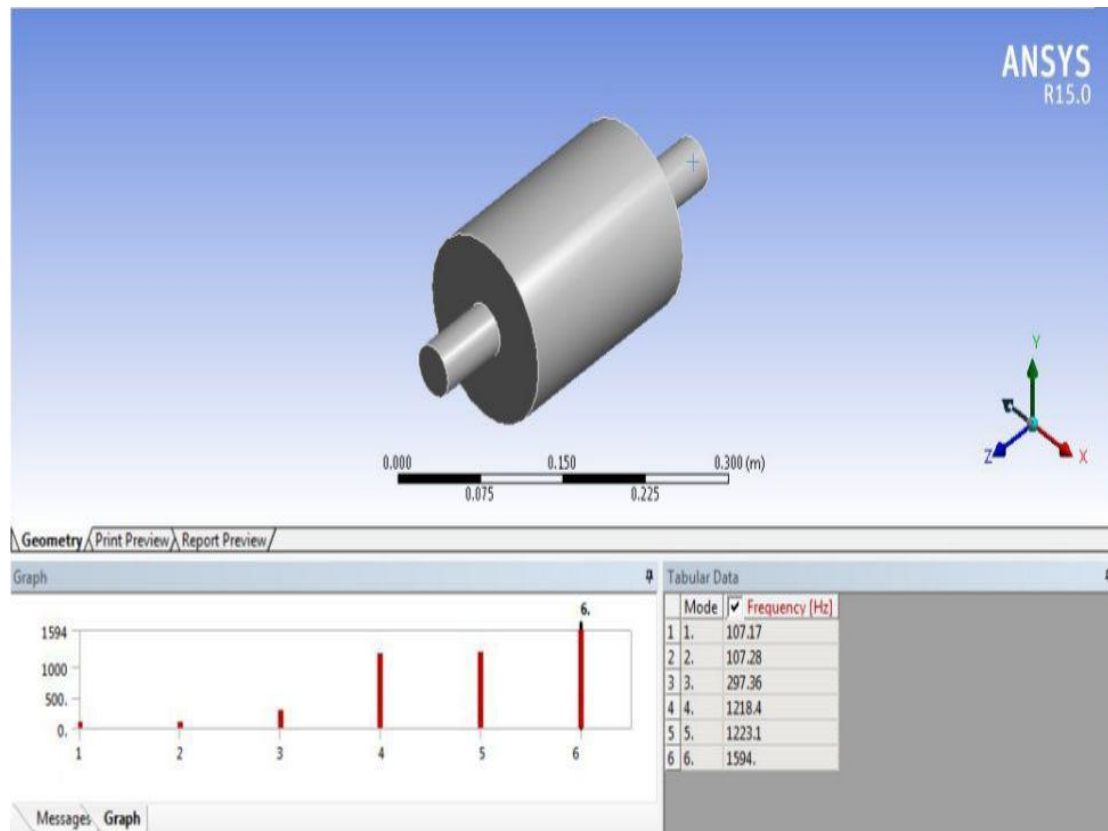


Figure (5.10) The Natural frequencies of the first six-modes.

Table (5.4) The values of natural frequencies.

Number of modes	Natural Frequencies (HZ)
first Mode	107.28
second Mode	297.36
third Mode	1223.1
fourth Mode	1594

5.3.2. The response for uncracked and cracked shaft:

The behavior of the response with the change of critical velocity due to the change of the depth of the crack, is very important to detect the crack in rotary systems.

The response was known as the critical velocity of several depths of the crack (**uncrack,0.2R,0.4R,0.6R,0.8R**) as shown in the figures (5.11) to (5.16), then it was compared the numerical results with the analytical results, and were excellent.

It was noted that the percentage of variance between **uncrack** test and (**0.8R**) test about critical speed and response is (**7.97%**) and (**19.74%**) sequentially.

The error value in uncrack test between analytical analysis and numerical analysis relative to the critical velocity and response is (**0.3%**) and (**7.31%**) respectively.

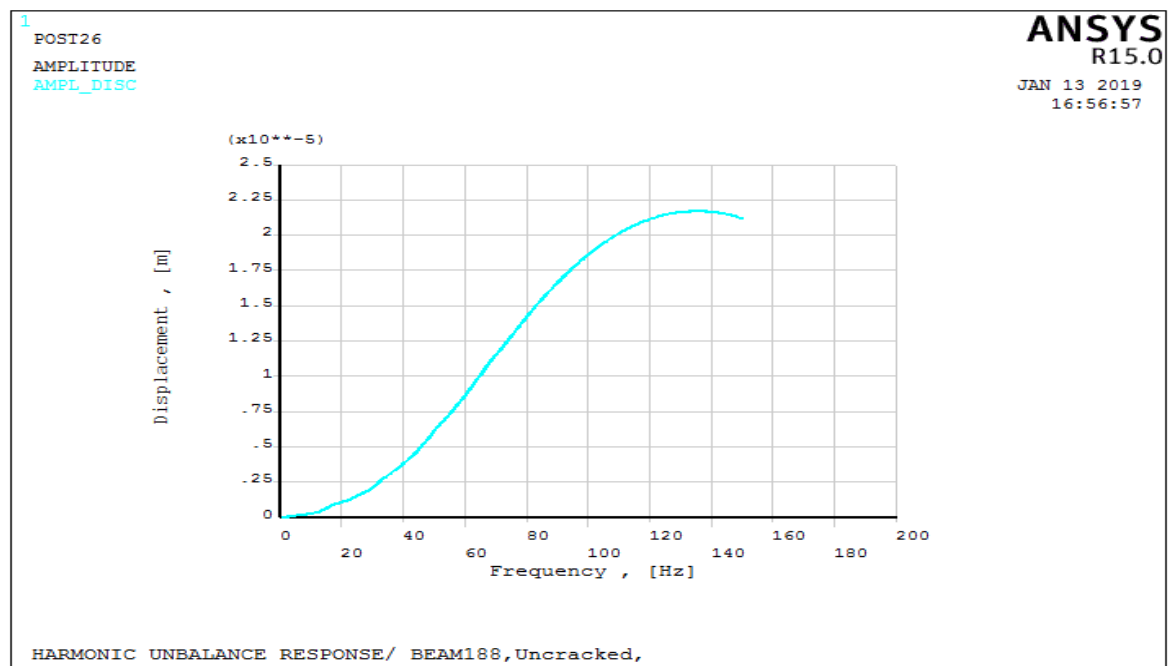


Figure (5.11) the response behavior in uncracked shaft.

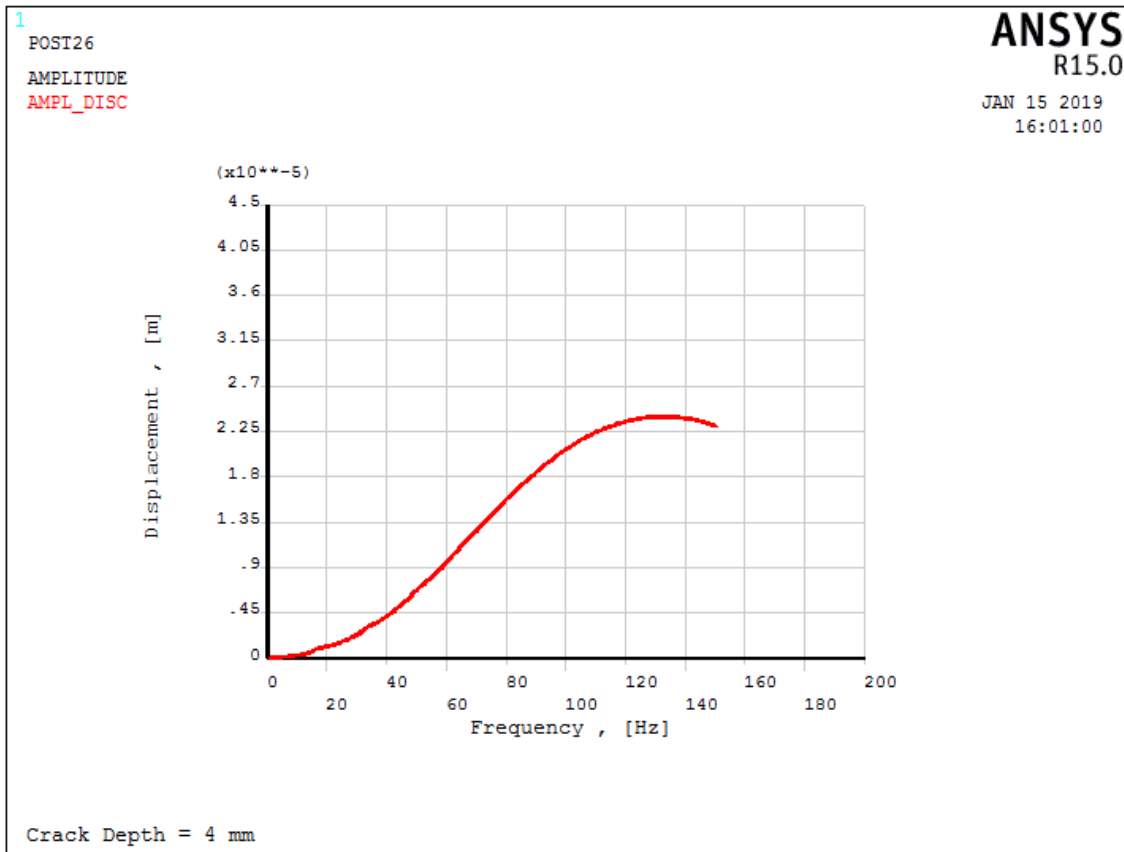


Figure (5.12) the response behavior at (0.2R).

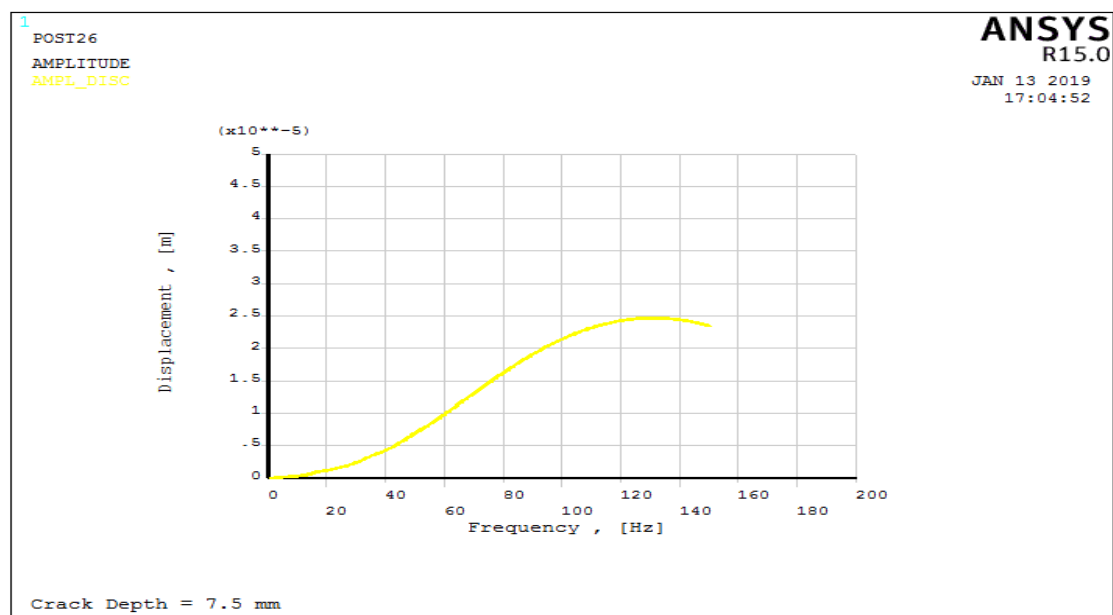


Figure (5.13) the response behavior at (0.4R).

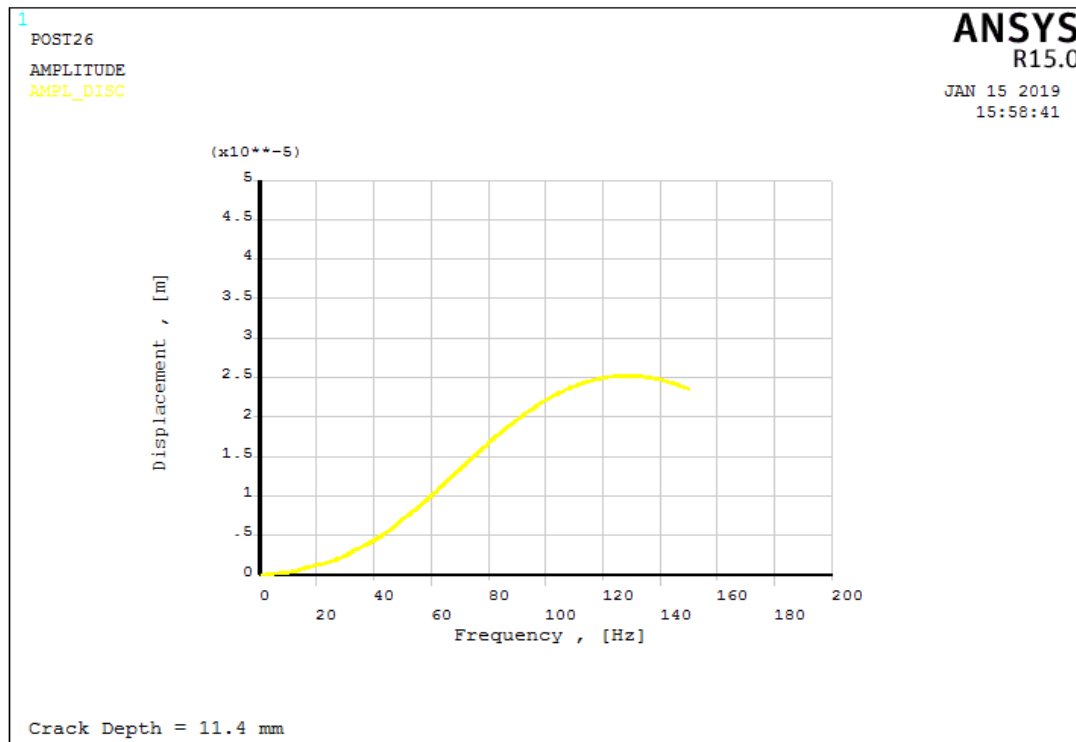


Figure (5.14) the response behavior at (0.6R).

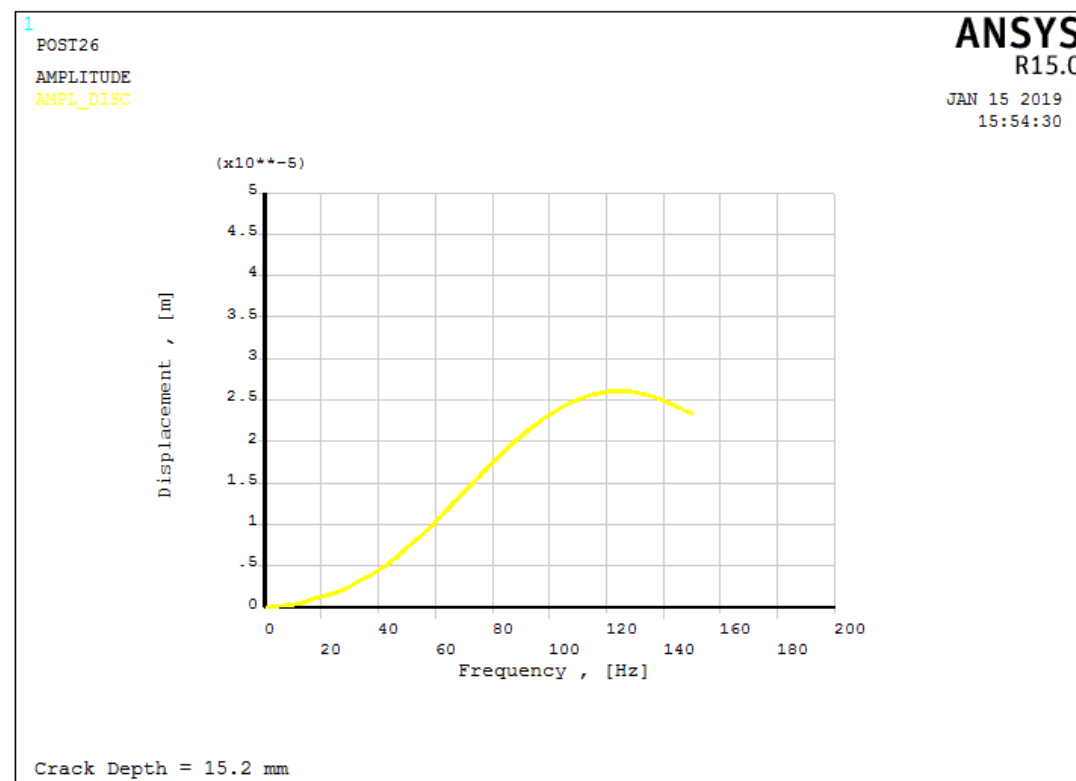


Figure (5.15) the response behavior at (0.8R).

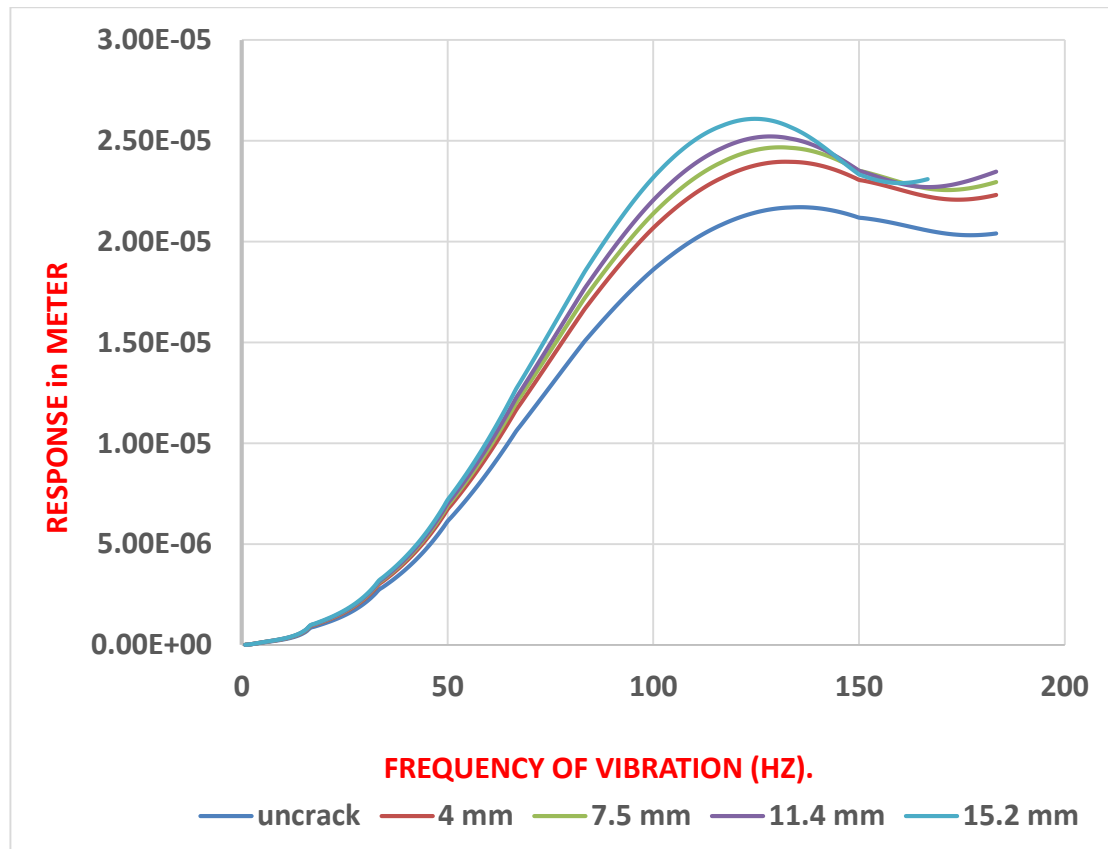


Figure (5.16) the response behavior with different depths.

Table (5.5) The values of response and critical speed with different crack depths.

CRACK DEPTH RATIO	CRITICAL SPEED (RPM)	RESPONSE (mm)
UNCRACK	8150	0.021789
0.2	7900	0.023969
0.4	7849	0.0246815
0.6	7699	0.0252251
0.8	7500	0.026092

5.4. The Experimental Results of rotor have single crack: -

5.4.1. Free vibration test of uncracked rotor: -

The natural frequency was found by the Hammering test, where the results were close to the results of the numerical analysis. The percentage of error between Experimental work and the numerical analysis in the second mode and the third mode and the fourth mode were **(14.245%)** and **(13.58%)** and **(10.60%)** sequentially.

The reason for the difference between numerical analysis and experimental analysis is the difference in the type of fixed of shaft ends, where are a Simply supported type in numerical analysis and journal bearing in experimental analysis, and it was given different values to stiffness and damping factors. Figure (5.17) and (5.18) shows the signal obtained from the vibration test.

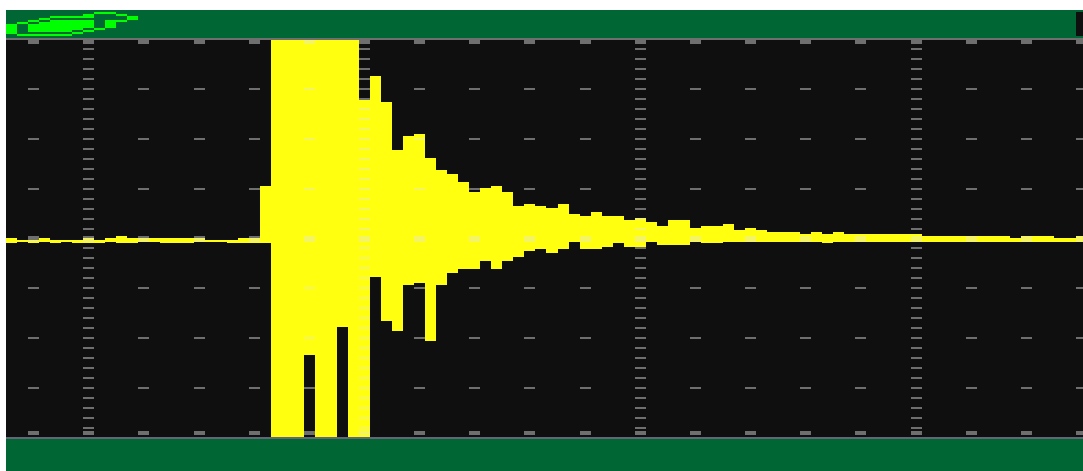


Figure (5.17) the Vibration wave from Hammering test.

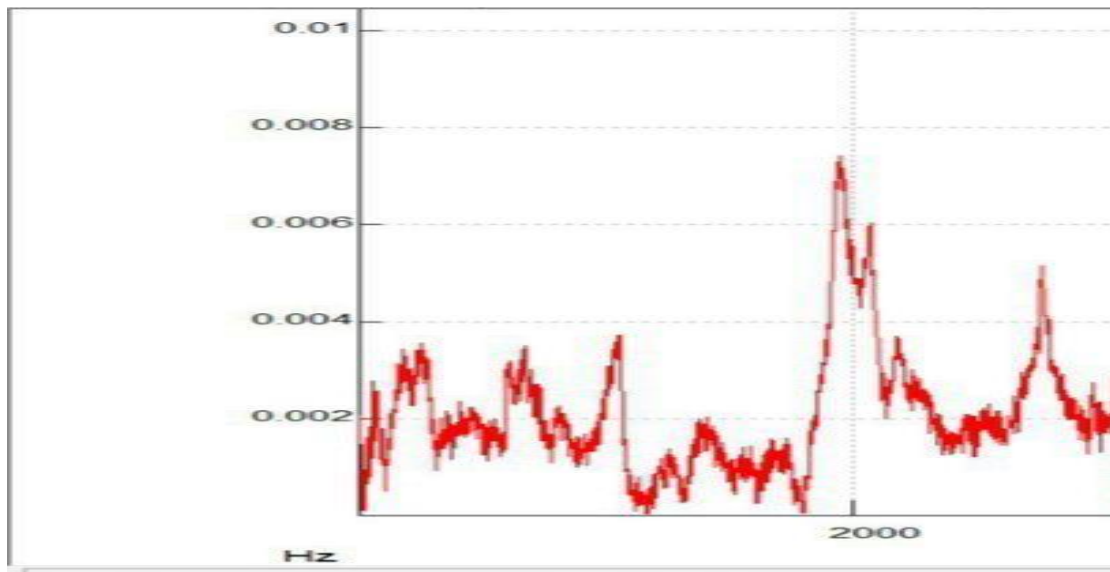


Figure (5.18) the Vibration wave processed by FFT.

Table (5.6) Comparison of natural frequencies between experimental and numerical results

Number of modes	Natural Frequencies (numerical analysis)	Natural Frequencies (Experimental work)
first Mode	107.28	90.3
second Mode	297.36	255
third Mode	1223.1	1057
fourth Mode	1594	1425

5.4.2. The response for uncracked and cracked shaft:

In the experimental work, an accelerometer mounted on the journal bearing was used to measure vibration parameters, Then the signal transferred to the amplifier and then to the oscilloscope. The wave data from the oscilloscope were taken, and it can be shown as a variable vibration wave with time, Where the acceleration is shown in the form of a small voltage, where each **(1) millivolt** is equal to **(10.17 m / s ^ 2)**, The acceleration value will be variable with time.

The data will be exported to the Sigview software, to process the wave by (Fast Fourier Transform **FFT**) to convert the domain from time to frequency, so it will be get acceleration variable with frequency.

The frequency of the wave at the crack site is the same as at the accelerometer site, but the response is uneven because the load is variable from the disc to the bearing on the shaft, where the bearing site is a value lower. So the values of the frequencies will be real, and acceleration values are as the indication of the variable response when the crack site.

Three tests were performed, at **uncracked** shaft, (**a/R= 0.2**), and (**a/R=0.4**). Below are the results of the three tests in **Table (5.7)**. It was found that the critical velocity at (uncrack shaft), (0.2R) and (0.4R) are **(7900) RPM**, **(7750) RPM**, and **(7500) RPM** respectively, and the acceleration are **(10.291) m/s²**, **(11.5043) m/s²** and **(12.4429) m/s²** sequentially. It was observed the descent in critical velocity with the expected rise in response at increasing crack depth.

Table (5.7) The values of acceleration in (m/s^2) with different crack depths.

RPM	UNCRACK	0.2R	0.4R
1000	0.1006	0.1025	0.1259
2000	0.2956	0.3001	0.34546
3000	0.917	1.0575	0.917
4000	1.5475	1.5912	2.7037
5000	1.8263	1.9011	5.3912
6000	2.0756	3.3551	8.1609
7000	3.9488	5.5485	9.9491
7500	8.2662	9.237	12.4429
7750	9.4575	11.5043	12.0581
7900	10.291	10.8119	11.8732
8250	8.3456	9.0841	11.0313
8500	6.6972	7.8675	10.7873
9000	5.1918	5.766	6.8758

The increase in acceleration with increased depth of the crack confirm the increased Variable displacement around the shaft axis. To continue the locking and opening cases during the cycle, it is necessary to increase the speed of motion at crack zone to complete the cycle, and this generates an increase in acceleration.

Note from **Figure (5.19)** that the curve **(0.4R)** is moving away from **(0.2R)** more than estrangement of curve **(0.2R)** from **uncrack** curve, this is because the decrease in area of the cross section is higher in the case of **(0.4R)** from **(0.2R)**.

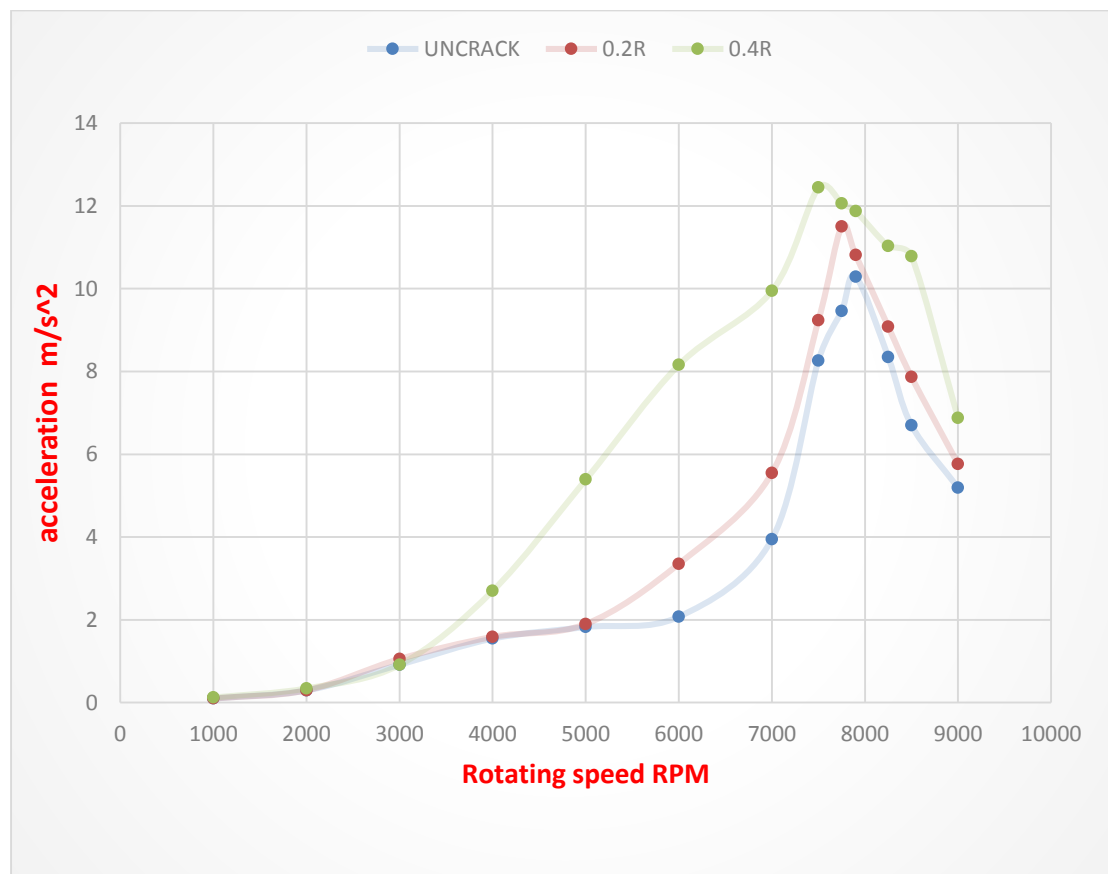


Figure (5.19) the acceleration behavior with different depths.

Table (5.8) The Critical speeds values to several depths of all analyses.

Crack Depth tests	Critical speed in analytical analysis	Critical speed in Numerical analysis	Critical speed in experimental work	The error value between experimental and analytical analysis	The error value between experimental and Numerical analysis
Uncrack test	8125	8150	7900	2.78%	3.07%
0.2R test	7925	7900	7750	2.21%	1.89%
0.4R test	7750	7849	7500	3.23%	4.45%

The following below are part from the Figures of vibration waves for **uncracked** shaft, and part from waves Figures after processing by (FFT), and all these from **Figure (5.20) to (5.23)**.

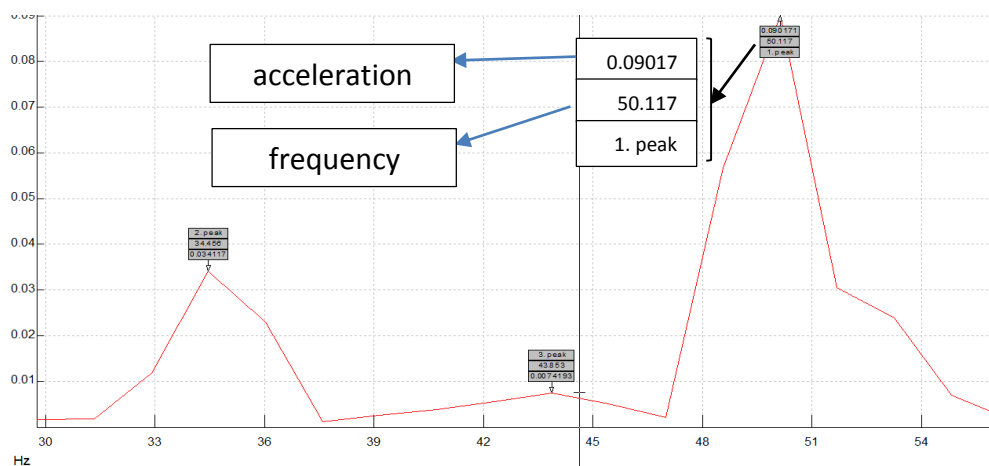


Figure (5.20) the vibration wave at 3000 RPM after processing by (FFT)

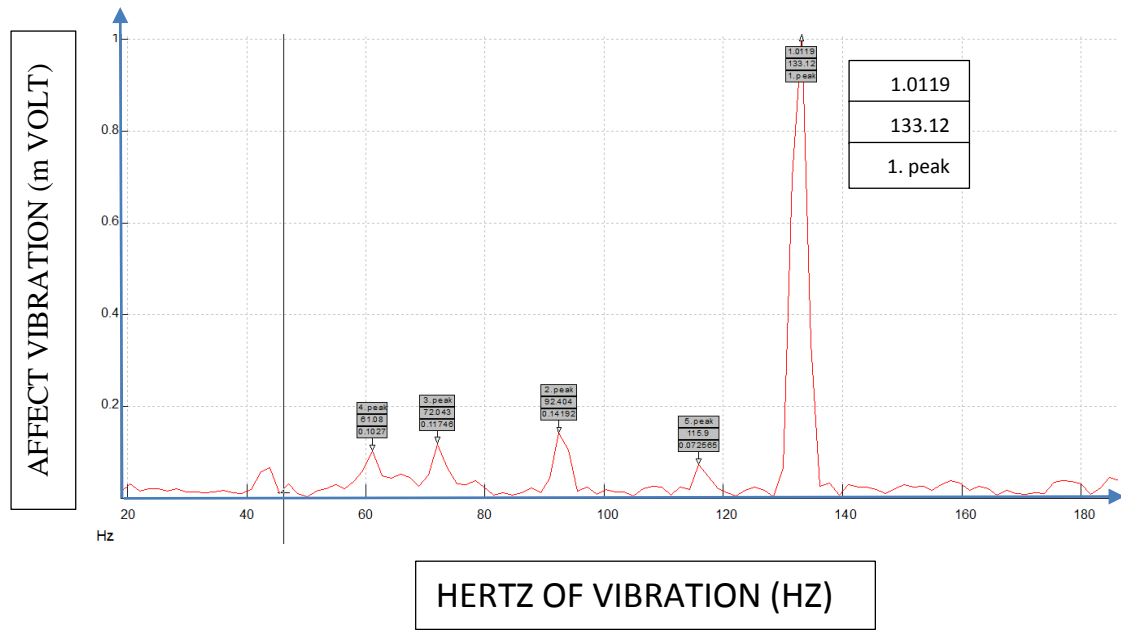


Figure (5.21) the vibration wave at 7900 RPM after processing by (FFT)

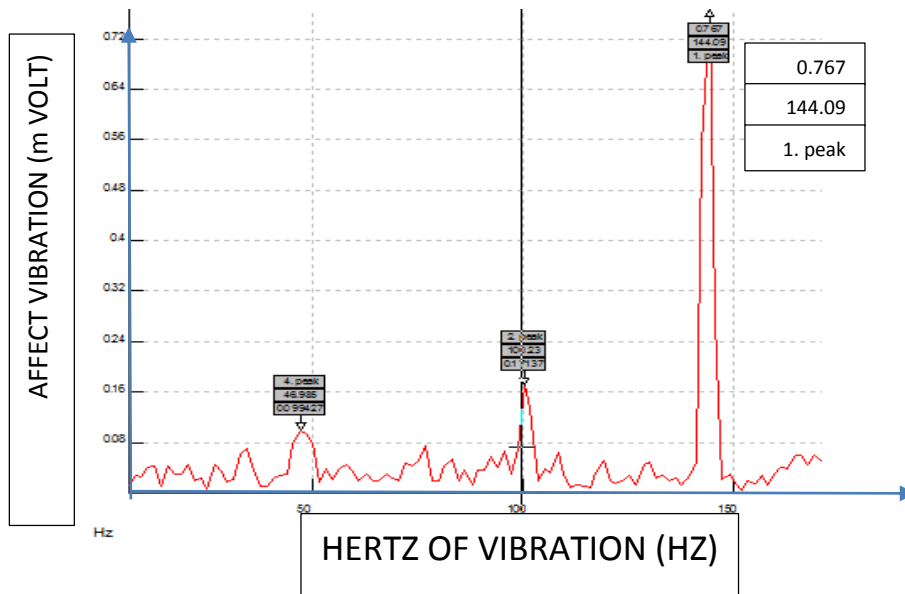


Figure (5.22) the vibration wave at 9000 RPM after processing by (FFT)

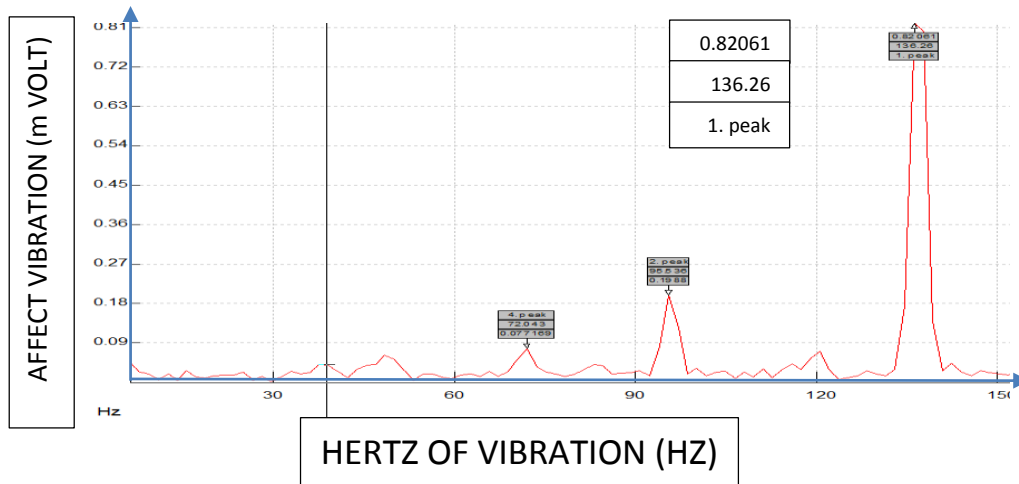


Figure (5.23) the vibration wave at 8250 RPM after processing by (FFT)

The following below are part from the Figures of vibration waves for ($a/R=0.2$) test, and part from waves Figures after processing by (FFT), and all these from **Figure (5.24) to (5.26)**.

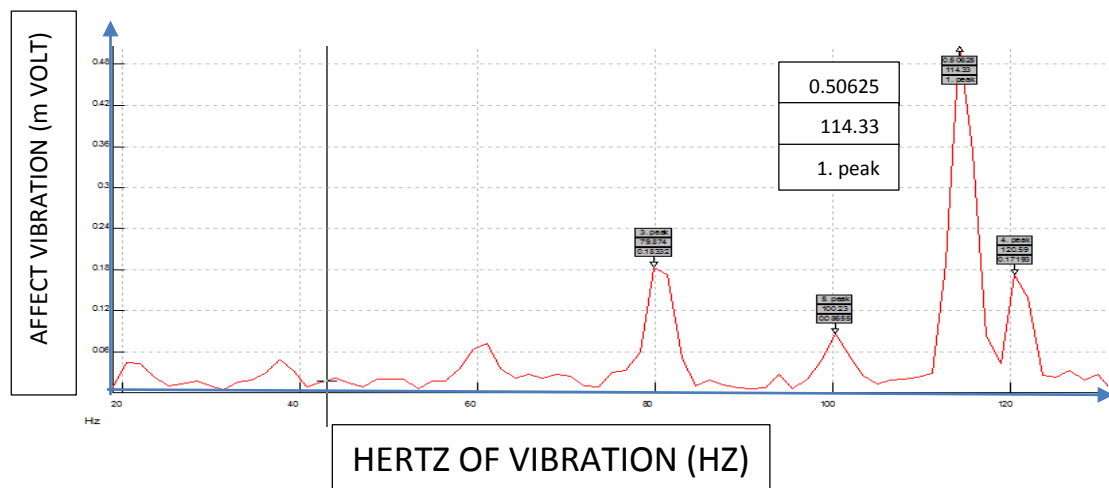


Figure (5.24) the vibration wave at 7000 RPM after processing by (FFT).

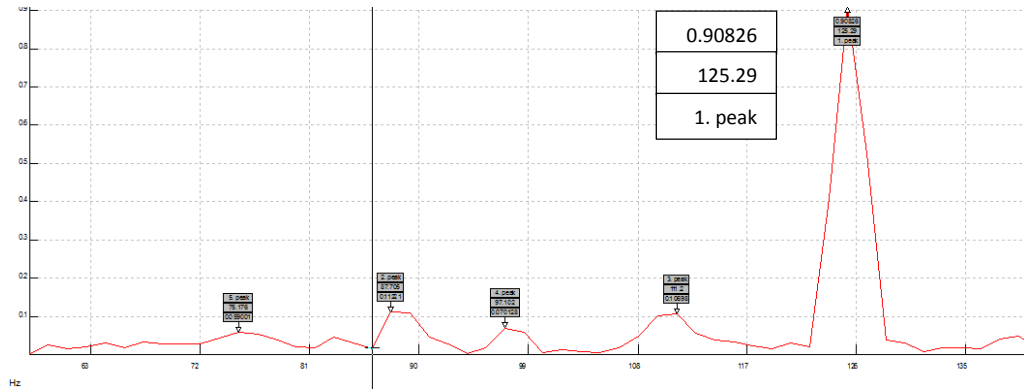


Figure (5.25) the vibration wave at 7500 RPM after processing by (FFT).

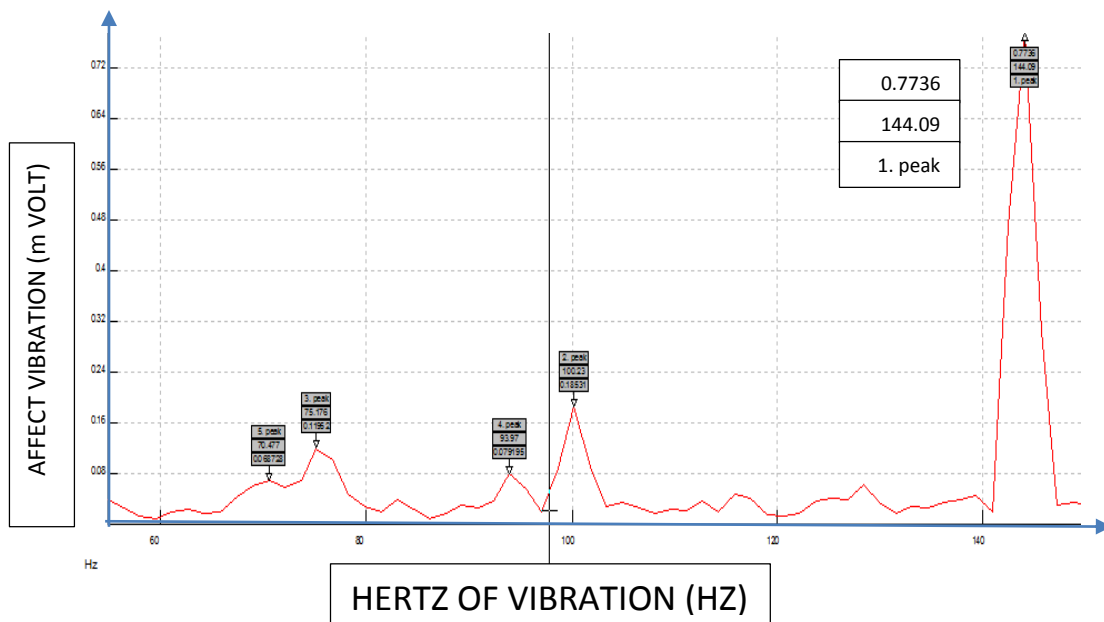


Figure (5.26) the vibration wave at 8500 RPM after processing by (FFT).

The following below are part from the Figures of vibration waves for ($a/R=0.4$) test, and part from waves Figures after processing by (FFT), and all these from **Figure (5.27) to (5.29)**.

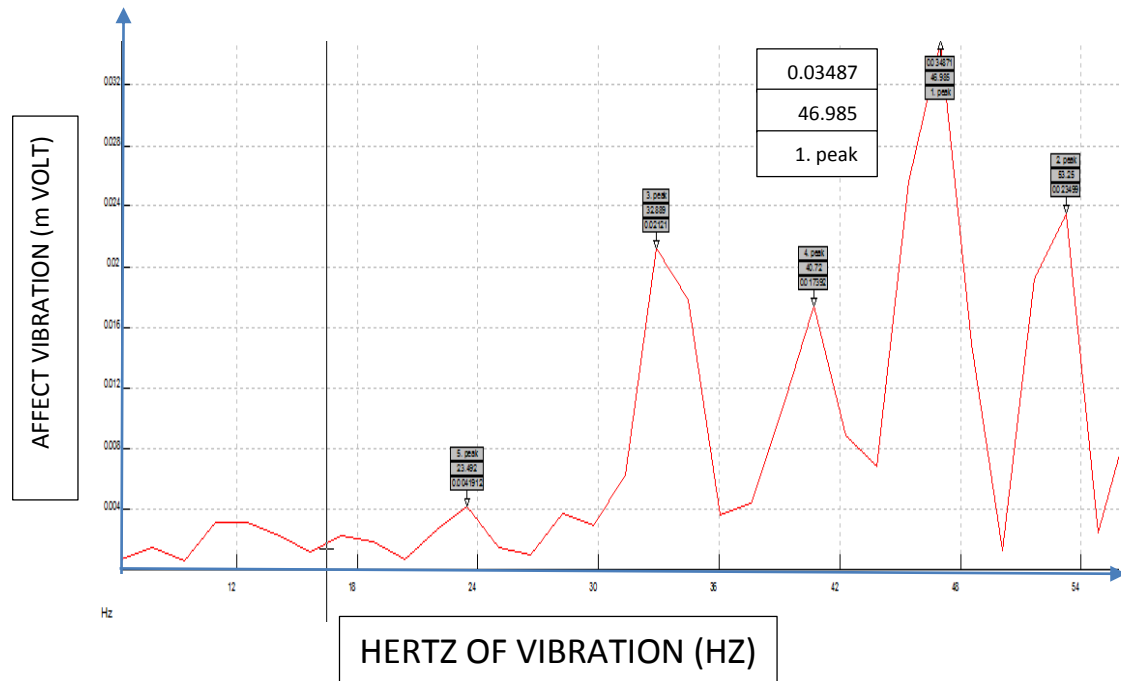


Figure (5.27) the vibration wave at 2000 RPM after processing by (FFT).

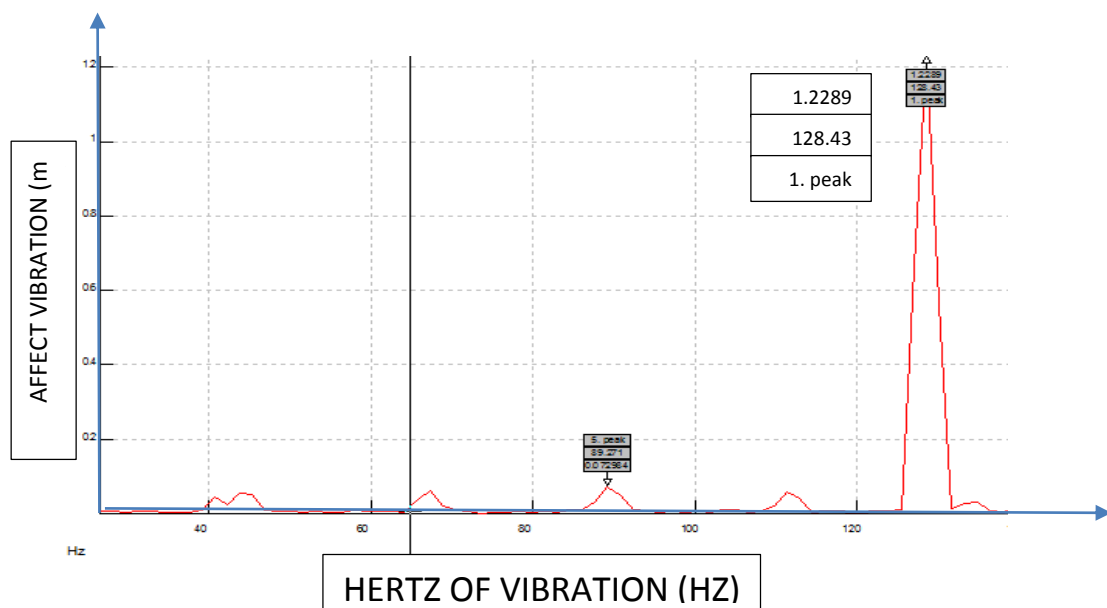


Figure (5.28) the vibration wave at 7500 RPM after processing by (FFT).

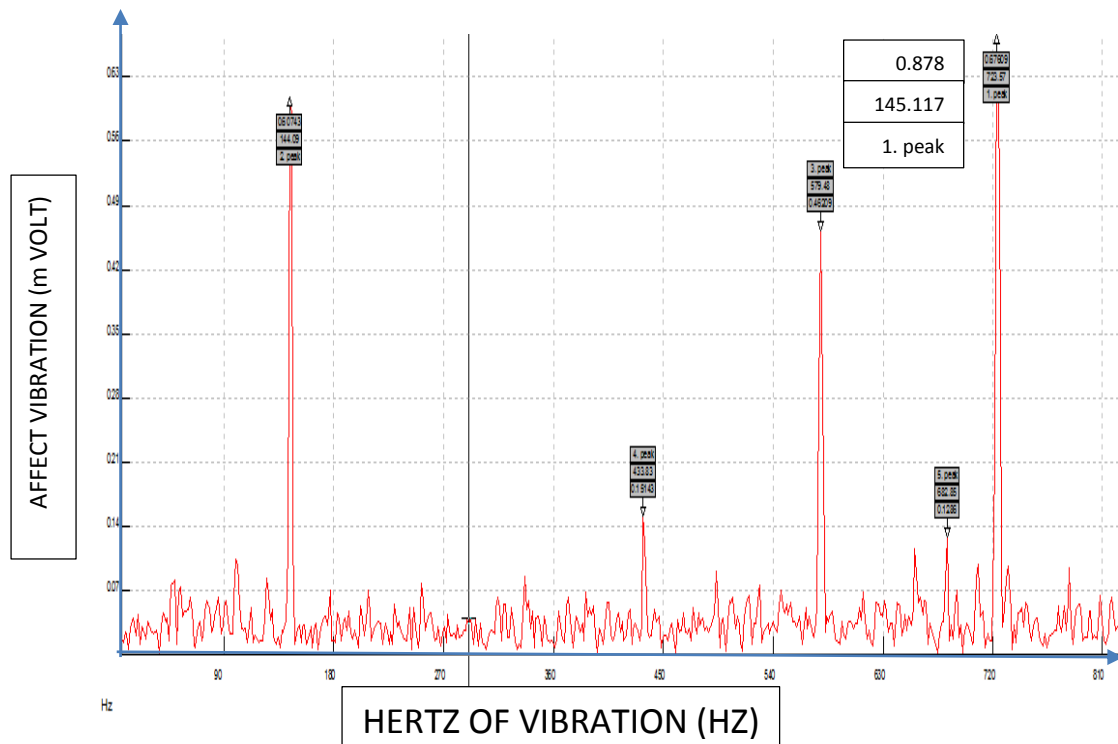


Figure (5.29) the vibration wave at 9000 RPM after processing by (FFT).

5.5. The results from analytic study for model have Two crack in shaft:

In this analysis, it was fabricated two cracks and each crack at a certain angle. The angle of inclined of the first crack (θ_1) and the second crack (θ_2). when looking from the side, we have angle between the first crack and the second called (γ).

Three tests were conducted, it is (90,30), (90,60) and (90,90). In all tests it was concluded that increasing the depth of the crack caused an increase in response with a decrease in critical velocity

From **tables (5.9), (5.10) and (5.11)**, it was observed increased the response and decreased critical velocity when the crack depths are increasing. It was concluded that increased the response and decreased critical velocity when the inclined angle of the second crack is increase.

In the third chapter, from equations **(3.83) and (3.84)**, it was found that the flexibility depends on the incline angle of the crack, Where the flexibility increases when the angle of inclination increases, if the flexibility increases the critical velocity will decrease and the response will increase also.

Table (5.9) the value of response and critical speed at
 $(\theta_1 = 30^\circ, \theta_2 = 90^\circ, \gamma = 0^\circ)$.

Cracks depths (mm)	Critical speed(RPM)	Response (mm)
Uncrack test	8125	0.0295
7.5 , 4	7400	0.0385
15 , 8	6600	0.0426
15 , 15	6520	0.0481

**Table (5.10) the value of response and critical speed at
($\theta_1 = 60^\circ, \theta_2 = 90^\circ, \gamma = 0^\circ$)**

Cracks depths (mm)	Critical speed(RPM)	Response (mm)
Uncrack test	8125	0.0295
7.5 , 4	7200	0.0411
15 , 8	6460	0.0442
15 , 15	6258	0.0503

**Table (5.11) the value of response and critical speed at
($\theta_1 = 90^\circ, \theta_2 = 90^\circ, \gamma = 0^\circ$)**

Cracks depths (mm)	Critical speed(RPM)	Response (mm)
Uncrack test	8125	0.0295
7.5 , 4	7010	0.0424
15 , 8	6320	0.0463
15 , 15	6070	0.0531

Figure (5.30) to (5.32) shows increased response with a decrease in critical velocity when crack depth is increased in both sides. So increasing the crack depth with increased crack angle will increase the percentage failure in the rotor.

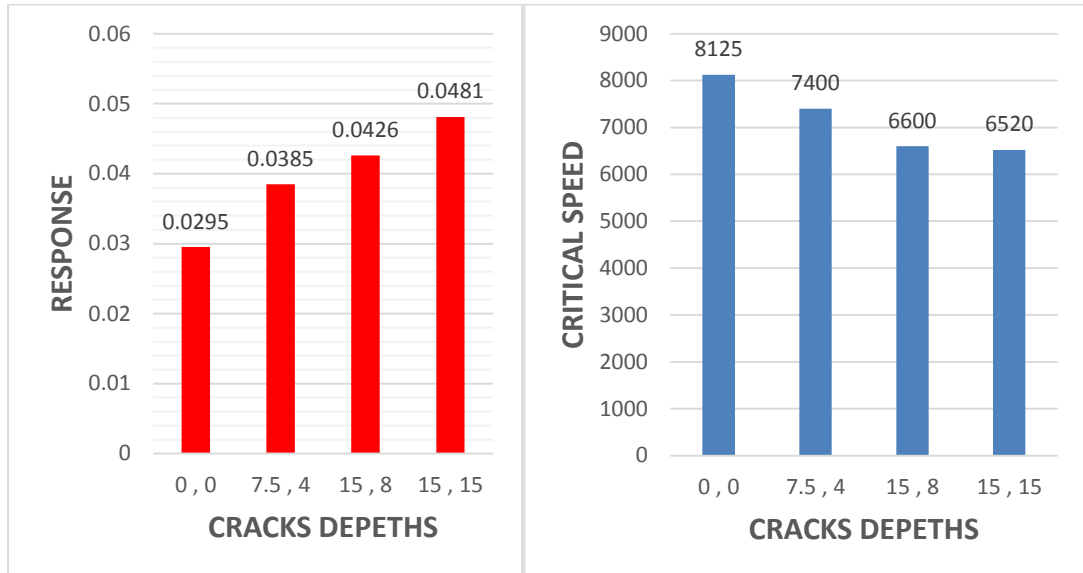


Figure (5.30) the response and critical speed at $(\theta_1 = 30^\circ, \theta_2 = 90^\circ, \gamma = 0^\circ)$.

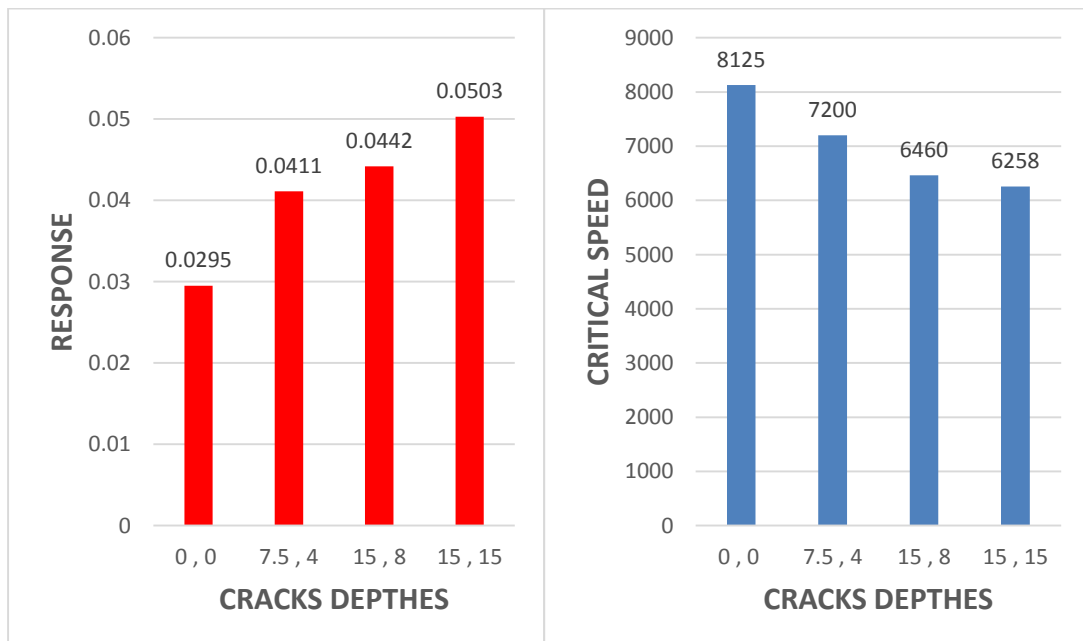


Figure (5.31) the response and critical speed at $(\theta_1 = 60^\circ, \theta_2 = 90^\circ, \gamma = 0^\circ)$

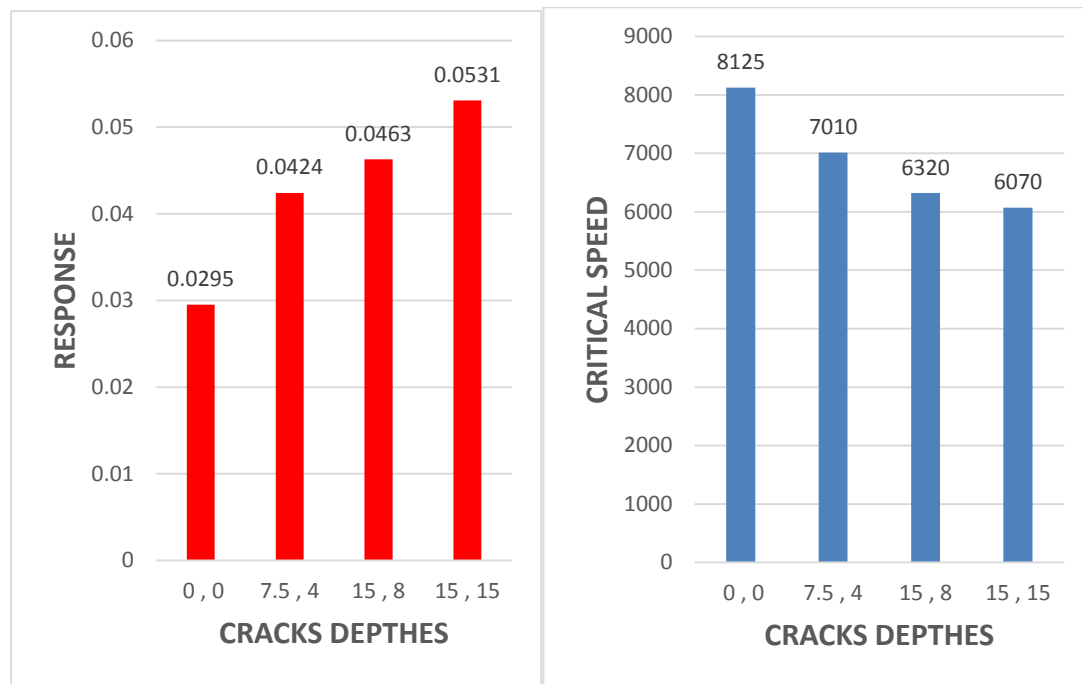


Figure (5.32) the response and critical speed at
 $(\theta_1 = 90^\circ, \theta_2 = 90^\circ, \gamma = 0^\circ)$

From Table (5.12) and Figure (5.33), it was concluded that the higher the depth of the crack with the stability of the angle, the greater the risk. Where the percentage of critical velocity decreases is greater than the remainder of the other cases

Table (5.12) The Percentage value of decreases ratio for critical speed between crack angles.

Cracks depths (mm)	Comparison between $\theta_1 = 30^\circ, \theta_2 = 60^\circ$	Comparison between $\theta_1 = 30^\circ, \theta_2 = 90^\circ$	Comparison between $\theta_1 = 60^\circ, \theta_2 = 90^\circ$
7.5 , 4	2.70%	5.27%	2.63%
15 , 8	2.12%	4.24%	2.16%
15 , 15	4.01%	6.90%	3.00%

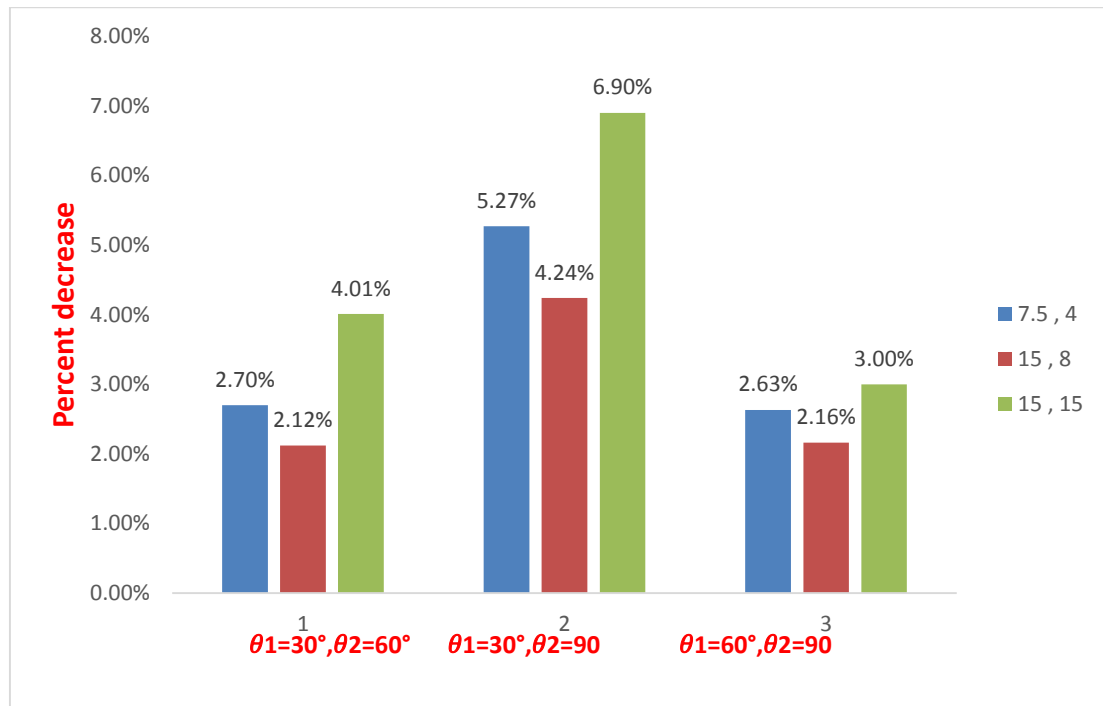


Figure (5.33) The Percentage value of decreases ratio for critical speed between crack angles.

From Table (5.12) and Figure (5.33), It was concluded that increasing the depth of the crack leads to increased displacement, which results in increased repaidetely forces on the dynamic system. The high speed of rotation increases the stresses on the rotor due to increased Angular Momentum.

Table (5.13) The Value of increases ratio for response.

Cracks depths (mm)	Comparison between $\theta_1 = 30^\circ, \theta_2 = 60^\circ$	Comparison between $\theta_1 = 30^\circ, \theta_2 = 90^\circ$	Comparison between $\theta_1 = 60^\circ, \theta_2 = 90^\circ$
7.5 , 4	2.75%	10.12%	3.16%
15 , 8	3.75%	8.68%	4.75%
15 , 15	5.16%	11.73%	5.56%

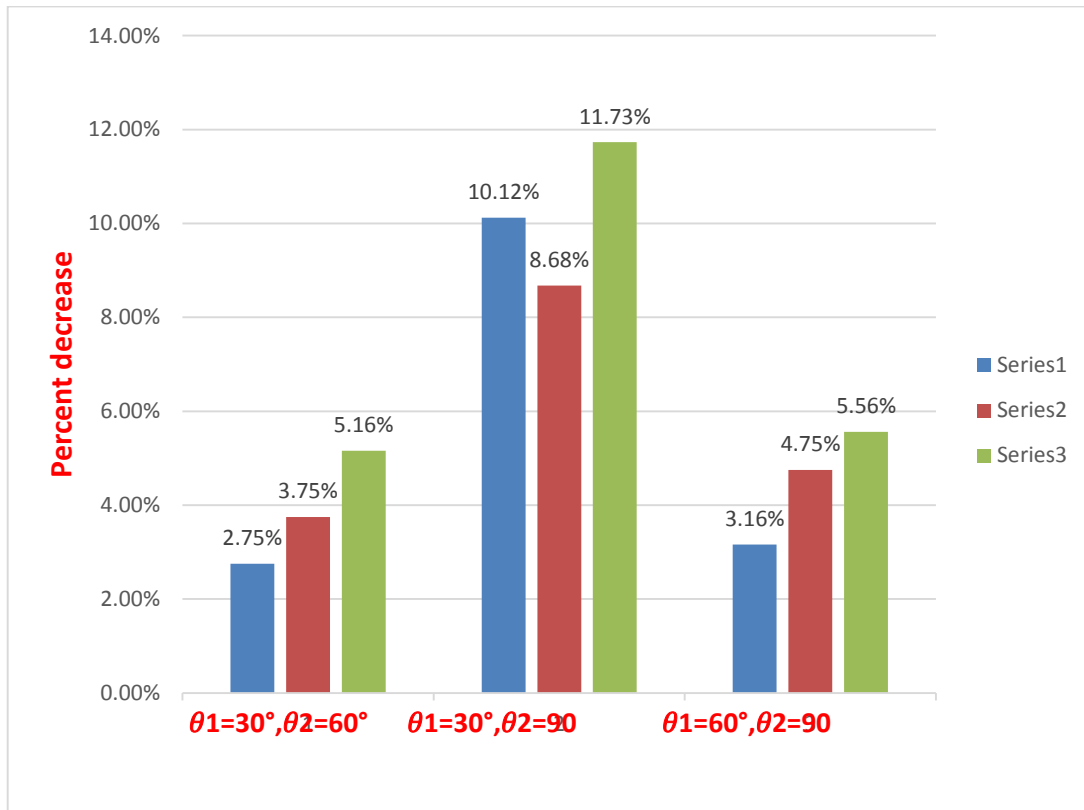


Figure (5.34) The Percentage value of increases ratio for response between crack angles.

Figure (5.33) to **(5.35)** shows that when the angle of the crack slope increased, the cross sectional area of rotor is decreased and therefore the flexibility increased. So the response will increase with the critical speed decrease.

Also it was noted that the presence of two crack in the rotor is more dangerous than having a single crack, and this was increasing the rate of rapid failure, thus increasing the dynamic system damage rotor.

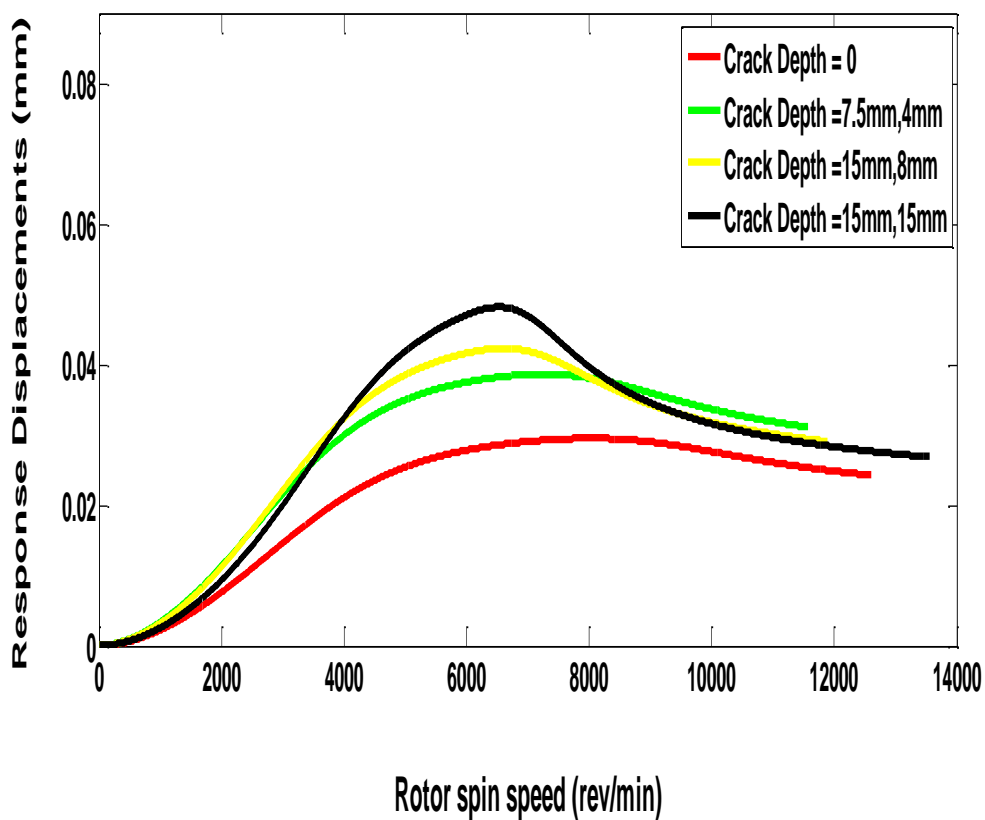


Figure (5.33) the response and critical speed at $(\theta_1 = 30^\circ, \theta_2 = 90^\circ, \gamma = 0^\circ)$.

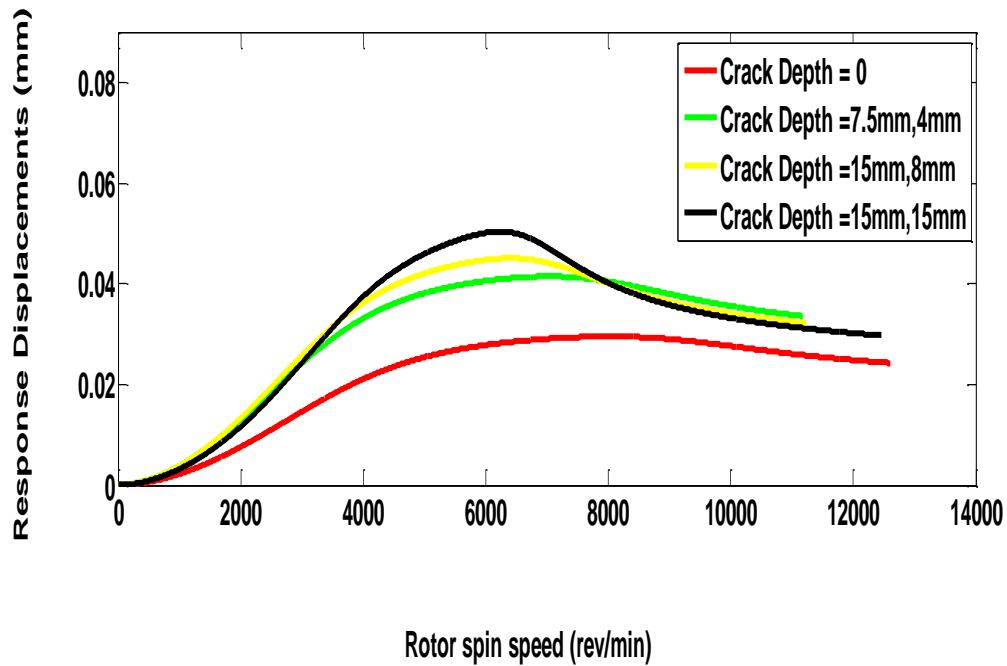


Figure (5.34) the response and critical speed at
 $(\theta_1 = 60^\circ, \theta_2 = 90^\circ, \gamma = 0^\circ)$.

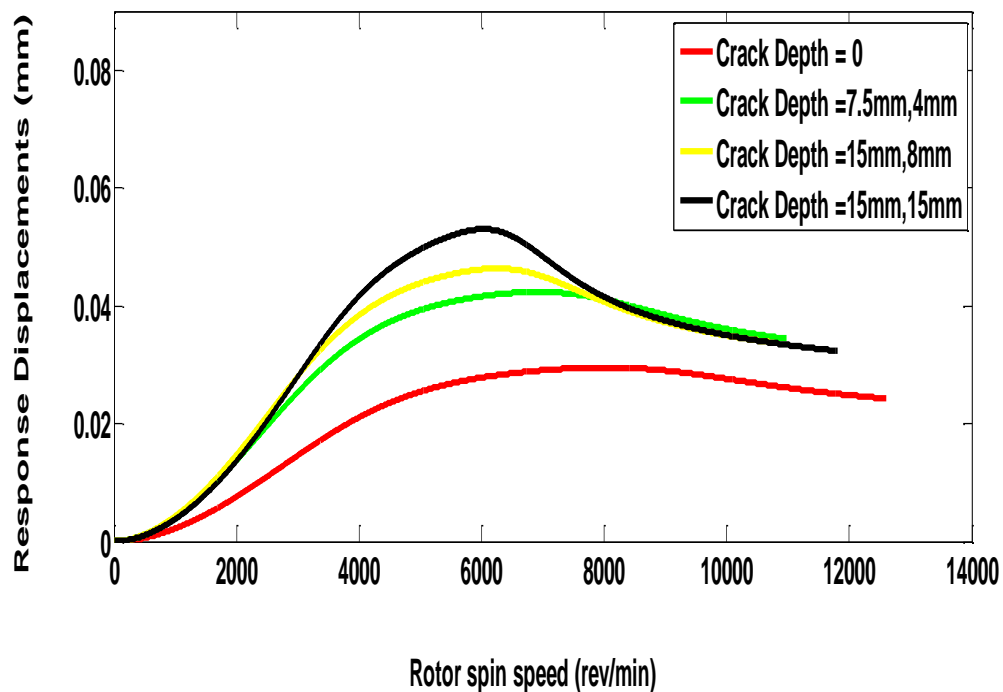


Figure (5.35) the response and critical speed at
 $(\theta_1 = 90^\circ, \theta_2 = 90^\circ, \gamma = 0^\circ)$.

CHAPTER SIX

Conclusions and Recommendations

6.1. Conclusions: -

The following conclusions were obtained from this study.

- 1- The effect increasing the crack depth on the vibration parameters lead to an increase in the response and a decrease in critical speed.
- 2- Increasing the size the orbit is a good indication of the presence of crack, it was observed that if the depth of the crack increased, the size of the Orbit is increased also.
- 3- When the crack depth is increased to $(0.8R)$ of the radius, then it will expect sudden failure at any time with high growth speed for crack.
- 4- In the experimental work at uncracked shaft, it is observed that the speed of rotation is very close to the frequency resulting of the vibration, so it is possible to consider the wave from type $(1X)$.
- 5- For the shaft that contains two crack, it was concluded that when the angle of the crack is increased with the horizontal direction, the critical speed will decrease and the response will increase, and the change will be significant when the angle is (60) degrees or more.
- 6- The higher response of the cracked rotor leads to higher crack growth. This is due to the higher stresses that concentrated at the crack zone.

6.2. Recommendations: -

For the future work related to the rotor studying, the following recommendations can be suggested:

- 1- Study of the effect of thermal stresses resulting from the combustion products in the gas Turbine.
- 2- Study the impact of shocks resulting from failed confinements and their effect on the formation or growth of the crack.
- 3- Studying the effect of torsion stresses on the crack and its effect on the growth of the crack with bending stresses.
- 4- Study the effect of temperature on the properties for the oil layer and its effect on the vibration parameters in the journal bearings.

References

- [1] C. Athanasios Chasalevris, "Vibration Analysis of Nonlinear-Dynamic Rotor-Bearing Systems and Defect Detection", Mechanical Engineering and Aeronautics, University of Patras, (2009).
- [2] A.W. Rankin, B.R. Senguin, "Report of Investigation of the Turbine Wheel Fracture at Turners Creek" Transactions of the ASME 78(10), (1956) 1527.
- [3] C. Schabtach, E.L. Folgeman, A.W. Rankin, D.H. Winner "Report of the Investigation of Generator Rotors Fractures", Transactions of the ASME 82(18), (1957) 1623.
- [4] M. Yoshida, "Steam Turbine Rotor Accidents and Its Countermeasure", Turbomachinery.1976; 4(11):782.
- [5] A. Muszynska, "Demonstration of Various Rotors Instabilities (Exhibit of Bently Rotor Dynamics Research Corporation Liberator Rig at Symposium on Instability in Rotating Machinery)", NASA, Conference Publication (1985); pp409-413.
- [6] R.A. Gasch, "Survey of the Dynamic Behavior of a Simple Rotating Shaft with a Transverse Crack", Journal of Sound and Vibration, (1993); 160(2):313-332. .
- [7] H.D. Nelson and I.M. Mcvaugh," The Dynamics of Rotor-Bearing Systems Using Finite Elements", Journal of Engineering for Industry, May, (1976)/pp593-600.
- [8] A.AL-Shudeifat and A. Butcher, "New Breathing Functions for The Transverse Breathing Crack of the Cracked Rotor System": Approach for Critical and Subcritical Harmonic Analysis, Journal of Sound and Vibration,12. August. (2010).

References

- [9] H.D. Nelson and I.M. Mcvaugh, "The Dynamics of Rotor-Bearing Systems Using Finite Elements", *Journal of Engineering for Industry*, May, (1976)/pp593-600.
- [10] Stefanos A. Paipetis, Thomas G. Chondros "Analytical Methods in Rotor Dynamics" *Mechanical Engineering and Aeronautics*, University of Patras (2000).
- [11] E.T. John Penny and I. Michael Friswell, "The Dynamics of Cracked Rotors" (2002).
- [12] M.A. Mohiuddin, and Y.A. Khulief, "Dynamic Response Analysis of Rotor-Bearing Systems with Cracked Shaft", DOI: 10.1115/1.1423950, Vol. 124, *Transactions of the ASME*, (2002).
- [13] A.K. Drape, K. Gupta, A. Chawla, "Dynamics of Two-Cracked Rotor", *Journal of Sound and Vibration*. (2003)259(3), pp649-675.
- [14] Marc Thomas, A.A Lakis, L. Hamidi, M. Massoud, "Rotor Health Monitoring by Modal Analysis", Department of Mechanical Engineering, University of Montreal (Qc) Canada, (2003).
- [15] J. Darryl Chauvin, "An experimental Investigation of Whirl Instability Including Effects of Lubricant Temperature in Plain Circular Journal Bearings", Louisiana State University, Agricultural and Mechanical College, May, (2003).
- [16] J.J. Sinou, "Effects of a Crack on the Stability of a Non-Linear Rotor System", *International Journal of Non-Linear Mechanics* doi: 10.1016/j.ijnonlinmec.2007.04.002, Elsevier Ltd, (2007).

[17] Paolo Pennacchi, Andrea Vania” Diagnostics of a crack in a load coupling of a gas turbine using the machine model and the analysis of the shaft vibrations”, Journal of Elsevier, (2007).

[18] P. Todorovič, B. Jeremic, I. Mačuzic, A. Brkovic, Proso, "Vibration Analysis of Cracked Rotor During Run-up", Tribology in Industry, volume 30, No.1&2, (2008).

[19] P. Todorovič, B. Jeremic, I. Mačuzic, A. Brkovic, U. Proso, "Vibration Analysis of Cracked Rotor During Run-up", Tribology in Industry, volume 30, No.1&2, (2008).

[20] J.J. Sinou, "An Experimental Investigation of Condition Monitoring for Notched Rotors through Transient Signals and Wavelet Transform", Experimental Mechanics 49 (2009) 683-695", DOI: 10.1007/s11340-008-9193-6, Elsevier Ltd. (2009).

[21] Z.K. Peng, Z.Q. Lang, G. Meng F.L. Chu, "The Effects of Crack on the Transmission Matrix of Rotor System", Shock and Vibration, 18(2011), pp91-103.

[22] M. Chouchane, S. Naimi, J.L. Ligier, " Stability Analysis of Hydrodynamic Bearings with a Central Circumferential Feeding Groove", 13th World Congress in Mechanism and Machine Science, Guanajuato, México, 19-25 June, (2011).

[23] C.D. Untaroiu, A. Untaroiu, M. Boiangiu, "Dynamic Stability Analysis of Periodically Time-Varying Rotor System with a Transverse Crack", scientific research, Engineering, (2011), 3, 719-725, <http://www.SciRP.org/journal/eng>, (2011).

[24] B.S.N. Murthy, J. Srinivas, M. Balaji, M. Ram Mohana Rao, "Dynamic Analysis of Cracked Rotor-Bearing System with Fractional-

References

Order Damping", International Journal of Engineering Science Invention (IJESI), ISSN Conline: 2319-6734, (2012), pp47-50.

[25] R. Ramezanpour, M. Ghayour, S. Ziaei-Rad "Dynamic Behavior of Jeffcott Rotors with an arbitrary Slant Crack Orientation on the Shaft", Applied and Computational Mechanics,6 (2012), pp35-52.

[26] M. Serier, A. Lousdad, K. Refassi, A. Megueni, "Analysis of Parameters Effects on Crack Breathing and Propagation in Shaft of Rotor Dynamic Systems", Materials Research, (2013),16(4), pp867-873.

[27] M.J. Patil and Ali Vaziri, "Vibration Analysis of a Cracked Shaft", International Journal of Advance Engineering Technology, EISSN 0976-3945, June, (2013), pp103-104.

[28] N. Tenali and S. Kadivendi, "Rotor Dynamic Analysis of Steam Turbine Rotor Using ANSYS", International Journal of Mechanical Engineering and Robotics Research (IJMERR), Vol.1, January, (2014).

[29] R. Peretz¹, L. Rogel², J. Bortman³, and R. Klein⁴, "Detection of Cracks in Shafts via Analysis of Vibrations and Orbital Paths" Department of Mechanical Engineering, Ben-Gurion University of the Negev, (2013).

[30] J.F. Al Draji, "Studying the effect of cracks on the static and dynamic behavior of the rotor axis system in the bearings", Department of Mechanics, collage of Engineering, University of Baghdad, (2016).

[31] Nizar Ferjaoui *, Sami Naimi, Mnaour Chouchane, "Bifurcation analysis of a flexible balanced cracked rotor-bearing system", Mechanical Engineering, National Engineering School of Monastir, University of Monastir, (2016).

[32] Deepak P Hujare¹, Nitesh R Girase, and Madhuri G Karnik, “Crack detection in Shaft by Finite Element Analysis and Experimental Modal Analysis”, *European Journal of Advances in Engineering and Technology*, (2016), 3(10): 18-24.

[33] I. Michael Friswell, E.T. John Penny, D. Seamus Garvey, W. Arthur Lees, "Dynamics of Rotating Machines", Cambridge University press, 32 Avenue of the Americas New York NY 10013-2473 USA, First Published 2010, Reprinted 2012, pp177-183.

[34] N. Bachschmid, R. Pennacchi, E. Tanzi, "Cracked Rotors, "A survey on Static and Dynamic Behavior Including Modeling and Diagnosis", ISBN 978-3-624-01484-0, @ 2010 Springer-Verlag Berlin Heidelberg.

[35] C. Won Lee, "Vibration Analysis of Rotors" 1993 Springer Science + Business Media Dordrecht, originally published by Kluwer Academic, pp99-120.

[36] J.S. Rao, “History of Rotating Machinery Dynamics" Springer Science + Business Media B.V. 2011, pp188-196 & pp 242-248.

[37] ANSYS, Inc, "ANSYS Mechanical APDL Rotor Dynamic Analysis Guide" Southpointe, 275 Technology Drive Canonsburg, PA15317, (2012).

[38] H. Saruhan” Design Optimization of Rotor-Bearing Systems” *Journal of Engineering Sciences*, 2003 (3) 319-326.

[39] J. Claude Luneno, "Cases of Coupled Vibrations and Parametric Instability in Rotating Machines", Department of Engineering Sciences and Mathematics Division of Mechanics of Solid Mechanics, Lulea University of Technology, SE-97187 Sweden, pp2-6.

References

- [40] 1S. Dinakaran, 2S. Ramesh, “Stability Analysis of Journal Bearing: Dynamic Characteristics”, 1Department of Mechanical Engineering, Pawai College of Technology, Namakkal-637018, 2Department of Mechanical Engineering, Vel Tech High Tech Dr. Rangarajan Dr. Sakunthala Engineering College, Avadi, Chennai-600062, Tamilnadu, India.
- [41] B.E. Oka-Avae, “Analogue Computer Simulation of a Rotor System Containing a Transverse Crack”, SIMULATION 1993.
- [42] José M. Machorro-López, et al,” CRACK DETECTION IN SHAFTS OF ROTATING MACHINERY USING ACTIVE SENSING WITH AN EXTERNAL EXCITATION ON A BEARING”, Transactions of the ASME, (2008).

1. finding the eccentricities and the forces in bearings by MATLAB program.

```

clc;
clear;
c = 0.1e-3 ; D = 38e-3 ; Lb = 25e-3 ; RT = 9000;
vis = 0.12 ; Rb=D/2;
%*****
**
% CALCULATE BEARINGS REACTION FORCES
a= 81.7e-3; b= 66.6e-3;h= 185.93e-
3;g=9.81;p=7850;Dd=137.4e-3;Ds=38e-3;
Ls=a+b+h;
md = pi*(Dd/2)^2*p*h; wd = md*g;
ma = pi*(Ds/2)^2*a*p; wa = ma*g;
mb = pi*(Ds/2)^2*b*p; wb = mb*g;
F2=(1/Ls)*(wb*(b/2+h+a)+wd*(h/2+a)+wa*a/2)
F1=(1/Ls)*(wa*(a/2+h+b)+wd*(h/2+b)+wb*b/2)
F0 = F2; % reaction force of bearing near the
pulley
M = md+(17*(ma+mb)/35);
Ms=ma+mb;
% c = clearance , Rb= bearing radius , Lb= bearing
length;
% e= journal displacement from bearing center ;
% RT = journal rotational speed in RPM , vis =
Viscosity in pa.s;
% Dd = disk diameter ,Ds = shaft diameter p=
density of disk and diameter
omega =RT*2*pi/60;
Fu = vis*Rb*Lb^3*omega/(2*c^2);
Ss = D*omega*vis*Lb^3/(8*F0*c^2);
% ecr = e/c; % ECCENTRICITY RATIO (ecr)
% Newton-Raphson method with numerical
approximations to the derivative.
ecr = 1;
err = 100;
for i =1:100;
maxit = 100;
tol = 1.0e-6;
icount = 0;
while (err > tol & icount <= maxit)
h = min(0.01*ecr,0.01);

```

```

icount = icount + 1;
f = ecr^8-4*ecr^6+(6-Ss^2*(16-pi^2))*ecr^4-
(4+pi^2*Ss^2)*ecr^2+1;
fp = (ecr+h)^8-4*(ecr+h)^6+(6-Ss^2*(16-
pi^2))*(ecr+h)^4-(4+pi^2*Ss^2)*(ecr+h)^2+1;
fn = (ecr-h)^8-4*(ecr-h)^6+(6-Ss^2*(16-
pi^2))*(ecr-h)^4-(4+pi^2*Ss^2)*(ecr-h)^2+1;
df = (fp-fn)/(2*h);
ecrnew = ecr - f/df;
if (icount > 1)
err = abs((ecrnew - ecr)/ecrnew);
end
fprintf(1,'icount = %i xold = %e f = %e df = %e
xnew = %e err = %e \n',icount, xold, f, df, xnew,
err);
fprintf(1,'%i %e %e %e %e %e \n',icount, xold, f,
df, xnew, err);
ecr = ecrnew;
end
%*****
*****

```

2. The relationship between eccentricity with stiffness and damping at change in spin speed was represented by the MATLAB program.

```

% BEARING DIAMETER = 38 mm ; BEARING LENGTH = 25
mm ; lubrication oil SAE = 10 W

% Dynamic viscosity at 20 C = 0.12 Pa s and at 40
C = 0.032 Pa s
% STIFFNES OF BEARING NEAR DRIVE PULLEY
clc;
clear;
c = 0.1e-3 ; D = 38e-3 ; L = 25e-3 ; vis = 0.032 ;
Rb=D/2;
% c = clearance , Rb= bearing radius , L= bearing
length do = wear depith,
% e= journal displacement from bearing center ,
% RT = journal rotational speed in RPM , vis =
Viscosity in pa.s;
%*****
*****

```

APPENDIX-A

```

% ROTATIONAL SPEED RANGE 0 --- 7000 RPM
step=10; % speed
increment
hrpmv =7000; % high rpm
value (hrpmv)
RT=7000;%:step:hrpmv;
omega = (RT.*2.*pi)./60 ; % ROTATIONAL SPEED
IN rad/s

%*****
%*****
% CALCULATE BEARINGS REACTION FORCES
a= 81.7e-3; b= 66.6e-3;h= 185.93e-
3;g=9.81;p=7850;Dd=137.4e-3;Ds=38e-3;
Ls=a+b+h;
md = pi*(Dd/2)^2*p*h; wd = md*g;
ma = pi*(Ds/2)^2*a*p; wa = ma*g;
mb = pi*(Ds/2)^2*b*p; wb = mb*g;
F1=(1/Ls)*(wb*(b/2+h+a)+wd*(h/2+a)+wa*a/2); %
reaction force of bearing near the Free End
F2=(1/Ls)*(wa*(a/2+h+b)+wd*(h/2+b)+wb*b/2); %
reaction force of bearing at pulley End
m = md+ma+mb; % total mass
A = pi*(Ds/2)^2;
ma = (17/35)*p*A*Ls;
%m = md+ma;
%*****
%*****
% BEARING NO.1 AT FREE END

Ss = (D.*omega.*vis*L^3)./(8*F1*c^2);
ecr = 1;
err = 100;
for i =1:100;
maxit = 100;
tol = 1.0e-6;
icount = 0;
while (err > tol & icount <= maxit)
h = min(0.01*ecr,0.01);
icount = icount + 1;
f = ecr.^8-4*ecr.^6+(6-Ss.^2*(16-pi.^2)).*ecr.^4-
(4+pi.^2.*Ss.^2).*ecr.^2+1;

```

APPENDIX-A

```

fp = (ecr+h).^8-4.*(ecr+h).^6+(6-Ss.^2.*(16-
pi.^2)).*(ecr+h).^4-
(4+pi.^2.*Ss.^2).*(ecr+h).^2+1;
fn = (ecr-h).^8-4.*(ecr-h).^6+(6-Ss.^2.*(16-
pi.^2)).*(ecr-h).^4-(4+pi.^2.*Ss.^2).*(ecr-
h).^2+1;
df = (fp-fn)./(2.*h);
ecrnew = ecr - f./df;
if (icount > 1)
err = abs((ecrnew - ecr)/ecrnew);
end
fprintf(1,'icount = %i xold = %e f = %e df = %e
xnew = %e err = %e \n',icount, xold, f, df, xnew,
err);
fprintf(1,'%i %e %e %e %e %e \n',icount, xold, f,
df, xnew, err);
ecr = ecrnew;
end
% ecr = xnew
%%end
end
y = ecr;
z = 16*ecr.^2+pi.^2*(1-ecr.^2);
s = ((1-ecr.^2).^2)./(ecr.*z.^0.5);          %
sommerfeld number
ho = 1./z.^1.5;
% *****
% stiffness bearing no.1

K11S = -2*s.*((2*pi.^2*ecr.^3-4*pi.^2*ecr-
32*ecr.^3)./((1-ecr.^2).^2.*z));
K12S = -2*s.*((-pi.^3+2*pi.^3*ecr.^2+16*pi*ecr.^4-
pi.^3*ecr.^4)./(2*(1-ecr.^2).^2.5.*z));
K21S = -
2*s.*(pi/2).*((pi.^2+32*ecr.^2+32*ecr.^4+pi.^2*ecr
.^2-2*pi.^2*ecr.^4)./((1-ecr.^2).^2.5.*z));
K22S = 2*s.*2.*ecr.*((pi.^2+(32+pi.^2)*ecr.^2+(32-
2*pi.^2)*ecr.^4)./((1-ecr.^2).^3.*z));
%*****
% Dimensionless K
K11 = (K11S.*F1)./c;
K12 = (K12S.*F1)/c;
K21 = (K21S.*F1)./c;
K22 = (K22S.*F1)./c;

```

APPENDIX-A

```

%*****
% Damping bearing no.1
C11S=(ho./ecr).*(2*pi*(1-
ecr.^2).^0.5).*(pi^2*(1+2*ecr.^2)-16*ecr.^2));
C12S=-ho*8.*(pi^2*(1+2*ecr.^2)-16*ecr.^2);
C21S=C12S;
C22S=(ho./(ecr.*(1-
ecr.^2).^0.5)).*(2.*pi.*(pi^2.*(1-
ecr.^2).^2+48.*ecr.^2));
C11 = (C11S.*F1)./(c*omega);
C12 = C12S.*F1./ (c*omega);
C21 = C21S.*F1./ (c*omega);
C22 = C22S.*F1./ (c*omega);
%disp([K11' K12' K21' K22'])
%disp([C11' C12' C21' C22'])
%*****
*****
% BEARING NO.2 AT PULLEY END

Ss = (D*omega.*vis*L^3)./(8*F2*c^2);
ecr = 1;
err = 100;
for i =1:100;
maxit = 100;
tol = 1.0e-6;
icount = 0;
while (err > tol & icount <= maxit)
h = min(0.01*ecr,0.01);
icount = icount + 1;
f = ecr.^8-4*ecr.^6+(6-Ss.^2*(16-pi.^2)).*ecr.^4-
(4+pi.^2.*Ss.^2).*ecr.^2+1;
fp = (ecr+h).^8-4.*(ecr+h).^6+(6-Ss.^2.*(16-
pi.^2)).*(ecr+h).^4-
(4+pi.^2.*Ss.^2).* (ecr+h).^2+1;
fn = (ecr-h).^8-4.*(ecr-h).^6+(6-Ss.^2.*(16-
pi.^2)).*(ecr-h).^4-(4+pi.^2.*Ss.^2).* (ecr-
h).^2+1;
df = (fp-fn)./(2.*h);
ecrnew = ecr - f./df;
if (icount > 1)
err = abs((ecrnew - ecr)/ecrnew);
end

```

APPENDIX-A

```

%fprintf(1,'icount = %i xold = %e f = %e df = %e
xnew = %e err = %e \n',icount, xold, f, df, xnew,
err);
%fprintf(1,'%i %e %e %e %e %e \n',icount, xold, f,
df, xnew, err);
ecr = ecrnew;
end
% ecr = xnew
%%end
end
y = ecr;
z = 16*ecr.^2+pi.^2*(1-ecr.^2);
s = ((1-ecr.^2).^2)./(ecr.*z.^0.5);           %
sommerfeld number
ho = 1./z.^1.5;
% stiffness bearing no.2

K11S = -2*s.*((2*pi.^2*ecr.^3-4*pi.^2*ecr-
32*ecr.^3)./(1-ecr.^2).^2.*z));
K12S = -2*s.*((-pi.^3+2*pi.^3*ecr.^2+16*pi*ecr.^4-
pi.^3*ecr.^4)./(2*(1-ecr.^2).^2.5.*z));
K21S = -
2*s.*(pi/2).*((pi.^2+32*ecr.^2+32*ecr.^4+pi.^2*ecr
.^2-2*pi.^2*ecr.^4)./(1-ecr.^2).^2.5.*z));
K22S = 2*s.*2.*ecr.*((pi.^2+(32+pi.^2)*ecr.^2+(32-
2*pi.^2)*ecr.^4)./(1-ecr.^2).^3.*z));
%*****
% Dimensionless K
K112 = (K11S.*F2)./c;
K122 = (K12S.*F2)/c;
K212 = (K21S.*F2)./c;
K222 = (K22S.*F2)./c;
%*****
% Damping bearing no.2
C11S=(ho./ecr).*((2*pi*(1-
ecr.^2).^0.5).*(pi^2*(1+2*ecr.^2)-16*ecr.^2));
C12S=-ho*8.*(pi^2*(1+2*ecr.^2)-16*ecr.^2);
C21S=C12S;
C22S=(ho./(ecr.*(1-
ecr.^2).^0.5)).*(2.*pi.*(pi^2.*(1-
ecr.^2).^2+48.*ecr.^2));
C112 = C11S.*F2./(c*omega);
C122 = C12S.*F2./(c*omega);
C212 = C21S.*F2./(c*omega);

```

APPENDIX-A

```
C222 = C22S.*F2./(c*omega);  
%disp([K111' K121' K211' K221'])  
%disp([C111' C121' C211' C221'])  
%*****  
*****
```


Appendix-B

1. The Dynamic Parameters for bearings Coefficients, [33].

$$a_{xx} = h_o \times 4(\pi^2(2 - \varepsilon^2) + 16\varepsilon^2) \quad B - 1$$

$$a_{xy} = h_o \times \frac{\pi((\pi^2(1-\varepsilon^2)^2)-16\varepsilon^4)}{\varepsilon\sqrt{1-\varepsilon^2}} \quad B - 2$$

$$a_{yx} = -h_o \times \frac{\pi(\pi^2(1 - \varepsilon^2)(1 + 2\varepsilon^2) + 32\varepsilon^2(1 + \varepsilon^2))}{\varepsilon\sqrt{1 - \varepsilon^2}} \quad B - 3$$

$$a_{yy} = h_o \times 4(\pi^2(1 + 2\varepsilon^2) + \frac{32\varepsilon^2(1 + \varepsilon^2)}{(1 - \varepsilon^2)}) \quad B - 4$$

$$b_{xx} = h_o \times \frac{2\pi\sqrt{1-\varepsilon^2}(\pi^2(1+2\varepsilon^2)-16\varepsilon^2)}{\varepsilon} \quad B - 5$$

$$b_{xy} = b_{yx} = -h_o \times 8(\pi^2(1 + 2\varepsilon^2) - 16\varepsilon^2) \quad B - 6$$

$$b_{yy} = h_o \times \frac{2\pi((\pi^2(1 - \varepsilon^2)^2) + 48\varepsilon^2)}{\varepsilon\sqrt{1 - \varepsilon^2}} \quad B - 7$$

$$h_o = \frac{1}{(\pi^2(1 - \varepsilon^2) + 16\varepsilon^2)^{3/2}} \quad B - 8$$

2. parameters for Direct compliance, [21].

$$KI5 = \sigma 5 \sqrt{\pi y} F2\left(\frac{y}{hx}\right), \quad KII5 = KIII5 = 0, \quad \sigma 5 = \frac{4M_y \sqrt{R^2 - x^2}}{\pi R^4} \quad B - 9$$

$$KI4 = \sigma 4 \sqrt{\pi y} F1\left(\frac{y}{hx}\right), \quad KII4 = KIII4 = 0, \quad \sigma 4 = \frac{4M_x x}{\pi R^4} \quad B - 10$$

$$F1\left(\frac{y}{hx}\right) = F0\left(\frac{y}{hx}\right) \left[0.752 + 2.02 \frac{y}{hx} + 0.37 \left(1 - \sin \frac{\pi y}{2 hx}\right)^3\right] \quad B - 11$$

$$F2\left(\frac{y}{hx}\right) = F0\left(\frac{y}{hx}\right) \left[0.923 + 0.199 \left(1 - \sin \frac{\pi y}{2 hx}\right)^4\right] \quad B - 12$$

$$E' = \frac{E}{1 - \vartheta^2} ; \quad Fo\left(\frac{y}{h_x}\right) = \sqrt{\frac{\tan \frac{\pi y}{2h_x}}{\frac{\pi y}{h_x} \cos \frac{\pi y}{h_x}}} \quad B - 13$$

3. The flexibility for a slant crack finding from equations. [21]

$$[C] = [G1][\Delta Cij][G2] + [Cs] \quad B - 14$$

Where

$$\Delta Cij = \frac{\partial^2 W}{\partial M_i \partial M_j} , \quad [G1] = \left[\frac{ba}{L} , \frac{ba}{L} , 1 , 1 \right] , \quad [G2] = \left[\frac{ba}{L} , \frac{ba}{L} , 1 , 1 \right] \quad B - 15$$

$$[Cs] = \mathit{diag.} \left(\frac{a^2 b^2}{3EIL} , \frac{a^2 b^2}{3EIL} , \frac{L}{2GJp} , \frac{L}{2AE} \right) \quad B - 16$$

The shear stress and maximum tension to combined loads element is

$$\sigma_{max.} = \frac{2T}{\pi R^3} \sin(2\theta) + \frac{M_z}{\pi R^2} \sin^2 \theta \quad B - 17$$

$$\tau_{max.} = -\frac{2T}{\pi R^3} \cos(2\theta) + \frac{M_z}{\pi R^2} \sin \theta \cos \theta \quad B - 18$$

where.

$$\sigma^2_{max} = \left(\frac{M_z}{\pi R^2} \sin^2 \theta + \frac{2T}{\pi R^3} \sin 2\theta \right)^2 \quad B - 19$$

$$\tau^2_{max} = \left(-\frac{2T}{\pi R^3} \cos 2\theta + \frac{M_z}{\pi R^2} \sin \theta \cos \theta \right)^2 \quad B - 20$$

To find the element C(3,4), it must calculate the second derivatives of σ^2_{max} and τ^2_{max} with respect to q_1 and T .

$$\frac{\partial^2 \sigma^2_{max}}{\partial M_z \partial T} = \frac{\partial^2}{\partial M_z \partial T} \left(\frac{M_z}{\pi R^2} \sin^2 \theta + \frac{2T}{\pi R^3} \sin 2\theta \right)^2 = 2 \left(\frac{2}{\pi R^3} \right) \left(\frac{1}{\pi R^2} \right) \sin^2 \theta \sin 2\theta \quad B - 21$$

$$\begin{aligned} \frac{\partial^2 \tau^2 max}{\partial M_z \partial T} &= \frac{\partial^2}{\partial M_z \partial T} \left(-\frac{2T}{\pi R^3} \cos 2\theta + \frac{M_z}{\pi R^2} \sin \theta \cos \theta \right)^2 \\ &= -2 \left(\frac{2}{\pi R^3} \right) \left(\frac{1}{\pi R^2} \right) \sin \theta \cos 2\theta \end{aligned} \quad B - 22$$

The element C(3,4) of the flexibility matrix is proportional to function (H) in the equation as follows

$$H(\theta) = \frac{\partial^2 \sigma^2 max}{\partial M_z \partial T} + \frac{\partial^2 \tau^2 max}{\partial M_z \partial T} = 2 \left(\frac{2}{\pi R^3} \right) \left(\frac{1}{\pi R^2} \right) F(\theta) \quad B - 23$$

Where

$$F(\theta) = \sin^2 \theta \sin 2\theta - \sin \theta \cos \theta \cos 2\theta \quad B - 24$$

4. The equations of the terms for finding the flexibility of the rotor, it's have two cracks, the first slant crack and the second transverse crack.

$$\bar{I}g1 = \iint_{A1} \tilde{\alpha}^2 \alpha F^2 d\alpha dw \quad B - 25$$

$$\bar{I}g1 = \iint_{A2} \tilde{\alpha}^2 \alpha F^2 d\alpha dw \quad B - 26$$

$$\bar{I}g2 = \iint_{A2} \tilde{\alpha}^2 \alpha w F \tilde{F} d\alpha dw \quad B - 27$$

$$\bar{I}g3 = \iint_{A2} w^2 \alpha \tilde{F}^2 d\alpha dw \quad B - 28$$

$$\bar{I}g2 = \iint_{A1} w^2 \alpha \tilde{F}^2 d\alpha dw \quad B - 29$$

$$\bar{I}g3 = \iint_{A1} \tilde{\alpha} \alpha w F \tilde{F} d\alpha dw \quad B - 30$$


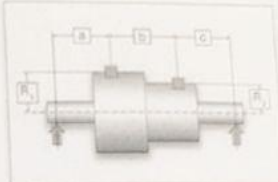
1. Balancing report from Doraa Refinery:

Balancing report

Type data

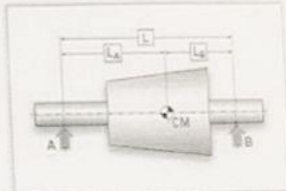
Rotor type	*
Last change	2/6/2019 1:28 PM
Set speed	750 rpm

ABC geometry

Position of correction planes		
Distance a	52 mm	
Distance b	185 mm	
Distance c	62 mm	
Radius 1	68 mm	
Radius 2	68 mm	

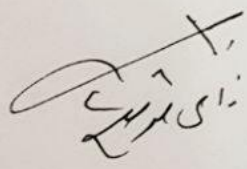
ISO 1940-1:2003 calculation


Calculation based on	Quality grade G	
Deviation (+/-)%	0	
Balancing quality grade	G 6.3	
Mass of rotor	24.0 kg	
Service speed	8000 rpm	
Distance of bearings L	299 mm	
Distance bearing A - center of mass	145 mm	
Distance bearing B - center of mass	155 mm	
Dynamic Tolerance 1	93.3	g-mm
Dynamic Tolerance 2	87.2	g-mm

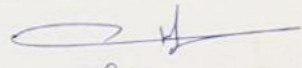


Measuring Results, Run: 12 2/6/2019

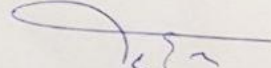
Rotor ID	695 rpm		
Measuring speed			
Unbalance	63.7 g-mm	203°	in Tol
Correction Plane 1	36.3 g-mm	8°	in Tol
Correction Plane 2			
Correction	936 mg	203°	in Tol
Correction Plane 1 - Mass (Remove)	534 mg	8°	in Tol
Correction Plane 2 - Mass (Remove)			







جاء من قبل
رئيس
019/017



رئيس
رئيس قسم

2. Table (1) The values of the dimensionless compliance in vertical and cross coupling directions, [1].

a/R	\bar{C}_{55}	\bar{C}_{44}
0.04	0.002839	0.000041
0.08	0.016094	0.000351
0.12	0.04368	0.001498
0.16	0.08912	0.004382
0.2	0.142261	0.009502
0.24	0.221466	0.017941
0.28	0.31727	0.030710
0.32	0.43367	0.04922
0.36	0.56612	0.074125
0.4	0.72304	0.109167
0.44	0.904937	0.153903
0.48	1.10735	0.211690
0.52	1.34193	0.285412
0.6	1.88307	0.494015
0.64	2.21216	0.638209
0.68	2.58835	0.817116
0.72	2.99793	1.03831
0.76	3.45437	1.31194
0.8	3.97224	1.65530

الخلاصة

تتعرض دوارات التوربينات الغازية لأنواع واتجاهات مختلفة من الاحمال مثل الحمل المحورية، والانحناء، والقص الحراري. تتغير هذه الاحمال بشكل دوري أثناء عملية التشغيل التي يمكن أن تؤدي إلى بديّة تصدع في عمود الدوران. عندما تنتشر هذه التشققات إلى أقصى حد، فإنها ستؤدي إلى فشل مفاجئ في العمود الدوار.

يمكن اكتشاف وجود التصدع من خلال مراقبة معاملات الاهتزاز للدوار، يحدث تغيير في معاملات الاهتزاز عند تشقق العمود. التغييرات الذي تمت ملاحظتها بوضوح في هذه المعاملات هي التردد الطبيعي واستجابة الاهتزاز.

في هذه الدراسة، يتم دراسة اهتزاز دوار التوربينات الغازية في محطة الحلة الغازية/2 بوجود شقوق وبدونها. تم تصميم الدوار بطريقة تحليلية وعددية وتجريبية. أجريت الدراسة العددية باستخدام برنامج ANSYS للدراسة التجريبية. تم بناء جهاز اختبار لتمثيل الدوار الحقيقي، خلال التجارب كان نطاق سرعة الدوار يتغير من صفر إلى 10000 دورة في الدقيقة. من الناحية التجريبية، تم تصميم نموذجين من أعماق الشق يبلغان 0.2 و 0.4 من نصف قطر العمود إلى جانب العمود غير متشقّق.

تم تصنيع الدوار بدقة عالية ثم تم اجراء عملية موازنه له للدوران بسرعة أعلى. تم قياس اهتزاز الدوار باستخدام مقياس التسارع المتصل بجهاز **Oscilloscope**. تم اكتشاف السرعة الحرجة عندما وصلت قراءة مقياس التسارع إلى أعلى قيمة لها.

في الدراسة التحليلية، تم تصميم نموذج شق واحد وشق مزدوج بأعماق واتجاهات مختلفة. بينما في التحليل العددي، تم تصميم العمود ليكون له شق واحد بأعماق مختلفة.

أظهرت النتائج التي تم الحصول عليها من هذه الدراسة وجود اتفاق جيد بين النمذجة التحليلية والعددية والتجريبية. في حالة العمود السليم، تم العثور على السرعة الحرجة، وكانت نسبة الخطأ بين التحليل التجريبي والتحليل العددي (3.07%)، وبين التحليل التحليلي والتحليل التجريبي (2.78%). تم التوصل بعد نمذجة الدوار واجراء التحليلات عليه أنه عند زيادة عمق الشق، فان السرعة الحرجة سوف تنخفض بينما تزداد الاستجابة ويزداد حجم مدار الدوار.



جمهورية العراق

وزارة التعليم العالي والبحث العلمي

جامعة كربلاء

كلية الهندسة

مراقبة حالة عمود التوربين الغازي في محطة كهرباء الحلة / 2 باستخدام مقاييس الاهتزاز في بيئات مختلفة.

رسالة مقدمة الى

مجلس كلية الهندسة / جامعة كربلاء

وهي جزء من متطلبات نيل درجة الماجستير في علم الهندسة الميكانيكية

من قبل

حسين إبراهيم منصور اللوبوي

بكالوريوس الهندسة الميكانيكية / جامعة كربلاء لسنة 2006-2007

بإشراف

الأستاذ المساعد

د. أمجد مال الله الحمود

الأستاذ المساعد

د. محسن عبدالله الشمري

2019م

1440 هـ